CORE-COLLAPSE SUPERNOVAE IN THE GREAT SURVEY ERA

BY

AMY Y. LIEN

DISSERTATION

Submitted in partial fulfillment of the requirements
for the degree of Doctor of Philosophy in Astronomy
in the Graduate College of the
University of Illinois at Urbana-Champaign, 2011

Urbana, Illinois

Doctoral Committee:

Professor Brian Fields, Chair
Professor Robert Brunner
Professor You-Hua Chu
Professor Paul Ricker

Abstract

A new class of wide-field, repeated-scan optical sky surveys, such as LSST, is coming online, and will map the sky in the time domain with unprecedented depth, completeness, and dynamic range. A main science goal of LSST is to detect Type Ia supernovae, but the survey will also revolutionize our understanding of core-collapse events. LSST will observe $\sim 10^5$ core-collapse supernovae per year out to $z \sim 1$ and obtain the cosmic supernova rate by *direct counting*, in an unbiased way and with high statistics. Many science applications will therefore be feasible. Here, we discuss synergies with neutrino detectors, radio observations, and gamma-ray telescopes. The cumulative (anti)neutrino production from all core-collapse supernovae within our cosmic horizon gives rise to a diffuse supernova neutrino background (DSNB) which is on the verge of detectability. The observed flux depends on supernova physics, but also on the cosmic history of supernova explosions. The high precision measurement of the cosmic supernova rate will allow precise predictions of DSNB and make it a strong probe of optically *invisible* supernovae, which may be unseen either due to unexpected large dust obscuration in host galaxies, or because some core-collapse events proceed directly to black hole formation and fail to give an optical outburst. Another way to uncover optically invisible supernovae would be the next generation radio telescope, the Square Kilometer Array (SKA). SKA will be capable of unbiased synoptic searches over large fields of view with remarkable sensitivity and explode the radio core-collapse supernova inventory from the current number of several dozen in the local universe to ~ 600 yr^{-1} deg^{-2} out to $z \sim 5$. SKA will be complementary to LSST and together provide crucial information for dust evolution and star-formation at high redshift. Furthermore, supernovae are an impor-

tant astrophysical input of the diffuse extragalactic gamma-ray background (EGB), which arises from an ensemble of unresolved extragalactic gamma-ray sources. Although the EGB has been detected by the *Fermi Gamma-Ray Space Telescope*, its source spectrum remains unsettle. We will discuss the EGB contributions from cosmic rays accelerated by supernovae in both star-forming and quiescent galaxies. LSST will provide crucial information about supernovae and their host galaxies, and therefore enable more precise EGB predictions that will disentangle the EGB emissions from different source candidates.

To my family

Acknowledgments

Throughout all the content in this thesis, I found it the hardest to complete the acknowledgments, for this work certainly would not be done without the help and support from many people, and it is impossible to express my full gratitude in just a few paragraphs. However, here is my little attempt to convey my appreciation to people that are closely related to my life as a graduate student.

First and foremost, I would like to thank my advisor, Prof. Brian Fields, for his endless support and patience guiding me through my graduate life. His enthusiasm and optimism have always been a great inspiration that constantly reminds me how fun it is to do astronomy. Besides providing unlimited brilliant and interesting scientific ideas, Brian has also carefully prepared me with many skills that I will need to survive in the real academic world, such as paper writing, how to make a good presentation, and teaching. I cannot recall how many times that he had spent hours and hours with me discussing my presentation slides, sitting through my practice talks, and encouraging me to talk to people in conferences. For this, I am greatly indebted for the generosity and all the time and effort he put in that helped me overcome my timidity and become comfortable with and truly enjoy all kind of scientific interactions.

I would also like to thank my collaborators and letter writers, Prof. John Beacom, Prof. Athol Kemball, and Prof. Leslie Looney. My graduate life would not be so smooth without their help and support, and it was really a wonderful experience working with them. John's meticulous approach toward science has deeply influenced me to be a better scientist. Also, I will never forget the kind spirit and the encouragement from Prof. Kemball. I am

also very grateful for having the wonderful TA experience with Leslie, who is certainly an outstanding teacher and a great cook of Thanksgiving dinners.

Additionally, this thesis work definitely would not be completed without the help from Nachiketa Chakraborty, the best groupmate, who has supported me and this work in every possible way. I greatly enjoy our collaboration and all the scientific (and non-scientific) discussions. Most importantly, I am truly grateful for Nachi's invaluable friendship.

I am also thankful for all the helpful and inspiring conversations with many professors in the astronomy department, particularly Prof. Robert Brunner, Prof. You-Hua Chu, and Prof. Paul Ricker. Their suggestions have greatly improved this work.

Most of all, I would like to thank You-Hua for all of her support even beyond academic assistance. As a foreign graduate student, I am surprised how much Urbana-Champaign can feel like home with the kind friendship, the best Taiwanese cooking, and sprinkle donuts from You-Hua. I thank her for her generosity and for selflessly taking care of all the graduate students.

Moreover, I would really like to thank Jeri Cochran, Mary Magaret O'Connor, and Sandie Osterbur, who have been the nicest assistants that I have ever met. I would not have survived through graduate school without their help with all the complicated paperwork. I would also like to thank Kevin Pointer for always magically fixing the computer problems. Additionally, I really appreciate all the help from Bryan Dunne, who knows all the complicated rules in the university, and also provided extremely helpful suggestions about teaching.

I would especially like to express my gratitude to Jeri Cochran, who has been more than a friend to me. I am truly thankful for all the friendship and love she shared. She warmed my heart in every imaginable way, and I am blessed to have someone who loves me as a daughter here in the US. I will always miss the sprinkle donuts and kettle corn that showed up on my desk, and the knitting time we spent together.

Furthermore, I would like to thank all the current and former graduate students in the astronomy department for their friendship and support. I would like to especially thank

Brett Hayes, Nick Indriolo, Nick Hakobian, Jonathan Seale, Hsin-Fang Chiang, and Jana Bilíková for all the time we spent together in the department doing homework and playing hacky sack. I also thank all of my class (everybody listed above), and former students Ashley Ross and Britt Lundgren, for all the fun parties and the nights we spent at Crane Alley. Additionally, I appreciate the company from the Taiwanese dinner group, Rosie Chen, Shiya Wang, Hsin-Fang Chiang, Tai-Lin Tseng, Karen Yang, Chao-Chin Yang, Chi-Ju Chou, Yuan-hung Chien, Hsin-Lun Kuo, Katherine Lee, Kuo-Chuan Pan, and Yu-Ching Lee. I am especially thankful for all the help and support from my roommate, Karen Yang, throughout these years.

Particularly, I would like to thank my best officemates and dearest girl friends, Jana Bilíková and Hsin-Fang Chiang, who have been extremely generously supporting me both mentally and practically. I enjoyed every single minute we spent together. My graduate life would not be so delightful without your company. At the final stage of my thesis work, I am especially grateful for Jana so kindly proofreading my thesis, and Hsin-Fang being so thoughtful and encouraging even when she was in Taiwan.

I thank Brett Hayes, my boyfriend, for always being there whenever I needed him. His generous support helped me survived through even the most stressful times. This place would not feel so much like home without him, and I am truly grateful for having him in my life. I would also like to thank his three kitties, Loki, Cody, and Bast, for being the best stress relievers and always cheering me up.

Finally, I owe my deepest gratitude to my family. I thank my dad and my mom for a loving childhood and introducing me to the fascinating science world. I am greatly indebted to them for all their support and encouragement for me to pursue my dream far abroad. I thank my sister, Helen Lien, for being the best friend and company in my life, and always mailing me my favorite Taiwanese snacks. I am truly blessed for having such a wonderful family. None of these would have happened without their selfless support and love, and I sincerely dedicate this thesis to my beloved family.

Table of Contents

Chapter 1

Introduction

Core-collapse supernovae are the violent explosions resulting from deaths of massive stars. These events have fascinated astronomers for many centuries for their extraordinary luminosities and energy output. The importance of core-collapse supernovae touches many fields in astrophysics, such as star-formation, neutrino physics, and high-energy astrophysics.

1.1 History of Supernova Observations

The history of supernova observations traces back to more than 1000 years ago. In 185 AD, Chinese astronomers recorded in the "Book of Later Han" a "guest star" that was visible in the night sky for about 8 months. "Guest star" is a Chinese term commonly referring to supernovae. Therefore many people believe that this is the first record of a supernova observation (e.g. Pisarski et al., 1984; Zhao et al., 2006). However, some studies suggested that this "guest star" might be a comet instead of a supernova (Chin & Huang, 1994). The earliest confirmed record of a supernova observation is SN 1006. It was widely seen throughout the northern hemisphere and this supernova observation can be found in literatures of many countries, including China, Egypt, Iraq, Japan, and Switzerland. It is generally believed that SN 1006 is a Type Ia supernova. Its supernova remnant is the first object from which the X-ray synchrotron emission from nonthermal electrons arising from diffusive shock acceleration was proposed and detected (Reynolds & Chevalier, 1981; Koyama et al., 1995). This remnant has provided a great environment for studying the relation between the shock waves from supernovae and the production of cosmic rays and

very high energy ($\gtrsim 100$ GeV) gamma rays (e.g. Tanimori et al., 1998; Acero et al., 2010).

To date, there are ~ 5 recorded Galactic supernovae (Stephenson, 2007), among which are the famous SN 1054 and SN 1604. SN 1054 is famous for its supernova remnant, the Crab Nebula, where a pulsar has been detected and confirmed that SN 1054 is a core-collapse supernova. SN 1604 was discovered by an Italian observer, Johannes Kepler, and has been the last visible Galactic supernova with confirmed record. Based on the age estimation of another well-known supernova remnant Cassiopeia A, some suggested that John Flamsteed has seen the supernova that created this remnant (Ashworth, 1980). However, since John Flamsteed did not recognize the object matching the position of Cassiopeia as a supernova and the object did not appear in other records, some argued that this object might have been a mistake in his catalog (Stephenson & Green, 2005). The invention of telescope extended supernova detections from the Milky Way to other galaxies. Since the first detection of the extragalactic supernova SN 1885A in M31, the number of supernova discoveries has increased exponentially to a total count of ~ 5600 (Fig. 1.1).

In the past decade, Type Ia supernovae have been studied intensively because of their critical role in cosmological distance measurement that has revealed an accelerating universe (e.g., Phillips, 1993a; Riess et al., 1998). The Sloan Digital Sky Survey II (SDSS-II), a 3-year extension of the original SDSS (SDSS-I), had a special survey mode dedicated to search for Type Ia supernovae and found 516 Type Ia events during the survey seasons (Dilday et al., 2010).

Although most of the current transient surveys are designed to observe Type Ia supernovae, core-collapse events will also be found by these surveys due to their similar observational characteristics and hence comparable survey requirements. Core-collapse supernovae are only slightly ($\sim 2^{\rm mag}$) dimmer than Type Ia events. Also, core-collapse and Type Ia supernovae have similar duration of their lightcurves. The luminosities of both supernova types decrease $\sim 1^{\rm mag}$ in ~ 10 days, which means that the same survey cadence is sufficient to discover both of these events. In this work, we will explore the importance of core-collapse

supernovae in astronomy, particle astrophysics, and cosmology.

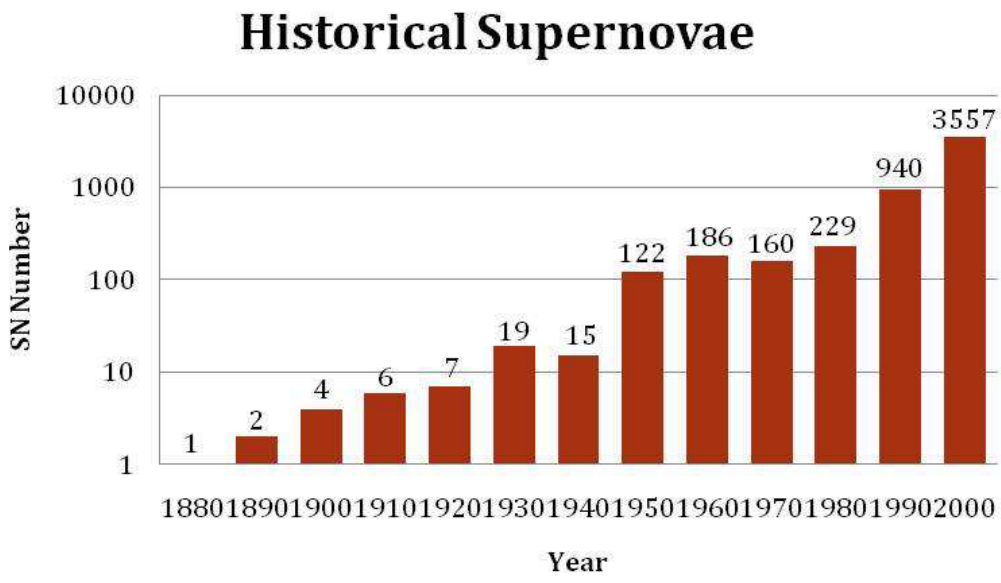

Figure 1.1: Historical supernovae discoveries in 10-year bins. Data compiled from http://www.cbat.eps.harvard.edu/lists/Supernovae.html.

1.2 Brief Overview of Core-Collapse Supernovae

1.2.1 Observational Characteristics of Core-Collapse Supernovae

Observationally, core-collapse supernovae include Type Ib, Type Ic, and Type II supernovae, which are categorized by their lightcurves or spectroscopic features. Comparing to the spectral features of Type II supernovae, all Type I events (Ia, Ib, and Ic) show no hydrogen lines in their spectra. The spectra of Type Ibc supernovae also lack of strong silicon lines compared to Type Ia events. However, Type Ib supernovae have prominent helium lines while Type Ic supernovae only present weak or no helium lines. Type Ib and Ic supernovae are often referred to together as Type Ibc (or Type Ib/c) supernovae because of their similar observational characteristics. Recent observations have shown that Type Ibc supernovae represent $\sim 25\%$ of all core-collapse supernovae (Li et al., 2011b). Currently Type Ibc events are

studied intensively due to their connection with Gamma-ray Bursts (GRBs) (e.g., Galama et al., 1998).

There are several subtypes in Type II supernovae, which include Type II-P, II-L, IIn, and IIb supernovae. Type II-P supernovae show plateau features in their lightcurves. This is the most common supernova type and represents $\sim 70\%$ of all Type II supernovae (Li et al., 2011b). The remaining $\sim 30\%$ are roughly equally distributed between Type II-L, IIn, and IIb supernovae (Li et al., 2011b). Type II-L supernovae display linear-declined features in their lightcurves. Type IIn supernovae show particularly narrow emission lines compared to other Type II events, and hence are labeled as IIn where "n" stands for narrow. In addition, Type IIn events tend to have narrow P-Cygni profiles in the hydrogen Balmer lines. Type IIb supernovae have weak hydrogen lines and are thus initially classified as Type II events, but these lines fade away and the spectra become similar to those of Type Ib events. Table 1.1 summarizes the observational features that distinguish different supernova types.

Table 1.1: Observational characteristics of different supernova types

SN type		Observational Features
I	Ia	No hydrogen; prominent Si II .
	Ib	No hydrogen; prominent He I.
	Ic	No hydrogen; no Si II, no He I.
II	II-P	Plateau feature in lightcurve.
	II-L	Linear-declined feature in lightcurve.
	IIn	Narrow emission lines in spectrum.
	IIb	Transfer from Type II to Ib.

The observational features of core-collapse supernovae basically depend on the mass loss of the progenitors prior to the explosions. Type Ibc supernovae result from massive stars with their hydrogen and/or helium envelopes largely stripped away. Type IIb supernovae retain only a small fraction of their hydrogen envelopes initially, but lose them at later stages of explosion. The progenitors of Type II-P and II-L events possess most of their mass when the explosion happens. The plateau phase in Type II-P is generated by the recombination of

the ionized hydrogen produced by the shock wave. The progenitors of Type II-L supernovae are believed to have less mass in their hydrogen envelopes and hence do not show a long period of hydrogen recombination (Filippenko, 1997). The distinguishing spectral features of Type IIn supernovae suggest that these events are surrounded by dense circumstellar medium that is formed from the mass loss of the progenitor stars decades to centuries before the explosions (see e.g., Filippenko, 1997; Kiewe et al., 2010; Smith et al., 2011).

Although the cosmic core-collapse supernova rate was estimated soon after the first measurement of the cosmic star-formation rate (Madau et al., 1996, 1998), the direct measurements of the cosmic core-collapse supernova rate only become possible recently (Dahlen et al., 2004; Cappellaro et al., 2005). Observationally, supernova rates used to be measured in units of rate per galaxy. However, it was soon realized that a supernova rate depends on the stellar mass of each galaxy. Therefore, nowadays the supernova rate is commonly expressed in units that are normalized to some quantities which represent the galaxy stellar mass, such as the galaxy luminosity. For example, the unit "SNu" is defined as the number of supernovae per century per 10^{10} $L_{\odot}$. This kind of unit makes it easier to discuss supernova rates in different galaxy types. It has been found that supernova rate strongly depend on the galaxy morphology (e.g., Mannucci et al., 2005; Sullivan et al., 2006). In general, core-collapse supernova rates are approximately zero in early-type galaxies, as expected, and Type Ia supernova rates are higher in late-type galaxies than in early-type galaxies.

Observations have shown a rapid growth of the cosmic core-collapse supernova rate out to redshift $z \sim 1$. However, the normalization of the cosmic core-collapse supernova rate remains quite uncertain. Additionally, very little information exists about the cosmic supernova rate beyond redshift $z \sim 1$. Direct measurements of the cosmic supernova rate are mostly available only at low redshift $z \lesssim 0.4$ and come from relatively small or incomplete supernova samples (Cappellaro et al., 1999; Dahlen et al., 2004; Cappellaro et al., 2005; Hopkins & Beacom, 2006; Botticella et al., 2008a; Dahlen et al., 2008a; Kistler et al., 2008a; Bazin et al., 2009; Smartt et al., 2009; Dahlen et al., 2010; Li et al., 2011a; Horiuchi et al.,

2011). To the author's knowledge, the largest single-survey core-collapse sample published to date is that of the Lick Observatory Supernova Search (LOSS) (Leaman et al., 2011; Li et al., 2011b,a; Maoz et al., 2011). LOSS observed 440 core-collapse supernovae in selected galaxy sample in the local universe. They derived a volume-limited core-collapse supernova rate in the local universe after correcting for the sample incompleteness. The most complete volumetric sample so far was obtained by the SuperNova Legacy Survey (SNLS) (Bazin et al., 2009; Palanque-Delabrouille et al., 2010). SNLS performed a synoptic survey and detected 117 core-collapse supernovae out to redshift $z \sim 0.4$ with a medium redshift $z = 0.29$. Dahlen et al. (2010) have directly measured the core-collapse supernova rate out to the highest redshift using the *Hubble Space Telescope*. These authors used a sample of 60 core-collapse supernovae to acquire the core-collapse supernova rate out to redshift $z \sim 1.1$. The direct measurements of cosmic core-collapse supernova rate currently have uncertainties of $\sim 40\%$ in the normalization in local universe (Hopkins & Beacom, 2006), and the uncertainties increase rapidly with larger redshifts.

Cosmic core-collapse supernova rate can also be estimated from the star-formation rate. Since core-collapse supernovae are the deaths of short-lived massive stars, core-collapse supernova rate $\mathcal{R}_{\rm SN}$ is directly proportional to the star-formation rate $\dot{\rho}_\star$ and can be expressed as

$$\mathcal{R}_{\rm SN} = \dot{\rho}_\star \, \frac{\int_{\rm SN} \xi(m) dm}{\int_{\rm star} m \xi(m) dm} \tag{1.1}$$

where the fraction $\int_{\rm SN} \xi(m) dm / \int_{star} m \xi(m) dm$ is the fraction of massive stars that become core-collapse supernovae per unit mass. In Eq. 1.1, $\int_{\rm SN} \xi(m) dm$ integrates the initial mass function $\xi(m)$ over the mass range in which stars end as supernovae. $\int_{\rm star} m \xi(m) dm$ integrates over the mass range of all stars. The extra mass factor in the integrand of the denominator accounts for the fact that $\dot{\rho}_\star$ is a mass rate density in units of $[M_\odot \ {\rm yr}^{-1} \ {\rm Mpc}^{-3}]$, as opposed to an event rate density $\mathcal{R}_{\rm SN}$ in units of $[{\rm yr}^{-1} \ {\rm Mpc}^{-3}]$.

There exist many more measurements of the cosmic star-formation rate than those of the cosmic core-collapse supernova rate, although most star-formation rate measurements are

indirect. Current methods usually involve observing the total luminosity of a galaxy at wavelengths that are mostly contributed to by massive stars, such as UV, H_α, and far-infrared. Thus the star-formation rate can be estimated from the total luminosity via appropriate conversion factors (Hopkins, 2004). Observations conducted at different wavelengths consistently show a rapid rise in the cosmic star-formation rate out to redshift $z \sim 1$ (e.g., Hopkins, 2004; Hopkins & Beacom, 2006, and references therein). Hopkins & Beacom (2006) fitted the current measurements for the cosmic star-formation rate with simple analytic functions and analyze the uncertainties in its normalization. Horiuchi et al. (2009) updated some parameters in the best-fitted function in Hopkins & Beacom (2006) with more recent measurements derived from gamma-ray bursts at higher redshift (Yüksel et al., 2008; Kistler et al., 2008b) With these new data, the uncertainty in the normalization of the cosmic star-formation rate is $\sim 20\%$ (Horiuchi et al., 2009).

Recently Horiuchi et al. (2011) have noticed a mismatch between the cosmic core-collapse supernova rate from direct measurements and the one estimated from the cosmic star-formation rate. The direct measurements are lower by a factor of 2. These authors have carefully examined possible causes for this discrepancy and concluded that the most likely cause would be the existence of intrinsically dim or invisible supernovae. It is theoretically possible that stars with mass $m \gtrsim 40 M_\odot$ form black holes directly without any (or only very dim) optical explosions (MacFadyen & Woosley, 1999; Fryer, 1999; MacFadyen et al., 2001; Heger et al., 2003).

1.2.2 Theoretical Understanding of Core-Collapse Supernovae

The explosion mechanism of supernovae is still poorly understood. Current theories suggest that stars with $m \gtrsim 8 M_\odot$ will be likely to end their lives as core-collapse supernovae, and a supernova progenitor mass range of $8 - 50 M_\odot$ in Eq. 1.1 is commonly adopted. However, the exact cutoff of the mass range is quite uncertain. It is generally believed that a star with mass around $8 - 25 M_\odot$ ends its life as a regular supernova that leaves behind a neutron star

after a successful optical explosion. However, stars with masses above $\sim 25M_{\odot}$ are believed to form black holes either from direct collapse or fall back of the expending material that does not have sufficient velocity (see review in Heger et al., 2003, and references therein). Some studies suggest that stars above $\sim 40M_{\odot}$ directly collapse into black hole without releasing any optical signals, while stars with masses around $25 - 40M_{\odot}$ form black holes from fall back and display some dim optical signals (Fryer, 1999; Heger et al., 2003; Nakazato et al., 2008). However, all of these mass ranges contain large uncertainties, as it is hard to constrain the mass of the progenitors and the outcome via direct observations. Moreover, current simulations have difficulties producing enough momentum for the shock to leave the surface of a progenitor star to create a successful explosion. It is currently believed that 3-dimensional simulations and/or better understanding of neutrino transportation in core-collapse supernovae may hold the key to producing a successful explosion in supernova theory (e.g., Scheck et al., 2006; Duan et al., 2006; Liebendörfer et al., 2005).

1.2.3 Core-Collapse Supernovae and Particle Astrophysics

More than 99% of the energy of a core-collapse supernova is released in the form of neutrinos and anti-neutrinos of all species. Therefore neutrinos are important for studying supernova physics. So far, little is known about the neutrino transportation inside a supernovae. This knowledge is not only crucial in understanding the energy transfer process and the explosion mechanism, but it is also important for the study of nucleosynthesis process that creates heavy elements. Because of the enormous amount of neutrinos produced by each core-collapse supernova, these events are the major sources of extragalactic neutrinos. All core-collapse supernovae in the universe contribute to a "diffuse supernova neutrino background (DSNB)" that is on the verge of detectability. DSNB can be detected via inverse-β decay. The detectable neutrino energy range on Earth is $\sim 10-26$ MeV and thus the major detector for DSNB is Super-Kamiokande (Super-K), which is currently the largest neutrino detector in the MeV energy range. Until now, no DSNB flux has been detected and hence super-K

has set an upper limit for the DSNB flux to be 1.2 cm^{-2} s^{-1} (Malek et al., 2003). This limit is close to the current theoretical prediction based on recent knowledge of supernova neutrino physics and the cosmic core-collapse supernova as well as star-formation history (Strigari et al., 2005; Yüksel & Beacom, 2007). If supernova neutrino physics can be better understood, this upper limit of DSNB will place a tighter constraint of the total cosmic core-collapse supernova rate. Additionally, since neutrinos can pass through almost everything, the DSNB can be one of the major methods for detecting invisible supernovae that are caused by either dust extinction or black hole formation.

Furthermore, core-collapse supernovae are among the major candidates for the production of cosmic rays. Therefore core-collapse supernovae are also important for high-energy astrophysics and for the study of energy feedback to the surrounding environment. Interactions between cosmic rays and interstellar gas generate gamma rays via pion decay (Stecker, 1971):

$$p_{\mathrm{cr}} + p_{\mathrm{ism}} \rightarrow p + p + \pi^0$$

$$\pi^0 \rightarrow \gamma + \gamma$$

Similar to the DSNB described in the previous paragraph, the ensemble of unresolved gamma-ray emission in each galaxy contributes to the "diffuse extragalactic gamma-ray background (EGB)" that is detected by the *Fermi Gamma-ray Space Telescope* (Abdo et al., 2009a). Besides core-collapse supernovae, Type Ia events can also produce cosmic rays, and hence gamma rays in galaxies. However, the source spectrum of the EGB remains unsettled. Current favored candidates that are considered to be possible sources of the EGB include star-forming galaxies, starburst galaxies, and blazars (e.g., Pavlidou & Fields, 2001; Prodanović & Fields, 2006; Fields et al., 2010; Makiya et al., 2011; Thompson et al., 2007; Stecker, 2007; Stecker & Venters, 2010; Venters & Pavlidou, 2011; Padovani et al., 1993; Stecker et al., 1993; Pavlidou & Venters, 2008; Mukherjee & Chiang, 1999; Inoue & Totani,

2009). Understanding the origin of the EGB is critical for understanding the galaxy evolution, mechanism of cosmic-ray acceleration, and star formation history.

1.3 Dawn of the Great Survey Era

Starting in 2000, the SDSS opened the era of large-sky synoptic surveys with CCD technology. The word "synoptic" in this context essentially means "repeatedly scanned". The SDSS telescope surveyed more than 8000 square degrees of the sky [1] and recorded all the data available during the survey lifetime. With this "movie" of the universe taken, astronomers are free to extract a wealth of information in almost every imaginable research field. Such strategy has successfully maximized the science potential of the survey.

After the great success of SDSS, the rapid improvement of CCD technology and data management open further possibilities for more ambitious synoptic surveys that will scan the sky with wider coverage, deeper exposures, and faster cadences. These automatic and untargeted surveys will obtain an unbiased sample of both Type Ia and core-collapse supernovae with unprecedented detection rates and redshift ranges.

In the past few years, several proto-type supernova synoptic surveys have either just finished or come online, such as ESSENCE [2], SNLS [3], DES [4], and Pan-STARRS 1 [5]. These proto-type surveys will lead to the next-generation synoptic surveys, such as the Large Synoptic Survey Telescope (LSST). LSST will be a 8.4 meter telescope located in Cerro Pachón, Chile. It will have a special three-mirror design that produces a particularly large field-of-view. In the scanning mode, the telescope will be capable of observing the entire available sky every $\sim$ 3 days. About 90% of the survey time will be carried out in this mode with a single-visit depth of $\sim 24^{\rm mag}$, which is much better than the $\sim 20^{\rm mag}$ to $22^{\rm mag}$ survey depths of the contemporary synoptic surveys. The remaining 10% survey time will

[1] http://www.sdss.org/.
[2] "Equation of State: SupErNovae trace Cosmic Expansion"; http://www.ctio.noao.edu/essence/.
[3] The "SuperNova Legacy Survey"; http://www.cfht.hawaii.edu/SNLS/.
[4] The "Dark Energy Survey"; http://www.darkenergysurvey.org/.
[5] The "Panoramic Survey Telescope & Rapid Response System"; http://pan-starrs.ifa.hawaii.edu/public/.

be carried out in a deep mode with greater single-visit depth of $\sim 27^{\rm mag}$. This time will be dedicated to very deep surveys of a variety of special regions.

All of the supernova synoptic surveys described above are optical. However, this might soon to be changed when the next generation radio telescope, the Square Kilometer Array (SKA), comes online. With its extraordinary survey sensitivity, SKA will bring new possibility to revolutionize current survey strategy in radio supernova observations from the target-based observations to synoptic searches.

In this work, we will first make predictions of core-collapse supernova discoveries for upcoming synoptic optical surveys and explore their science potential (Chapter 2). Based on these predictions, we will further discuss the possibility to study supernova physics and probe the invisible supernovae by synergies of optical surveys and neutrino detectors (Chapter 3). We will then extend our studies from optical wavelengths to radio regime and examine the possibility of performing a radio synoptic survey with SKA (Chapter 4). Afterwards, we will discuss the importance of supernova input in the EGB from both star-forming and quiescent galaxies (Chapter 5). Finally, we summarize the importance of core-collapse supernova in upcoming synoptic surveys and their future prospects (Chapter 6).

Chapter 2

Cosmic Core-Collapse Supernovae from Upcoming Sky Surveys

This chapter is previously published in The Journal of Cosmology and Astro-Particle Physics as Lien, A., & Fields, B. D. 2009, JCAP, 1, 47.

2.1 Abstract

Large synoptic (repeated scan) imaging sky surveys are poised to observe enormous numbers of core-collapse supernovae. We quantify the discovery potential of such surveys, and apply our results to upcoming projects, including DES, Pan-STARRS, and LSST. The latter two will harvest core-collapse supernovae in numbers orders of magnitude greater than have ever been observed to date. These surveys will map out the cosmic core-collapse supernova redshift distribution via direct *counting*, with very small statistical uncertainties out to a redshift depth that is a strong function of the survey limiting magnitude. This supernova redshift history encodes rich information about cosmology, star formation, and supernova astrophysics and phenomenology; the large statistics of the supernova sample will be crucial to disentangle possible degeneracies among these issues. For example, the cosmic supernova *rate* can be measured to high precision out to $z \sim 0.5$ for all core-collapse types, and out to redshift $z \sim 1$ for Type IIn events if their intrinsic properties remain the same as those measured locally. A precision knowledge of the cosmic supernova rate would remove the cosmological uncertainties in the study of the wealth of observable properties of the cosmic supernova populations and their evolution with environment and redshift. Because of the tight link between supernovae and star formation, synoptic sky surveys will also provide

precision measurements of the normalization and $z \lesssim 1$ history of cosmic star-formation rate in a manner independent of and complementary to the current data based on UV and other proxies for massive star formation. Furthermore, Type II supernovae can serve as distance indicators and would independently cross-check Type Ia distances measured in the same surveys. Arguably the largest and least-controlled uncertainty in all of these efforts comes from the poorly-understood evolution of dust obscuration of supernovae in their host galaxies; we outline a strategy to determine empirically the obscuration properties by leveraging the large supernova samples over a broad range of redshift. We conclude with recommendations on how best to use (and to tailor) these galaxy surveys to fully extract unique new probes on the physics, astrophysics, and cosmology of core-collapse explosions.

2.2 Introduction

A new generation of deep, large-area, synoptic (repeated-scan) galaxy surveys is coming online and is poised to revolutionize cosmology in particular and astrophysics in general. The scanning nature of these surveys will open the way for a systematic study of the celestial sphere in the time domain. In particular, ongoing and planned surveys are sensitive to the transient cosmos on timescales from hours to years, and to supernova flux limits down to $24^{\rm mag}$ and sometimes fainter. As we will see, these capabilities will reap a huge harvest in cosmic supernovae and will offer a new and direct probe of the cosmic supernova history out to high redshifts.

In the past decade, supernovae in nearby and distant galaxies have come to play crucial role for cosmology, via the use of Type Ia explosions as "standard" candles (e.g., Phillips, 1993a; Riess et al., 1996). These powerful beacons are detectable out to very high redshift and thus reveal the cosmic expansion history for much of the lifetime of the universe; the stunning result has been the detection of the acceleration of the Universe and the inference that dark energy of some form dominates the mass-energy content of the cosmos today (e.g.,

Riess et al., 1998; Perlmutter et al., 1999; Astier et al., 2006; Wood-Vasey et al., 2007). The detection of large numbers of Type Ia supernovae over a large redshift range, as well as their use as cosmological probes, represents a major focus of future galaxy surveys (e.g., Wang et al., 2004).

While studies of supernova Type Ia (thermonuclear explosions) justly receive enormous attention due to their cosmological importance, there has been relatively little focus on the detection of the more numerous population of core-collapse supernovae. These explosions of massive stars show great diversity in their observed properties, e.g. including several varieties of Type II events, but also Types Ib and Ic events. Despite their heterogeneous nature, some core-collapse events may nonetheless provide standard candles, via their early lightcurves whose nature is set by the physics of their expanding photospheres (Kirshner & Kwan, 1974; Baron et al., 2004; Dessart & Hillier, 2005, see below). Moreover, core-collapse events are of great intrinsic importance for cosmology, astrophysics, and particle physics. These events play a crucial role in cosmic energy feedback processes and thus in the formation and evolution of galaxies and of cosmological structure.

Synoptic surveys tuned for Type Ia events will also automatically detect core-collapse supernovae. Indeed, as survey coverage and depth increase, they will, for the first time, image a large fraction of *all* unobscured cosmic core-collapse supernovae out to moderate redshift. These photometric detections of supernovae and their light curves will shed new light on a wide variety of problems spanning cosmology, particle astrophysics, and supernova studies. Moreover, these data will "come for free" so long as surveys include core-collapse events in their analysis pipelines.

For example, Madau et al. (1998) already pointed out the link between the cosmic star formation history and the cosmic supernova history, and showed that when integrated over all redshifts, the all-sky supernova event rate is enormous, $\simeq 5 - 15$ events/sec in their estimate. Upcoming synoptic surveys will probe most or all of the sky at great depth, and thus are positioned to observe a large fraction of these events. Consequently, these surveys

will reveal the history of cosmic supernovae via directly *counting* their numbers as a function of redshift.

Already, recent and ongoing surveys have begun to detect core-collapse supernovae. However, to date, surveys have focused on Type Ia events, and thus core-collapse discovery and observation has been a serendipitous or even accidental byproduct of SNIa searches. As a result of these surveys, the supernova discovery rate is accelerating, and the current all-time, all-Type supernova count is ~ 5000 since SN1006.[1] Thus core-collapse data are currently sparsely analyzed and reported in an uneven manner. This situation will drastically improve in the near future, when the supernova count increase by large factors, culminating in up to $\sim$ 100,000 core-collapse events seen by LSST annually. In this paper we therefore will anticipate this future, rather than make extensive comparison with the present data though we will make quantitative contact with current results.

Our work draws upon several key analyses. The thorough and elegant work of Dahlén & Fransson (1999) laid out the framework for rates and observability of cosmic supernovae of all types. Their work assembled a large body of supernova data and applied it to make rate and discovery predictions for the wide variety of star formation histories and normalizations viable at that time, with a particular focus on forecasts for very high redshift (out to $z \sim 5$) observable by the infrared *James Webb Space Telescope*. Sullivan et al. (2000) estimated the rates for supernovae lensed by the matter distribution–particularly rich clusters–along the line of sight; these objects further extend the reach of infrared searches, and identified a possible supernova candidate from *Hubble Space Telescope* archival images of an intermediate-redshift cluster. Gal-Yam et al. (2002) made similar calculations of the infrared observability of supernovae, and identified additional events in archival data. Gal-Yam & Maoz (2004) and Oda & Totani (2005) presented forecasts for then-upcoming ground-based surveys. These studies considered all cosmic supernovae, but with a focus on Type Ia events, specifically with an eye towards revealing the Type Ia delay time as well as a parameterized characterization

[1] Central Bureau for Astronomical Telegrams (2008);
see also http://www.cfa.harvard.edu/iau/lists/Supernovae.html

of the cosmic star formation history based on Type Ia counts. In addition, these first studies reasonably chose to emphasize near-term (i.e., now-completed or ongoing) relatively modest surveys, or on future space-based missions such as SNAP, with little to no study of the impact of large synoptic surveys. Moreover, while these works included dust extinction effects in host galaxies, but because of their focus on Type Ia events, they did not study the possibility of a redshift evolution in extinction (Mannucci et al., 2007).

We build on the important studies of Dahlén & Fransson (1999), Gal-Yam et al. (2002); Gal-Yam & Maoz (2004), and Oda & Totani (2005) in several respects: (1) we explore the promise of synoptic surveys and forecast the very large numbers of supernovae they will find; (2) we focus on less-studied core-collapse events; (3) we incorporate the (pessimistic) possibility of strong dust evolution of Mannucci et al. (2007) which is a dominant obstacle to observing massive star death at high redshifts; (4) we present a strategy for *empirically* calibrating the obscuration properties across a broad range of redshift by studying the evolution of the supernova luminosity function; and (5) we study the unique opportunities that become available with the large supernova harvest of synoptic surveys; in particular, we show how the cosmic supernova rate can be recovered based on core-collapse counts, without assumption as to its functional form.

Our goal in this paper is to explore the impact synopic surveys will make on core-collapse supernova astrophysics and cosmology. We summarize key upcoming surveys in §2.3. In §2.4 we review expectations for the CSNR, core-collapse supernova observables, and the effect of cosmic dust and its evolution. We combine these inputs in §2.5 where we forecast the core-collapse supernova discovery potential for upcoming surveys. We quantify in detail the strong dependence of the supernova harvest on the survey limiting magnitude, which we find to be the key figure of merit for supernova studies. We discuss some of the supernova science payoff in §2.7, and conclude in §2.8 with some recommendations for synoptic surveys.

2.3 Synoptic Surveys

Current and future sky surveys build on the pioneering approach of the SDSS (York et al., 2000). Following SDSS, these surveys will produce high-quality digital photometric maps of large regions of the celestial sphere. The powerful innovation of the new surveys extends the original SDSS approach into the time domain. Each program will scan part of their survey domain frequently, with revisit periods of days and in some cases even hours, and maintain this systematic effort throughout the survey's multi-year operating lifespans. The result will be unprecedented catalogs of transient phenomena over timescales from hours to years. These surveys are thus ideal for supernova discovery and matched to supernova light curve evolution timescales; the result will be revolutionize our observational understanding of supernovae.

Table 2.1: Recent and Future Synoptic Sky Surveys

Survey Name	Scan Area $\Delta\Omega_{\rm scan}$ [deg^2]	SN Depth r-band $m_{\rm lim}^{\rm sn}$ [mag]	Scan Region	Expected Operation
SDSS-II	300	21.5	SDSS southern equatorial strip	2005–2008
DES	40	24.2	South Galactic Cap	2011–2016
Pan-STARRS	30000	23	$\sim 75\%$ of the Hawai'ian sky	2010–2020
LSST	20000	23–25	southern hemisphere	2014–2024

The science harvest in the time domain depends on both the depth of the scans and their breadth across the celestial sphere. These scale with collecting area A and sky coverage $\Omega_{\rm survey}$, respectively. Consequently, the figure of merit for scan power is the étendue $A\Omega_{\rm survey}$. Forthcoming projects are designed to maximize this quantity.

The viability of supernova discovery, typing, and followup by large-scale synoptic surveys has now been tested by the SDSS-II supernova search (Frieman et al., 2008). This program extended SDSS (York et al., 2000) into the time domain, scanning at a ~ 5 day cadence, identifying and typing supernova candidates from photometric data in real time, and following up with spectroscopic confirmation. This survey will serve as a testbed for the larger

future campaigns. It is thus very important and encouraging that SDSS-II has reported the discovery of 403 confirmed supernovae in the first two seasons of operation (Sako et al., 2008). The search algorithms and followup were focused on Type Ia events, for which light curves and spectra have been recovered over $0.05 < z < 0.35$; human input was used for supernova typing, but automated routines appear promising and will be essential for larger surveys. Follow-up spectroscopy (Zheng et al., 2008) yields accurate supernova and host-galaxy redshifts ($\sigma_z^{\rm sn} \approx 0.005$ and $\sigma_z^{\rm gal} \approx 0.0005$); host-galaxy contamination is found to be well-addressed by χ^2 fitting and a principal component analysis.

Table 2.1 lists several major current and future synoptic surveys, and gives the values or current estimates of their performance characteristics. The $m_{\rm lim}^{\rm sn}$ values are derived from the survey 5σ detections for single visit exposures, which have been corrected $1^{\rm mag}$ shallower as noted above. SDSS-II (Frieman et al., 2008) is recently completed, as discussed above; we adopt an r-band limiting magnitude of $21.5^{\rm mag}$ (J. Frieman, private communication). The Dark Energy Survey (DES; The Dark Energy Survey Collaboration, 2005) will push down to $m_{\rm lim}^{\rm sn} \sim 24.2^{\rm mag}$ in r-band; as we will see below, this will already enormously increase the supernova harvest. Finally, looking out farther into the next decade, Pan-STARRS (Jewitt, 2003; Tonry, 2003) and then LSST (The Large Synoptic Survey Telescope Collaboration, 2007; Tyson, 2002) will introduce a giant leap in both sky coverage and in depth. These ambitious projects represent a culmination of the synoptic survey approach, and we will make a particular effort to examine their potential for supernova science.

For our analysis, we will characterize each survey with four parameters

1. the survey supernova depth, i.e., single exposure limiting magnitude $m_{\rm lim}^{\rm sn}$ for supernova detection when used in scan mode; this is set by collecting area (and monitoring time)

2. the total survey scanning sky coverage, i.e., solid angle $\Delta\Omega_{\rm scan}$

3. the scan revisit time ("cadence") $\tau_{\rm visit}$

4. the total monitoring time $\Delta t_{\rm obs}$, which (for a single cadence) is proportional to the

total number $\Delta t_{\rm obs}/\tau_{\rm visit}$ of visits

For a fixed survey design and lifetime, these parameters are not independent, since exposure time comes at the expense of sky coverage and number of visits.

There are numerous challenges and complexities in the process of extracting supernovae and their redshifts from surveys (and for sorting out their types; see, e.g., Dahlén & Goobar, 2002; Poznanski et al., 2007; Kim & Miquel, 2007; Kunz et al., 2007; Blondin & Tonry, 2007; Wang, 2007). Tonry et al. (2003) gives thorough discussion of these issues with emphasis on Type Ia events; see also Dahlén & Fransson (1999), Gal-Yam & Maoz (2004) and Oda & Totani (2005), and the SDSS-II papers (Frieman et al., 2008; Sako et al., 2008; Zheng et al., 2008).

Our simple survey parameterization cannot capture all of these subtleties, nor do we intend to; rather, we hope our treatment will provide a rough illustration of the surveys' potential for core-collapse detection and science. Consequently, our parameter choices should be viewed as typical effective values, which may be different from (and weaker than) the raw survey specifications.

For example, supernova identification and typing requires knowledge of the light curve. Thus, one cannot only observe the supernova at peak brightness, but also follow it after (and ideally before). Tonry (2003) recommends following the supernova for least $\delta m = 1^{\rm mag}$ below peak brightness; we will adopt this value as well. Thus, the effective supernova detection depth is $m_{\rm lim}^{\rm sn} = m_{\rm max} - \delta m$, where $m_{\rm max}$ is the survey scan depth (i.e., depth for a single exposure).

Note also that some upcoming surveys (such as DES) will only repeatedly scan a fraction of the sky which they map; but only the *scanned* regions will host the discovery of supernovae and other transients. Also, some surveys (e.g., Pan-STARRS and LSST) envision multiple periodicities and associated limiting magnitudes; for simplicity we will choose conservative depths for the values given in Table 2.1, to be consistent with the advertised scanning sky coverage. Thus one should bear in mind that in our analysis we have chosen the minimal

parameterization one could use, which gives only a simplified and idealized sketch of the real surveys. Given this, and the ongoing planning of future survey characteristics, our forecasts for the surveys' supernova results should be understood as indicative of the order of magnitude expected, as opposed to high-precision predictions.

2.4 Core-Collapse Supernovae in a Cosmic Context

2.4.1 The Cosmic Core-Collapse Supernova Rate: Expectations

The total cosmic supernova rate (hereafter CSNR)

$$\mathcal{R}_{\rm SN}[z(t_{\rm em})] \equiv \frac{dN_{\rm SN}}{dV_{\rm com}\, dt_{\rm em}} \tag{2.1}$$

is the number of events per comoving volume per unit time $t_{\rm em}$ in the emission frame (i.e., cosmic time dilation effects in the observer's $z = 0$ frame are not included). The total rate, and the various differential rates below, can of course be specialized to distinguish different groups of supernovae classified by intrinsic type and/or dependence on local environment.

The present data on high-redshift core-collapse supernovae are too poor to construct an accurate CSNR. But the CSNR is intimately related to cosmic *star-formation* rate $\dot{\rho}_\star = dM_\star/dV_{\rm com}dt$ (Madau et al., 1998). The connection is

$$\mathcal{R}_{\rm SN} = \frac{X_{\rm SN}}{\langle m_{\rm SN}\rangle}\dot{\rho}_\star \tag{2.2}$$

where $X_{\rm SN}$ is the fraction, by mass, of stars which become supernovae, and $\langle m_{\rm SN}\rangle$ is the average supernova progenitor mass (see Supplement 2.9). A key point is that due to the short core-collapse progenitor lifetimes the two rates scale linearly, $\mathcal{R}_{\rm SN} \propto \dot{\rho}_\star$. The constant of proportionality depends on the initial mass function (IMF). If the IMF changes with time (or environment) this complicates the picture. In producing quantitative estimates we will follow most studies in assuming time-independent IMF. Thus the supernova/star-

formation rate proportionality is a constant fixed for all time, namely $\mathcal{R}_{\rm SN}/\dot{\rho}_\star = 0.00915\, M_\odot^{-1}$ (Supplement 2.9).

Uncertainties in the cosmic rates for both supernovae and star-formation remain considerable. As illustrated in detail by (Strigari et al., 2005), the cosmic star-formation rate is known to rise sharply towards redshift $z \sim 1$. In this low-to-moderate redshift regime, the *shape* of the rate versus redshift is fairly well known, but as emphasized by Hopkins & Beacom (2006) the *normalization* remains uncertain to within a factor ~ 2. At higher redshifts, the rate becomes even more uncertain, largely due to the paucity of data and also to uncertainties in our knowledge of the degree of dust obscuration. It is also worth noting that most studies to date directly or indirectly use massive stars as proxies for star formation. Consequently, the rate for cosmic massive star formation–and for cosmic supernovae–is less uncertain and IMF-dependent than the total rate.

To illustrate the effects of these uncertainties on the synoptic survey supernova harvest, we have adopted two possible CSNR forms. These appear in Figure 2.1, which shows the expected supernova rate assuming a perfect environment (i.e. no dust extinction, etc). The solid curve in Figure 2.1(a) is the CSNR derived from the cosmic star-formation rate of Cole et al. (2001) with parameters fitted by Hopkins & Beacom (2006) (hereafter the "benchmark" CSNR). This rate sharply rises to a peak at $z \sim 2.5$, followed a strong but less rapid declines out to high redshift. To investigate the impact of the falloff from the peak, we also show in the broken curve an alternate CSNR due to current observational data fitted by Botticella et al. (2008b) (hereafter the "alternative" CSNR). This rate also rise to redshift $z \sim 0.5$, though with a different slope; we somewhat arbitrarily set the alternative rate to a constant at $z > 0.5$ where the data are unclear; in any case we will find that few events from this high-redshift regime will be accessible to the all-sky surveys which are our focus.

Synoptic surveys will measure several observables associated with cosmic supernovae: their numbers and location, and some portion of their light curves in different bands. Spectroscopic redshifts of host galaxies can also be determined (when visible; see §2.7.5). Using

the number counts and redshift indicators, one can deduce an observed core-collapse rate, per unit redshift and per unit time and solid angle. This observed rate distribution directly encodes the CSNR via

$$\frac{dN_{SN}}{d\Omega dt_{\rm obs} dz} = \frac{dN_{SN}}{dV_{\rm com} dt_{\rm em}} \, \frac{dt_{\rm em}}{dt_{\rm obs}} \, \frac{dV_{\rm com}}{d\Omega dz} = \mathcal{R}_{\rm SN}(z) \frac{r_{\rm com}^2}{1+z} \frac{dr_{\rm com}}{dz} \tag{2.3}$$

where V_{com} is the comoving volume and $r_{com}(z)$ is the comoving distance out to redshift z. The $1+z$ factor corrects for time dilation via $dt_{\rm obs} = (1+z) dt_{\rm em}$.

Figure 2.1(b) shows the all-sky cumulative frequency of cosmic supernovae for an observer at $z = 0$, i.e.,

$$\frac{dN_{\rm SN}}{dt}(< z)_{\rm all-sky} = 4\pi \int_0^z \frac{dN_{SN}}{d\Omega dt_{\rm obs} dz} dz' = 4\pi \int_0^z \mathcal{R}_{\rm SN}(z') \, \frac{r_{\rm com}^2}{1+z'} \, \frac{dr_{\rm com}}{dz'} \, dz' \tag{2.4}$$

These curves give the total rate of observed cosmic supernova explosions out to redshift z for an idealized observer monitoring the entire sky out to unlimited depth and without any dust obscuration anywhere along the line of sight.

All of these idealizations will fail, some of them drastically, for real observational programs. Nevertheless, one cannot help but be tantalized by the enormous explosion frequencies indicated in Figure 2.1(b). With our benchmark CSNR, out to redshift $z = 1$, something like ~ 1 supernova explodes *per second* somewhere in the sky. Out to redshift $z = 2$, this rate increases to ~ 6 events/sec. Clearly, even with a small detection efficiency, synoptic surveys are poised to discover core-collapse supernovae in numbers far exceeding all supernovae in recorded history to date.

For numerical results in Figure 2.1 and throughout this paper, we adopt a flat cosmology with $\Omega_{\rm m} = 0.3$ and $\Omega_\Lambda = 0.7$. For the Hubble constant we adopt the value $H_0 = 71 \ {\rm km\,s^{-1}\,Mpc^{-1}}$, i.e., $h = 0.71$ where $H_0 = 100 \ h \ {\rm km\,s^{-1}\,Mpc^{-1}}$. These values are consistent with recent determinations using WMAP and large-scale structure (Spergel et al., 2007).

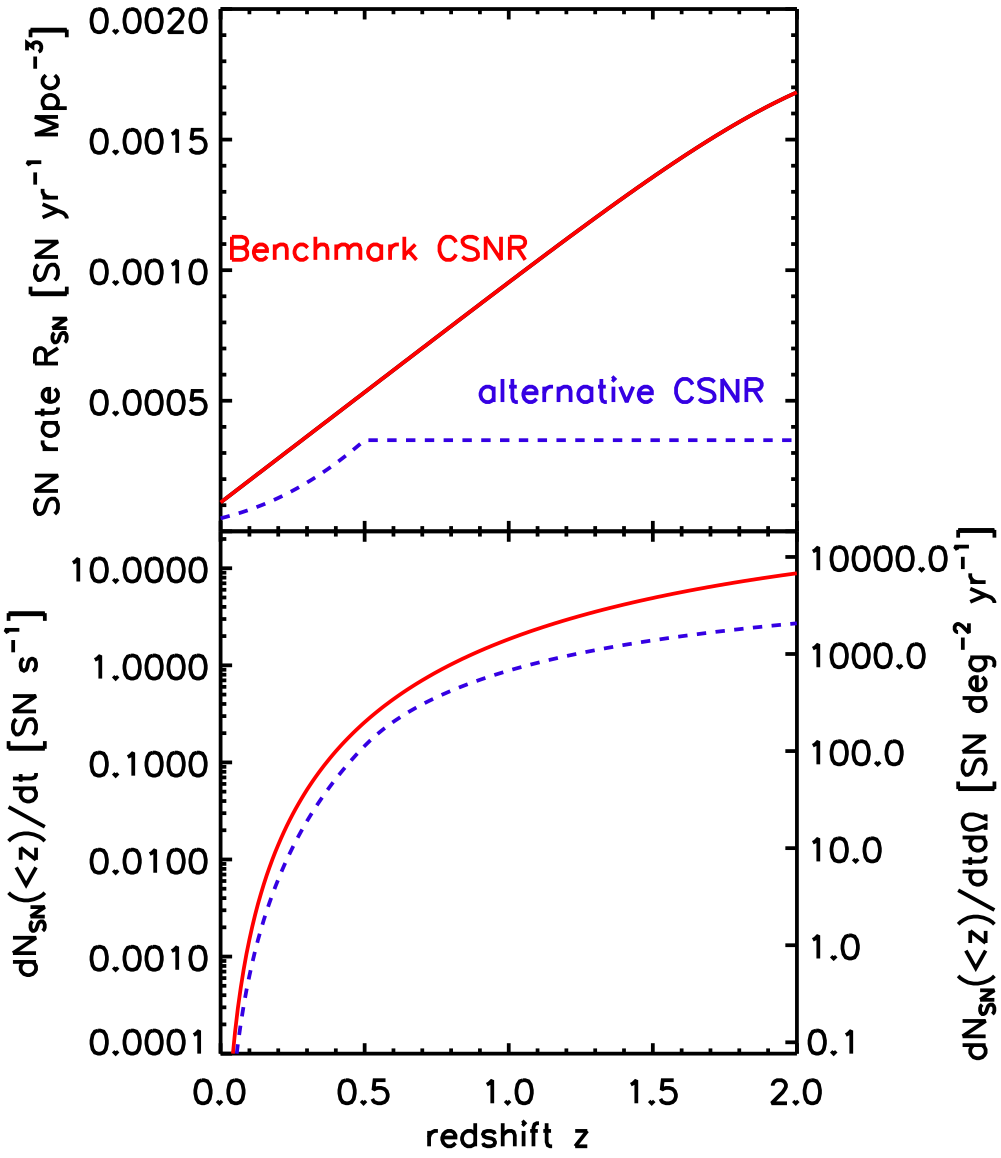

Figure 2.1: (a) *Top panel:* Possible cosmic core-collapse supernova rates as a function of redshift. The solid curve is the result calculated based on the Cole et al. (2001) cosmic star-formation rate; the broken curve is based on current supernova data (Botticella et al., 2008b); see Supplement 2.9. (b) *Bottom panel:* The idealized, all-sky cumulative rate of all supernovae observed over redshift 0 to z, for an observer with no faintness limit and with no dust extinction anywhere along the line of sight.

2.4.2 The Effect of Dust Obscuration

The enormous inventory of cosmic supernovae is, unfortunately, not fully observable even for arbitrarily deep surveys. In a realistic environment there are several factors that will hide the supernovae from us; dust extinction is one of the most important, and probably the most uncertain. Core-collapse supernovae mostly explode within regions of vigorous star formation which are thus likely to be dusty environments. Consequently, we expect that some core-collapse supernovae will be obscured to the point where they are not detected in synoptic surveys. The fraction of supernovae lost to dust obscuration, and particularly the possible redshift dependence of this extinction, represents a crucial systematic error which must be addressed before one can use survey data to infer information about supernova populations and their cosmic rates.

For the purposes of our present estimates of survey supernova yields, we follow the approach of Mannucci et al. (2007). These authors characterize losses due to dust extinction and/or reddening in the host galaxies via a fraction $\alpha_{\rm dust}(z)$ of undetected events at each redshift. This fraction could in principle differ for the various core-collapse types; for the present treatment we will assume it is the same for all such events. As core-collapse statistics become available from surveys, this issue can and should be revisited; more on this below. and in §2.6. The resulting fraction of *detected* supernovae is thus the complement $f_{\rm dust}(z) = 1 - \alpha_{\rm dust}(z)$, which measures the reduced supernova detection efficiency in the presence of dust. Expressed as an effective extinction A for the supernova population at z, we have $A_{\rm eff}(z) = -1.086 \ln f_{\rm dust}$.

Mannucci et al. (2007) estimate the fraction of missing supernovae by comparing the observed detections in the optical with those in radio and near-IR. They conclude that dust evolution is very strong; this becomes a dominant limitation to the discovery of core-collapse events at high redshift. In the local universe, Mannucci et al. (2007) find that the vast majority of the events occurring in massive starbursts (luminous infrared galaxies) are missed. Because these galaxies harbor only a small fraction of the local supernova

population, the overall optically missing fraction at $z = 0$ is estimated to be rather modest: $\alpha_{\rm dust} = 5 - 10\%$. If, however, high-redshift star formation occurs in starburst environments (i.e., luminous and ultra-luminous galaxies, which are highly extincted; see e.g. Smail et al., 1997; Hughes et al., 1998; Pérez-González et al., 2003; Le Floc'h et al., 2005; Choi et al., 2006) then the fraction of missing events rises sharply with redshift. Multiwavelength observations of light from pre-supernova massive stars also supports the idea of increasing dust obscuration at high redshift. Adelberger & Steidel (2000) find that ultraviolet light from massive stars in $z \sim 3$ galaxies is mostly reprocessed by dust into thermal submillimeter emission, so that the observable galaxy luminosities have $L_{\rm sub-mm}/L_{\rm UV} \sim 1 - 100$.

Mannucci et al. (2007) estimate the portion of supernovae which will be "catastrophic losses" to severe extinction, and propose that the missing fraction can be described by a linear relation $\alpha_{\rm dust}(z) = 0.05 + 0.28z$ for the core-collapse supernovae for redshift z<2. Thus, the fraction of the supernovae which remain optically detectable is $f_{\rm dust}(z) = 1 - \alpha_{\rm dust}(z) = 0.95 - 0.28z$ for $z < 2$. At higher redshift, Chen et al. (2007) and Gnedin et al. (2008) argue that $f_{\rm dust}$ is small; they find limits consistent with $f_{\rm dust} = 0.02$ for these redshifts.

We will smoothly match these two estimates, and adopt a fraction of the supernovae which can be detected after dust extinction of

$$f_{\rm dust}(z) = \begin{cases} 0.95 - 0.28z \ , & z < 3.3 \\ 0.02 \ , & z \geq 3.3 \end{cases} \tag{2.5}$$

For these values of $f_{\rm dust}$, the effective extinction varies from $A_{\rm eff} = 0.056^{\rm mag}$ at $z = 0$ to $A_{\rm eff} = 4.25^{\rm mag}$ at $z \geq 3.3$. In practice, we will find that cosmological dimming of supernovae beyond $z \sim 1$ is itself so large that surveys up to and including LSST will see relatively few events, so that the details of the adopted dust model in this regime will not affect our conclusions.

The strong redshift evolution of dust obscuration in the empirical Mannucci et al. (2007) model deserves comment. From a physical point of view, the rise in dust losses $\alpha(z)$ towards

high redshift implies that at earlier times, the birth environments of supernovae are significantly more enshrouded than those now. This interesting result itself deserves a deeper elucidation, one which will likely be easier to formulate and test in the presence of survey supernova data. From more practical point of view, our adoption of a model wherein dust losses grow rapidly with z should yield conservative (or at least not optimistic) predictions for the supernova harvest at large redshifts. That is, if it turns out that host galaxy effects do not change rapidly with cosmic time so that the efficiency of supernova detection remains close to the high local value, then our rate predictions at $z \sim 1$ would be boosted by a factor of ~ 1.5.

Note also that $f_{\rm dust}$ as Mannucci et al. (2007) and we have defined it to characterize the observable portion of the *ensemble* of supernovae at a particular redshift. Implicitly, *individual* supernovae are treated as either detectable or not, i.e., dust effects are considered negligible or total; our calculation treats total, catastrophic losses of supernovae using this $f_{\rm dust}$ formalism. We separately include the effect of partial extinction due to dust, where the apparent magnitude of supernova is reduced but still visible, as discussed in the next section. Of course in reality, all supernovae will experience some level of extinction in their host galaxies, with the *distribution* of host-galaxy extinctions changing with redshift. A more detailed study of dust effects on supernovae (and uses of supernovae to quantify and calibrate these effects) would be of interest for further investigation; see discussion in §2.6.

2.4.3 Supernova Observability at Cosmic Distances

2.4.3.1 The Supernova Luminosity Function

Locally, observations of core-collapse supernovae reveal diverse light curves with a wide range in peak luminosity and very different evolution after maximum brightness. The vast majority of supernovae discovered by synoptic surveys will lie at cosmological distances, and thus will be detectable mostly near their maximum luminosity. Thus we will focus on the observed distribution of peak brightness, and the timescales on which supernovae sustain it.

The distribution of peak absolute magnitude $M_{\rm peak}$ is given by the supernova luminosity function $\phi_{\rm snlf,x} = \phi_{\rm snlf,x}(M_{\rm peak}; z)$ which may have a redshift dependence; we choose a normalization such that at any z, $\int \phi_{\rm snlf,x}(M; z)\ dM = 1$, with this, we may write the cosmic supernova rate per absolute peak magnitude as

$$\frac{dN_{\rm SN}}{dV_{\rm com}\, dt_{\rm em}\, dM_{\rm peak}} \equiv \mathcal{R}_{\rm SN}(z)\ \phi_{\rm snlf,x}(M_{\rm peak}) \tag{2.6}$$

where here and throughout the possible redshift dependence of the luminosity function is understood.

Richardson et al. (2002) find the best-fit formulae for the supernova peak luminosity functions in B-band for different types of supernovae based on their tabulation of 279 supernovae of all types, for which absolute magnitudes were available at peak brightness. Of these, there were 168 events of all core-collapse types: II-P,L,n and I-ab. For each type, Richardson et al. (2002) fit the observed B-band absolute magnitude distributions with gaussian profiles, in some cases including two profiles where the data suggested "bright" and "dim" subclasses. Their results provide the basis for the luminosity functions used in this paper.

Note that we use the *observed* distributions rather than intrinsic, dust-corrected versions. Thus we automatically include the mean extinctions (ranging from $A \sim 0.1^{\rm mag} - 0.3^{\rm mag}$ for different types) found at low redshift. The reddening effect due to dust (ranging from $E \sim 0.02^{\rm mag} - 0.26^{\rm mag}$ across different bands and redshifts) is also added, based on the information given by Kim & Lee (2007). As noted in the previous section, catastrophic losses of supernovae due to large extinction and its possible evolution at high redshift is treated separately via our $f_{\rm dust}$ parameter.

We adjust the Richardson et al. (2002) distributions in two ways. First, we converted from their Hubble constant of $h = 0.6$ ot our adopted value $h = 0.71$. More importantly, we assume that each gaussian is a good representation of the data around the peak, but we do not allow the wings to extend arbitrarily far. Instead, we cut off the distributions

at $|M - M_{\rm mean}| > 2.5\sigma$, where no data exist in the Richardson et al. (2002) sample. We introduce these cutoffs in order to avoid extrapolating to very rare, bright events which in a large survey could extend the redshift reach considerably. Below (§2.5.2) we discuss the effect of this cutoff and its effect on the predicted supernova redshift range.

2.4.3.2 Supernova Discovery in Magnitude-Limited Surveys

Surveys will discover supernovae and monitor lightcurves in one or more passbands Here we will adopt the SDSS *ugriz* photometric system, which uses AB magnitudes (Fukugita et al., 1996).

The light curve of any supernova will suffer redshifting and time dilation effects. For passband x we put

$$m_x - M_x = 5 \log \left(\frac{d_L(z)}{d_0} \right) + K_x(z) + A_x(z) \equiv \mu(z) + K_x(z) - 1.086 \ln f_{\rm dust} \qquad (2.7)$$

with d_L the luminosity distance and $\mu(z)$ is the usual distance modulus with $d_0 = 10$ pc. The dust extinction A is included via the factor $f_{\rm dust}$ (eq. 2.5). The K-correction accounts for redshifting of the supernova spectrum, and is discussed in Supplement 2.11.

As noted above, at each redshift the effect of dust will be to obscure some fraction of supernovae. The remaining unobscured events will have apparent x-filter magnitudes of $m_x = M_x + \mu(z) + K_x(z)$. The expected m_x *distribution* thus reflects the underlying distribution of absolute magnitudes M_x. Since the Richardson et al. (2002) supernova luminosity function we use is in the B-band, we need to find the corresponding B-band magnitude in order to find the right corresponding number of supernovae; this transformation to m_B is straightforward and is given by $m_x = m_B + \eta_{xB}$, where

$$\eta_{xB} = -2.5 \log \frac{\int_{x_i}^{x_f} F(\lambda) S_x(\lambda) d\lambda}{\int_{B_i}^{B_f} F(\lambda) S_B(\lambda) d\lambda} + \text{zeropoint correction} \qquad (2.8)$$

is a color index which translates between the x and B magnitudes in the rest frame, and

zeropoint correction is the correction for different zeropoint of the SDSS magnitude system and the Johnson magnitude system. For the spectral shapes $F(\lambda)$ we use the prescriptions of Dahlén & Fransson (1999) as described in Supplement 2.11.

The absolute x-band magnitude distribution of unobscured supernovae at redshift z is $\phi_{\rm snlf,x}[M_x - \eta_{xB}]$, where $\phi_{\rm snlf,x}$ is the luminosity function in B-band as tabulated by Richardson et al. (2002). Therefore the distribution of a certain type of supernova *apparent* magnitudes m_x in x-filter is $\phi_{\rm snlf,x}[m_x - \mu(z) - K_x(z) - \eta_{xB}]$, Thus the fraction of all (unobscured) supernovae at z which fall within the survey x-band magnitude limit $m^{\rm sn}_{\rm lim}$ is a sum over the luminosity functions for all core-collapse types:

$$\begin{aligned} f_{\rm maglim}(z) &= \sum_{\rm types} \frac{\int^{m^{\rm sn}_{\rm lim} x} \phi_{\rm snlf,x}[m_x - \mu(z) - K_x(z) - \eta_{xB}]\ dm}{\int \phi_{\rm snlf,x}(m)\ dm} \\ &= \sum_{\rm types} \frac{\int^{m^{\rm sn}_{\rm lim} - \mu(z) - K_x(z) - \eta_{xB}} \phi_{\rm snlf,x}(m')\ dm'}{\int \phi_{\rm snlf,x}(m)\ dm} \\ &\equiv f_{\rm snlf}[< M_{\rm lim}(z, m^{\rm sn}_{\rm lim})] \end{aligned}$$

which is the cumulative fraction of supernovae whose absolute magnitude is brighter than

$$M_{\rm lim}(z, m^{\rm sn}_{\rm lim}) = m^{\rm sn}_{\rm lim} - \mu(z) - K_x(z) - \eta_{xB} \tag{2.9}$$

To develop some intuition, suppose the supernova peak brightnesses lie in a range $M_{\rm peak} \in (M_{\rm bright}, M_{\rm dim})$, and ignore for now the effects of dust. Then for low redshifts such that the absolute magnitude limit $M_{\rm lim}$ from eq. (2.9) is fainter than $M_{\rm dim}$, we can expect to see *all* supernovae, and $f_{\rm maglim} = 1$. For these redshifts, we can study the entire supernova luminosity function and test whether it varies with redshift. On the opposite extreme, for high redshifts such that $M_{\rm lim}$ is dimmer than $M_{\rm bright}$ we can see *no* supernovae, so $f_{\rm maglim} = 0$; this then defines the survey redshift cutoff (for fixed $m^{\rm sn}_{\rm lim}$). Finally, for intermediate z such that $m^{\rm sn}_{\rm lim} - M_{\rm dim} < \mu(z) + K_x(z) + \eta_{xB} < m^{\rm sn}_{\rm lim} - M_{\rm bright}$, we have $0 < f_{\rm maglim} < 1$; over these redshifts the survey samples the bright end of the supernova luminosity function.

Both magnitude limit and dust extinction reduce the expected supernova detection, and do so independently of each other. Consequently, we can find the net supernova detection probability by simply taking the product of the individual factors:

$$f_{\rm detect}(z; m^{\rm sn}_{\rm lim}) = f_{\rm maglim}(z; m^{\rm sn}_{\rm lim})\ f_{\rm dust}(z) \tag{2.10}$$

Figure 2.2 shows the resulting detectable fraction of supernovae. The left panel shows the shape of $f_{\rm maglim}$ for the g and r bands. At redshifts close to zero, $f_{\rm maglim} \approx 1$ which means that almost all supernovae are detected in the local universe. And it approaching to zero at high redshift, which reflects the fact that no supernovae can be detected at high redshift because of the survey deepness. Note that g and r bands are competitive for $m^{\rm sn}_{\rm lim} \leq 24$, but for higher $m^{\rm sn}_{\rm lim}$, $f_{\rm maglim}$ in g-band drops a lot faster than those in r-band especially around z ~ 0.4, which is cause by the effect of K-correction. The figure also shows that for higher $m^{\rm sn}_{\rm lim}$, $f_{\rm maglim}$ decays less rapidly. The right panel shows $f_{\rm detect}$ for different $m^{\rm sn}_{\rm lim}$, using our adopted dust model (eq. 2.5). We see $f_{\rm detect}$ shows the same trend as $f_{\rm maglim}$ except the detectable fraction is reduced due to dust and we can no longer observe all supernovae even in the local universe. It is also clear to see that going to fainter $m^{\rm sn}_{\rm lim}$ significantly boosts the detectable fraction at high redshift. For $m^{\rm sn}_{\rm lim} = 23^{\rm mag}$, $f_{\rm detectable}$ is almost zero at redshift $z \sim 1$ for both g and r bands. But going to $m^{\rm sn}_{\rm lim} = 26^{\rm mag}$, $\sim 55\%$ of the supernovae at redshift $z \sim 1$ remain visible both the g and r bands.

This means that deeper surveys (and/or scanning modes in which smaller areas are scanned more deeply) will probe supernovae out to much higher redshifts. Deep survey modes will also probe a much wider regime of the supernova luminosity function and light curves over a broad range of cosmic epochs, thus testing for redshift evolution in supernova properties. The clear lesson is that the scan $m^{\rm sn}_{\rm lim}$ is critical in determining the quality and reach of the supernova science. In particular, we urge that scans strategies include modes which push $> 1^{\rm mag}$ deeper than the all-sky depth.

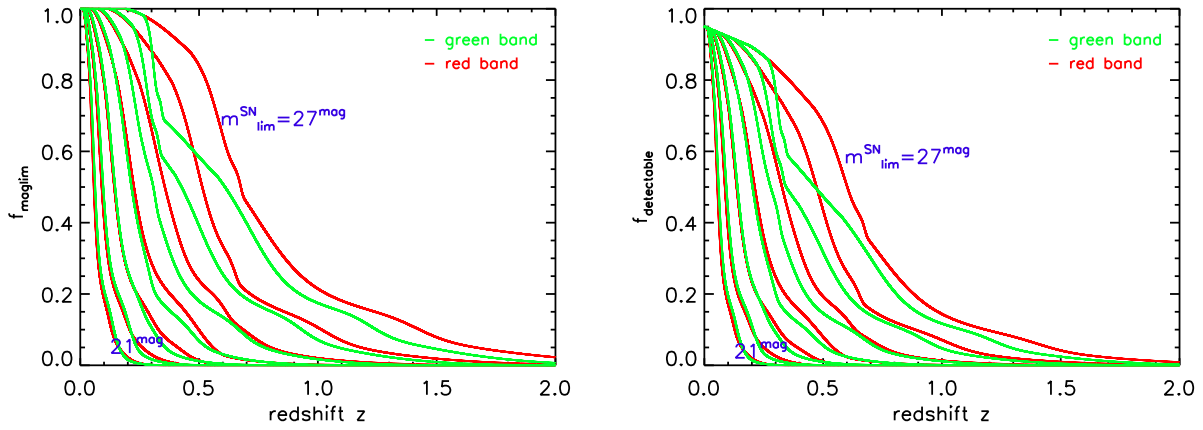

Figure 2.2: (a) The fraction of supernovae detected based on different survey deepness in g and r bands, with m^{sn}_{lim} ranging from 21^{mag} down to 27^{mag}; effects of dust obscuration are not included. (b) As in (a), but including the effects of dust obscuration strongly evolving with redshift as modeled by eq. (2.5).

2.4.3.3 Supernova Light Curves

The observed population of core-collapse supernovae shows a broad range of timescales and time histories in their decline from peak brightness (e.g., Doggett & Branch, 1985; Leibundgut & Suntzeff, 2003). The amplitude and time behavior of these curves encodes a wealth of information about the underlying physics of the supernovae as well as their interaction with the circumstellar and interstellar medium.

Empirically, light curves broadly fall into phenomenological categories, those whose magnitudes decline in a relatively steep, linear way (Type II-L) and those which linger near peak brightness with a relative plateau in magnitude (Type II-P). Patat et al. (1993) compiled 51 Type II light curves, and analysis in Patat et al. (1994) showed that plateau-type supernovae typically decline from peak brightness at rates which vary the range $(0.7^{mag} - 3.1^{mag})/100$ days, while linear-type events typically have $(3.9^{mag} - 5.7^{mag})/100$ days. Unfortunately, the lightcurves available at the time of these studies were poorly sampled near the peak itself, where the behavior is most critical for our purposes.

Fortunately, subsequent data, particularly using *Swift*, gives a clearer picture of the

early light curves for a few events. For plateau event SN 2005cs, data in Pastorello et al. (2006) show that $\sim$ 15 days after peak brightness, the supernova dimming was strongly depending on passband: $\Delta M_{15}(U) \simeq 1.8^{\rm mag}$, $\Delta M_{15}(B) \simeq 0.7^{\rm mag}$, $\Delta M_{15}(V) \simeq 0.18^{\rm mag}$, and $\Delta M_{15}(R) \sim 0.1^{\rm mag}$. Another Type II-P event, SN 2006bp, after $\sim$ 13 days declined by $\sim 1^{\rm mag}$ in U, but within errors was essentially constant in B and V (Dessart et al., 2008). For Type Ib, the recent event SN 2008D was seen from shock breakout (Modjaz et al., 2009); after dropping from this brief initial outburst, the flux increased for $\sim$ 15 days to a maximum. Afterwards, the brightness decline rates lengthen with wavelength, with a drop of $\Delta M \sim 1^{\rm mag}$ after $\sim$ 10 days in U-band, but after about 15 and 20 days in B and V respectively.

These multicolor data show that brightness decline in V and longer passbands comparable to if not slower than the typical range of $\Delta M_{15} \sim 1^{\rm mag} - 2^{\rm mag}$ found in Type Ia events (Phillips, 1993a). This implies that surveys timed for Type Ia discovery will automatically be well-suited and possibly even better-sampled for core-collapse events. In particular, we will find below that the r and also g passbands are the most promising for survey supernova detections. Thus, if cosmic supernovae follow the behavior of these local events, we expect that the light curves will remain within, e.g., $\Delta m \simeq 0.5^{\rm mag}$ of peak brightness (a factor 1.5 in flux) for a timescale of at least a week. In some cases this timescale will be longer, and possibly also with detections in the rising phase.

For synoptic surveys to detect core-collapse supernovae near their peak brightness, the cadence needs to be shorter than the (observer-frame) brightness decline time. Thus weekly revisits are sufficient for marginal detections, and cadences of $\sim 3-4$ days will often see the event three or more times. In the cases of plateau events, the supernova should remain near peak brightness for many such revisit times. Furthermore, due to cosmological time dilation effects, the observed brightness decline timescale $\tau_{\rm obs} = (1+z)\tau_{\rm rest}$ is increased by a factor of $1+z$, which extends the detection window and offers a greater opportunity to recover a well-sampled lightcurve. Also, we see that color evolution is not strong in V and R

bands. The UV and blue do fade more rapidly, and the supernova reddening depends on the type. For events where bluer rest-frame colors are available, this might be a useful means of photometrically determining supernova type.

2.5 The Cosmic Core-Collapse Supernova Rate: Forecasts for Synoptic Surveys

In this section we will work out general formalism for supernova observations by synoptic surveys. We then apply this formalism to specific current and proposed surveys

2.5.1 Connecting Cosmic Supernovae and Survey Observables

2.5.1.1 General Formalism

It is useful to define a differential supernova detection rate per unit redshift, solid angle, and apparent magnitude in x-band:

$$\frac{dN_{\rm SN,obs,x}}{dt_{\rm obs}\,dz\,d\Omega\,dm} = \mathcal{R}_{\rm SN}(z)\ \frac{r(z)^2}{1+z}\frac{dr}{dz}\ f_{\rm dust}(z)\ \phi_{\rm snlf,x}[m_x - \mu(z) - K_x(z) - \eta_{xB}] \qquad (2.11)$$

This expression adds the effects of supernova luminosity (cf eq. 2.6) and of dust obscuration (eq. 2.5) to the ideal rate of eq. (2.3). Throughout, we will for simplicity refer to the entire core-collapse supernova population, but the formalism could equally well distinguish the various core-collapse types, and compute the rates of each. An example of such a treatment is the Scannapieco et al. (2005) study of the rate and detectability of pair-instability supernovae.

The differential rate in eq. (2.11) relates the observables in a synoptic survey to underlying properties of cosmic supernovae. As such, a wealth of information can be recovered by a good statistical sample of supernovae over a redshift range: one probe different terms and their underlying physics. For example, at fixed z, the range of observed supernova magnitudes

in x-band m_x probes the supernova peak luminosity function $\phi_{\rm snlf,x}(M;z)$ at magnitudes $M_x = m_x - \mu(z) - K_x(z) - \eta_{xB}$. Comparing these results at different redshifts with local determinations can reveal any redshift- and/or environment-dependence in the core-collapse supernova luminosity function.

Another aspect of cosmic supernovae probed by synoptic surveys, and central focus of this paper, is the cosmic supernova rate. Whereas the supernova luminosity function can be determined from the distribution of supernova magnitudes at the *same* redshift, the cosmic supernova rate comes from the distribution of supernova *counts* across *different* redshifts. The observed differential rate for supernovae of all magnitudes in the x-band is

$$\Gamma_{\rm SN,obs,x}(z) \equiv \frac{dN_{\rm SN,obs,x}}{dt_{\rm obs}\,dz\,d\Omega} = \int^{m^{\rm sn}_{\rm lim}} dm\ \frac{dN_{\rm SN,obs,x}}{dt_{\rm obs}\,dz\,d\Omega\,dm} = \mathcal{R}_{\rm SN}(z)\ f_{\rm detect,x}(z;m^{\rm sn}_{\rm lim})\ \frac{r(z)^2}{1+z}\ \frac{dr}{dz} \tag{2.12}$$

Note that this is the idealized rate of eq. (2.3) reduced by the detection in x-band $f_{\rm detect,x}$.

One can get a sense of the orders of magnitude in play via the definition of a dimensionful scale factor

$$\begin{aligned}
\Gamma_{\rm SN,0} &= \mathcal{R}_{\rm SN}(0)\ d_H^3 = 7.2\times10^6\ \text{events yr}^{-1}\ \text{sr}^{-1}\left(\frac{\mathcal{R}_{\rm SN}(0)}{10^{-4}\ \text{yr}^{-1}\,\text{Mpc}^{-3}}\right) && (2.13)\\
&= 0.22\ \text{events sec}^{-1}\ \text{sr}^{-1}\left(\frac{\mathcal{R}_{\rm SN}(0)}{10^{-4}\ \text{yr}^{-1}\,\text{Mpc}^{-3}}\right) && (2.14)\\
&= 2.2\times10^3\ \text{events yr}^{-1}\ \text{deg}^{-2}\left(\frac{\mathcal{R}_{\rm SN}(0)}{10^{-4}\ \text{yr}^{-1}\,\text{Mpc}^{-3}}\right) && (2.15)
\end{aligned}$$

We may then define a dimensionless distance $u(z) = r(z)/d_H$, with $d_H = c/H_0$ the Hubble length, and write

$$\Gamma_{\rm SN,obs}(z) = \Gamma_{\rm SN,0}\ \frac{\mathcal{R}_{\rm SN}(z)}{\mathcal{R}_{\rm SN}(0)}\ \frac{u(z)^2}{1+z}\frac{du}{dz}\ f_{\rm detect,x}(z,m^{\rm sn}_{\rm lim}) \tag{2.16}$$

Figure 2.3 plots the observed supernova rate $\Gamma_{\rm SN,obs}$ per solid angle in r-band. For comparison, we show the idealized cases of $m^{\rm sn}_{\rm lim} = \infty$ and $f_{\rm dust} = 0$, as well as realistic cases

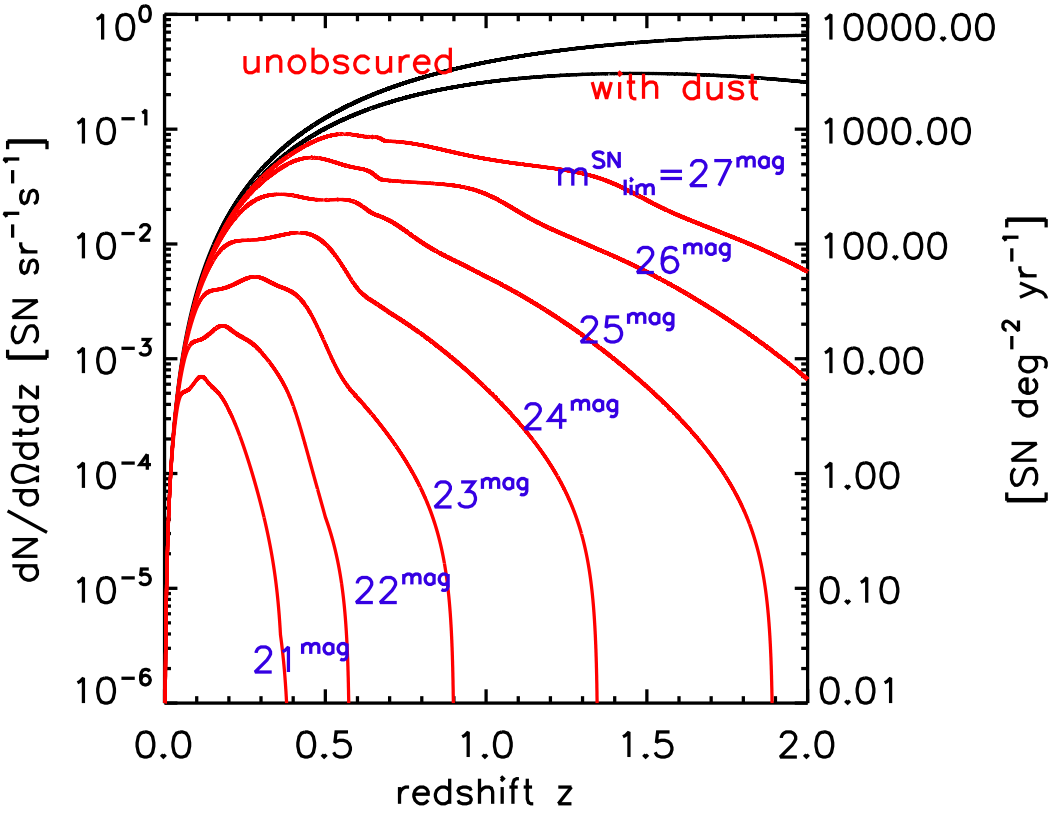

Figure 2.3: The cosmic supernova detection rate in r-band, expressed in number of events per solid angle per time, shown a function of redshift. The curve labeled "unobscured" ignores both effects of dust extinction or the flux limit of the survey (i.e., $f_{\rm detect} = 1$). The curve labeled "with dust" includes dust extinction only, but with $m^{\rm sn}_{\rm lim} = \infty$. The remaining curves are for surveys with $m^{\rm sn}_{\rm lim}$ as labeled, and include dust extinction. Note that the vertical axis is shown both in units of events per second per steradian (left scale) and events per year per square degrees (right scale).

in the presence of dust and with different $m^{\rm sn}_{\rm lim}$. The *amplitudes* of the curves in Figure 2.3 confirm the large numbers of events expected from eq. (2.13).

The *shapes* of the curves can also be readily understood. At low redshifts, the surveys see most of the supernovae that occur–i.e., the entire luminosity function is sampled; cf Figure 2.2. Hence at small z, the supernova sample is simply limited by the cosmic volume within z: $\Gamma \propto dV_{\rm com}/dz \sim r^2_{\rm com}\, dr_{\rm com}/dz \sim z^2$ Thus the detection rate initially rises quadratically with z; this volume effect is essentially independent of survey magnitude limit, as we see by

the overlap of the curves in this regime.

In the high redshift limit, several effects act to suppress supernova detectability. At $z > 1$, $r_{\rm com}$ rapidly saturates at the comoving horizon scale, and nearly all observable cosmic volume is sampled; in this regime, the volume factor *decreases* as $dV_{\rm com}/dz \sim dr_{\rm com}/dz \sim 1/H(z) \sim (1+z)^{-3/2}$. In addition, time dilation effects become large and add another factor of $(1+z)^{-1}$. For these reasons, even the idealized (unobscured, $m^{\rm sn}_{\rm lim} = \infty$) rate drops. Moreover, in some models (such as that of Cole et al., 2001), the CSNR itself is intrinsically expected to drop after a peak, perhaps somewhere in the range $z \sim 1-3$. On top of this, the effects of dust obscuration become large at $z \gtrsim 1$ and removes further supernovae in this range. Finally, a finite survey magnitude limit truncates still more events at high z.

The combination of the low-redshift rise and high-redshift drop acts to create a peak in supernova detectability. The position of the peak is sensitive to the CSNR itself, and the details of dust obscuration. But the peak position and amplitude are also both very sensitive to the survey magnitude limit; both rise sharply as survey depth $m^{\rm sn}_{\rm lim}$ increases. This illustrates a key conclusion which will be manifest in several other ways below: *for discovery of core-collapse supernovae at high redshifts, the most important aspect of a synoptic survey is its limiting magnitude; investment in deep scan modes ($m^{\rm sn}_{\rm lim} > 24$ mag) will reap substantial rewards.*

Figure 2.4 shows the same supernova rate redshift distribution as in Fig. 2.3, but for the five *ugriz* passbands with SDSS filters and efficiencies. For each band we fix $m^{\rm sn}_{\rm lim} = 24^{\rm mag}$. We see that the discovery rate is the highest in r for essentially all redshifts, with g-band counts very nearly the same except around the peak at $0.2 \lesssim z \lesssim 0.6$. The relative smallness of the counts in other bands traces back predominantly to low detector efficiency in i and z, and redshifting effects for u. The upshot is that for synoptic surveys, r and g bands are (in that order) clearly the most promising for supernova search.

We have thus far shown the *total* supernova rate redshift distribution, summed over all core-collapse subtypes. Figure 2.5 illustrates how the different subtypes contribute to the

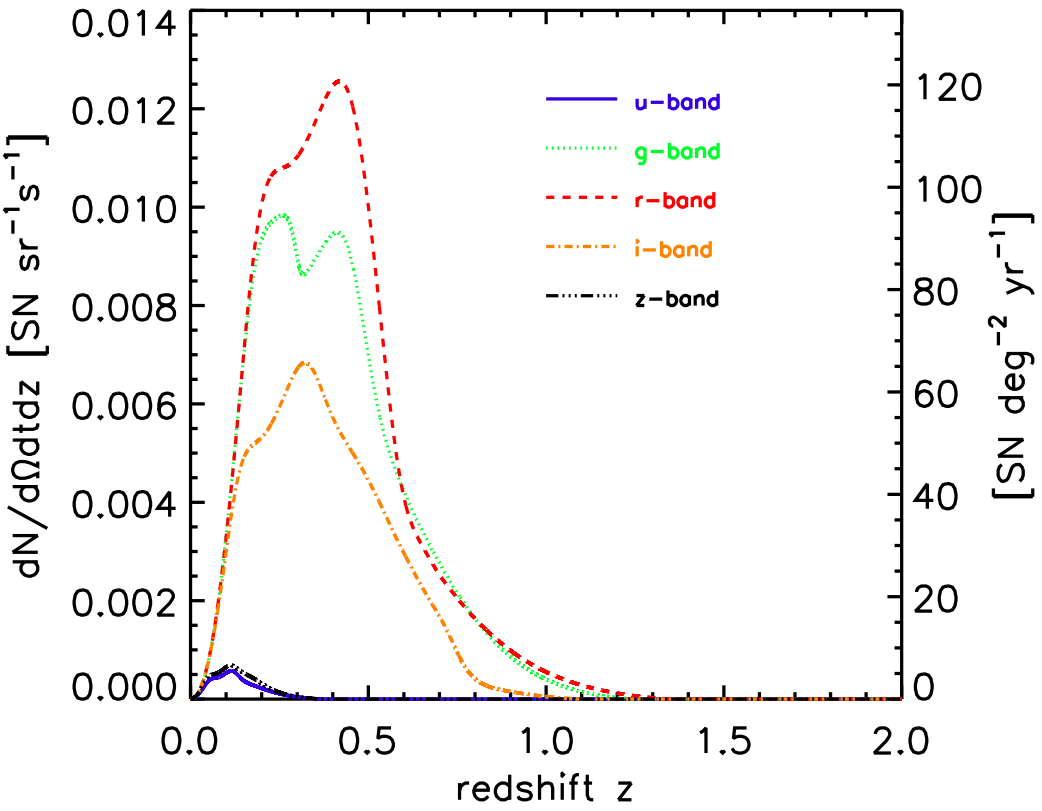

Figure 2.4: Number of supernovae per year per solid angle per redshift with $m_{\rm lim}^{\rm sn} = 24^{\rm mag}$ in different bands.

aggregate. Here we fix $m_{\rm lim}^{\rm sn} = 24^{\rm mag}$ and show results for the r and g bands. It is worth recalling that we have assumed the low-redshift Richardson et al. (2002) determination of luminosity functions and type distributions holds for all redshifts. In this scenario, we see that in both bands, Type IIn events give the largest contribution to the signal at $z \gtrsim 0.3$, and totally dominate the counts at $z \gtrsim 0.6$. This is expected, since it is the intrinsically brightest core-collapse subtype. Thus the redshift reach of supernova discovery (and associated results such as the CSNR) in synoptic surveys will depend sensitively on nature Type IIn events at $z \gtrsim 0.6$. It will thus be crucial to determine whether these events show evolution in their luminosity function and/or relative fraction of core-collapse events with redshift (e.g., via metallicity effects). Also, it is worth noting that the Richardson et al. (2002) luminosity

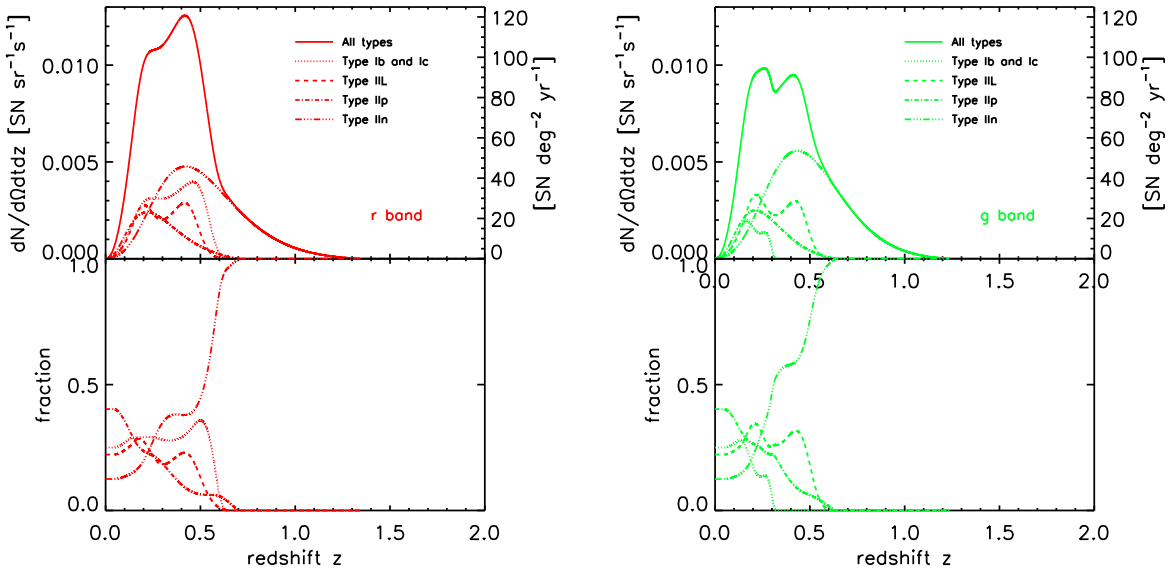

Figure 2.5: Supernova rate redshift distribution, as in Fig. 2.4, broken down by core-collapse type. Results shown for (a) r band, and (b) g band; both have $m_{\rm lim}^{\rm sn} = 24^{\rm mag}$. *Top panels:* detection rate distribution per subtype; *bottom panels:* fraction of each subtype rate relative to the total. We see that intrinsically bright Type IIn events dominate the counts at high redshift ($z \gtrsim 0.5$) and thus determine the redshift reach for core-collapse discovery.

function we have used is relatively narrow. As noted recently by Cooke (2008), some Type IIn events have now been observed with luminosities far above the range of values we consider. If so, then the redshift range of synoptic surveys could thus extend significantly further than in our estimates.

Figure 2.5 further predicts that the other core-collapse types should have observably distinct redshift ranges in different bands, again assuming no evolution in luminosity function or type distribution. The upper panels of Fig. 2.5 show the individual subtype detection rates, as well as their sum. Type II-L events have similar behavior in both r and g bands, peaking at $z \sim 0.45$ then rapidly dropping off. Although Type II-P events are the largest core-collapse subtype in the Richardson et al. (2002) sample, they are also by far the intrinsically dimmest, $\sim 1^{\rm mag} - 3^{\rm mag}$ fainter than the other types. We thus find that Type II-P have a smaller redshift range than Type II-L and IIn events. The counts and redshift range of Type Ib and Ic events are notably different in the two passbands. This traces to the effects of UV

lineblanketing which removes blue flux; thus at high redshift the K-correction first shifts photons out of the g band, with the r-band signal surviving until higher redshift. Note also that the "bright" and "normal" Type Ib and Ic events lead to the double-peaked structure in their redshift distribution.

The lower panels of Fig. 2.5 shows our forecast for subtype fraction detected as a function of redshift, i.e., the ratio of each subtype rate to the total. At $z = 0$, the subtype fractions go to the observed local values we have adopted from Richardson et al. (2002), as required by our model design. For $z \sim 0 - 0.2$, we see that all subtypes make significant contributions tot the total, and thus for this redshift range, the sharp rise in the total detection rate (top panel) is due to contributions from all subtypes. The features around the maximum in the total rate ($z \sim 0.2 - 0.5$) are due to the interplay between the rise of the Type IIn events and the successive dropout of the other types. Finally, we see that for $z \sim 0.5$, Type IIn events essentially completely set the total rate.

Because the highest-redshift detections will be dominated by Type IIn events, the nature of and evolution of this subtype will play a crucial role in setting the high-redshift impact of surveys for core-collapse events, as also pointed out by Cooke (2008). As we have noted, intrinsic evolution of the Type IIn fraction of core-collapse events would directly change–and be written into–the high-redshift signal. But at present, the uncertainties are very large even when evolution issues are set aside. Namely, published data are as yet very uncertain concerning the local, $z \approx 0$ fraction of core-collapse events which explode as Type IIn. Our forecasts use the Richardson et al. (2002) sample which finds 9 Type IIn events out of 72 core-collapse events, for a fraction of 12.5%. However, this *discovery* fraction are very uncertain. For example, the prior work of Dahlén & Fransson (1999) compiled their own core-collapse discovery statistics, and adopted a Type IIn event fraction of 2%, while noting that Cappellaro et al. (1997) recommend a Type IIn fraction of $\sim 2 - 5\%$. Because the high-redshift core-collapse detections will be dominated by Type IIn events, if these values better reflect the intrinsic fraction, this would dramatically reduce our predicted detection

rates for $z \gtrsim 0.5$ by factors of $\sim 2-6$, and thus also reduce the maximum redshift at which core-collapse events can be seen in surveys. Clearly, the small numbers available when all of these compilations were made render the Type IIn fraction estimates uncertain; indeed, to a lesser extent the estimates for the more common core-collapse types suffer similar problems.

In light of the uncertainties in the Richardson et al. (2002) and prior compilations, it is worth noting that considerably more supernova data already exists. A detailed, systematic study of the luminosity function and intrinsic subtype fractions of local events would be of the utmost value for forecasts of the sort we have presented. Moreover, precise and accurate local measurements will play an essential role as a basis of comparison for the future medium- to high-redshift data, in order to empirically probe for evolution within and among the core-collapse subtypes.

2.5.1.2 Unveiling the Cosmic Core-Collapse Supernova Rates

As noted above, synoptic surveys will revolutionize our understanding of the CSNR because they will directly determine the rate through *counting*. We now are in a position to determine the supernova counts for realistic (magnitude-limited, dust-obscured) surveys. Using these, we can demonstrate how the CSNR can be extracted. We can further determine its statistical uncertainty and the impact of survey depth and sky coverage.

Consider a survey with scan area $\Delta\Omega_{\rm scan}$ and limiting magnitude $m^{\rm sn}_{\rm lim}$, the total number of supernovae seen in x-band in time $\Delta t_{\rm obs}$, in a small redshift bins of width $\Delta z = z_f - z_i \ll 1$ centered around $z = (z_f + z_i)/2$ is

$$\Delta N_{\rm SN,obs,x} = \Delta\Omega_{\rm scan}\Delta t_{\rm obs}\ \Delta z\ \Gamma_{\rm SN,obs,x}(z) \tag{2.17}$$

$$= \Delta\Omega_{\rm scan}\Delta t_{\rm obs}\ \Delta z\ \Gamma_{\rm SN,0,x}\ \frac{\mathcal{R}_{\rm SN}(z)}{\mathcal{R}_{\rm SN}(0)}\ \frac{u(z)^2}{1+z}\frac{du}{dz}\ f_{\rm detect,x}(z; m^{\rm sn}_{\rm lim}) \tag{2.18}$$

Thus we see that the cosmic supernova rate is directly encoded in our binned data. This

means we can use the binned data to extract the supernova rate:

$$\mathcal{R}_{\rm SN}(z) = \frac{1}{\Delta\Omega_{\rm scan}}\ \frac{1}{\Delta z}\ \frac{1+z}{u(z)^2}\frac{dz}{du}\ f_{\rm detect,x}(z; m^{\rm sn}_{\rm lim})^{-1}\ \frac{\Delta N_{\rm SN,obs,x}}{d_H^3\ \Delta t_{\rm obs,x}} \tag{2.19}$$

this result is a major goal of this paper. Physically, we see that as we accumulate supernovae, i.e., as $\Delta N_{\rm SN,obs}$ fills out the redshift range accessible to the survey, we obtain an ever better measure of the SN rate.

We can also compute the statistical uncertainty in the CSNR derived from counts in surveys. The statistical error arises from the counting statistics in the supernova number. Expressing this as a fractional error, we have

$$\frac{\sigma(\mathcal{R}_{\rm SN})}{\mathcal{R}_{\rm SN}} = \frac{\sigma(\Delta N_{\rm SN,obs,x})}{\Delta N_{\rm SN,obs,x}} \approx \frac{1}{\sqrt{\Delta N_{\rm SN,obs,x}}} \tag{2.20}$$

But from eq. (2.18), we see that $\Delta N_{\rm SN,obs,x}$ scales linearly with the product of detected fraction and survey sky coverage, as well as monitoring time and redshift bin width. Thus we find the CSNR statistical error should scale as

$$\frac{\sigma(\mathcal{R}_{\rm SN})}{\mathcal{R}_{\rm SN}} = \frac{1}{\sqrt{\Delta\Omega_{\rm scan}\Delta t_{\rm obs}\ \Delta z\ \Gamma_{\rm SN,obs,x}(z)}} \tag{2.21}$$

$$\propto \frac{1}{\sqrt{f_{\rm detect,x}(z; m^{\rm sn}_{\rm lim})\ \Delta t_{\rm obs}\ \Delta\Omega_{\rm scan}}} \tag{2.22}$$

Consequently, for a fixed redshift bin size Δz, the CSNR accuracy grows with the product $\Delta t_{\rm obs}\,\Delta\Omega_{\rm scan}$, and implicitly with $m^{\rm sn}_{\rm lim}$ via the detection fraction. Thus survey sky coverage and magnitude limit (i.e., collecting area) enter together, and we see the payoff of a large survey étendue.

Thus, we can find the survey properties needed to achieve any desired precision in the CSNR at some redshift z. For a fixed $m^{\rm sn}_{\rm lim}$ and thus $f_{\rm detect}$, monitoring time and sky coverage enter together as the product $\Delta t_{\rm obs}\ \Delta\Omega_{\rm scan}$. Figure 2.6 shows the needed monitoring time $\Delta t_{\rm obs}\ \Delta\Omega_{\rm scan}$ to measure the CSNR to a statistical precisions of $\sigma_{\rm stat}(\mathcal{R}_{\rm SN})/\mathcal{R}_{\rm SN} = 10\%$, and

Table 2.2: Survey Discovery Potential for Core-Collapse Supernovae in r-band

Survey Name	Expected Total 1-year SNII Detections	SNII Redshift Range
SDSS-II*	1.70×10^2	$0.03 < z < 0.37$
DES	2.74×10^3	$0.06 < z < 1.20$
Pan-STARRS	5.14×10^5	$0.01 < z < 0.89$
LSST	3.43×10^5	$0.01 < z < 0.89$

Note: *Reflects SDSS-II supernova scan season of 3 months per calendar year.

with different survey $m_{\rm lim}^{\rm sn}$ in r-band. In both panels we choose $\Delta z = 0.1$ for the redshift bin size. The two panels show our baseline and alternative CSFR. From these figures we can see that these two different adopted CSNR behaviors both yield very similar results for the survey CSNR detectability.

Again the shapes of the curves can be understood. As shown in eq. (2.21), that the precision at each bin scales inversely with the supernova differential redshift distribution as $\Gamma_{\rm obs}(z)^{-1/2}$. Not surprisingly therefore, the least monitoring is needed to measure the CSNR for z near the peak in the redshift distribution On the other hand, redshifts in the high- and low-redshift tails of $\Gamma_{\rm SN,obs}$ require increasing monitoring, eventually to the point of unfeasibility.

Figure 2.6 makes clear that increasing $m_{\rm lim}^{\rm sn}$ brings a huge payoff reducing the needed monitoring $\Delta t\ \Delta\Omega_{\rm scan}$. To achieve a $\sigma(\mathcal{R}_{\rm SN})/\mathcal{R}_{\rm SN} < 10\%$ precision at redshift $z = 1$, the monitoring becomes about 1000 times smaller in r-band if we increase $m_{\rm lim}^{\rm sn}$ from $23^{\rm mag}$ to $26^{\rm mag}$. Clearly, for any survey, increasing $m_{\rm lim}^{\rm sn}$ will drastically shorten the observing time needed for the high redshift supernovae. In practice, given fixed survey lifetimes, this means that $m_{\rm lim}^{\rm sn}$ sets the maximum redshift reach over which the survey may determine the CSNR (via eq. 2.9).

2.5.2 Forecasts for Synoptic Surveys

For a given survey with a fixed scanning sky coverage $\Delta\Omega_{\rm scan}$, we can determine the total number of supernovae expected in each redshift bin. We can also forecast the accuracy of the resulting survey determination of the CSNR. Namely, we can turn our sky coverage–monitoring time result (Figure 2.6) into a specific prediction for the needed time to determine the CSNR to a given precision. In practice, this amounts to a determination of the redshift range over which different surveys can measure the CSNR. Our detailed predictions appear

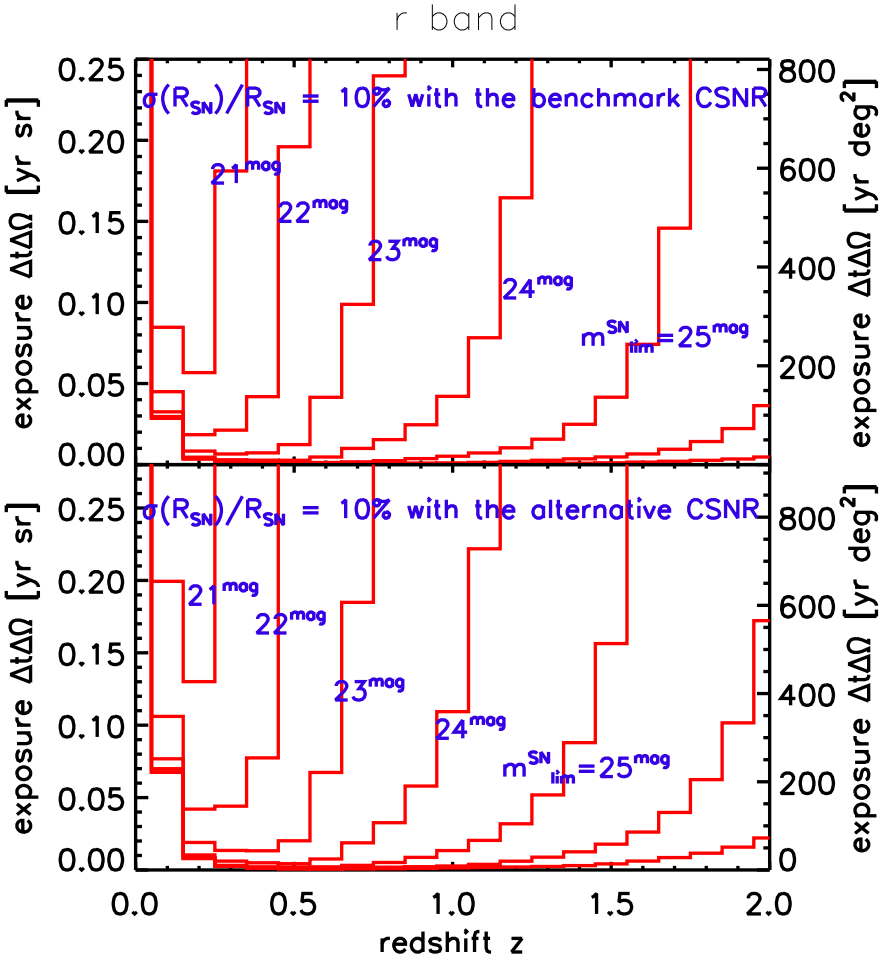

Figure 2.6: Survey CSNR discovery parameter, i.e., the product of survey monitoring time and sky coverage $\Delta t\,\Delta\Omega$ needed to measure the CSNR to a specified precision. Data are binned in redshift units of $\Delta z = 0.1$ vs. redshift. *Top panel:* discovery parameter needed to reach 10 % precision with our benchmark CSNR. *Bottom panel:* discovery parameter needed to reach 10 % precision with the alternative CSNR seen in Fig. 2.1.

in Supplement 2.10; here we summarize the results.

Several main lessons emerge from considerations of specific surveys. When Pan-STARRS and LSST are online, these surveys will collect a core-collapse supernova harvest far larger than the current set of events ever reported. This alone will make synoptic surveys a transformational point in the study of supernovae.

Moreover, synoptic surveys will detect core-collapse events over a wide redshift ranges. Table 2.2 summarizes the supernova redshift ranges correspond to the most likely $m^{\rm sn}_{\rm lim}$ of the surveys. The total supernova harvest depends sensitively on the survey depth, and in Supplement 2.10 the sensitivity to $m^{\rm sn}_{\rm lim}$ is shown. To determine the redshift ranges shown in Table 2.2, we set an (arbitrary) lower limit on the number of total supernova counts at $N_{\rm min} = 10$. We choose a lower redshift limit $z_{\rm min}$ such the cumulative survey supernova count in one year is $N_{\rm survey}(< z_{\rm min}) = N_{\rm min}$. Similarly, the upper limit $z_{\rm max}$ is set by $N(> z_{\rm max}) = N_{\rm min}$ is the number of supernovae detected within redshift $z = z_{min}$ within a year.

As seen in Tables 2.2 and 2.3, the future surveys will find abundant supernovae over a wide redshift range. At low redshifts, the surveys will detect nearly all of the supernovae within the nearby cosmic volume accessible in their sky coverage. So surveys with a large $\Delta\Omega_{\rm scan}$, such as LSST and Pan-STARRS, have $z_{\rm min}$ which does not depends on $m^{\rm sn}_{\rm lim}$. For DES, $\Delta\Omega_{\rm scan}$ is not as large, so that the number of supernovae brighter than $m^{\rm sn}_{\rm lim} = 21^{\rm mag}$ does not accumulate to $N(< z_{\rm min})$=10 until $z_{\rm min}$=0.081. But for depths fainter than $m^{\rm sn}_{\rm lim} = 24^{\rm mag}$, the survey does become volume-limited and the supernova counts accumulate to 10 at the same redshift. The upper limit of the redshift $z_{\rm max}$ depends not only on sky coverage but also survey depth. For planned survey depths, DES will gather core-collapse supernovae to about $z \simeq 1.20$; LSST will extend to $z \sim 0.89$, and could go further in modes with smaller sky coverage but deeper exposure.

The large supernova counts and wide redshift ranges together mean that surveys will, by direct counting, map out the CSNR to high precision out to high redshifts. Future

surveys should easily achieve 10% statistical precision for the CSNR for redshifts around which the survey's counts peak. We see that, with $m_{\rm lim}^{\rm sn} = 23^{\rm mag}$, LSST will reach out to $z \sim 0.89$, presuming that the relative fraction of the brightest, farthest-reaching events (of Type IIn and Ic) do not evolve with redshift. If so, then by direct counting future survey should witness the sharp CSNR rise. With deeper exposures and corresponding increases in redshift reach, surveys could begin to test for the behavior of the CSNR above $z = 1$, a regime that is currently poorly understood.

Both the survey yields of supernova discoveries, as well as their redshift ranges, are strong functions of survey depth. As shown in Table 2.3 of Supplement 2.10, each magnitude increase in survey depth yields a large enhancement (a factor ~ 3) in total supernova counts. This in turn leads to large enhancements in redshift range, and thus in the range over which the CSNR is measured. As shown in Supplement 2.10, increased monitoring time needed to achieve higher $m_{\rm lim}^{\rm sn}$ will come at some cost, though this will be partially offset by the higher supernova yield in a deeper exposure. Finally, for the large population of low-redshift supernovae, deeper surveys will lead to better lightcurve determination, allow for a more accurate photometry over a larger brightness range and thus longer timescales.

As noted in §2.4.3, our fiducial results are for supernova peak magnitudes whose luminosity functions (each of which is one or two gaussians for each core-collapse type) are nonzero only within $|M - M_{\rm mean}| < 2.5\sigma$ away from the mean. This arbitrary cutoff is meant as a compromise which shows the effect of nonzero width of the luminosity functions, without extrapolating too far into the tails in which there is as yet no data. To give a feel for the sensitivity of our results to the assumed luminosity function width we repeated our analysis for luminosity functions with larger and narrower $|M - M_{\rm mean}|$ ranges, (but with fixed observed intrinsic σ). We find that the total supernova counts vary less than 0.88% when $|M - M_{\rm mean}|$ ranges from 2σ to 3σ; this insensitivity reflects the fact that the bulk of supernova counts are from events near the means of the distribution. One the other hand, we found that the maximum observed supernova redshift (and thus the depth to which one can probe the

CSNR) is very sensitive to the choice of $|M - M_{\rm mean}|$. For example, the LSST maximum supernova redshift in 1 year is $z_{\rm sn,max} = 0.89$ for our fiducial choice of $|M - M_{\rm mean}| = 2.5\sigma$, as seen in Table 2.2. On the other hand for $|M - M_{\rm mean}| = 2\sigma$ and 3σ, we find $z_{\rm sn,max} = 0.73$ and 1.06, respectively. Here rare, intrinsically bright events determine the redshift reach, and the deeper the luminosity function reaches into the bright-end tail, the larger the resulting $z_{\rm sn,max}$. Thus we would expect the intrinsically brightest events, of Type Ibc and Type IIn, to give the greatest redshift reach. Indeed, Cooke (2008) has recently illustrated how Type IIn events can be mapped out to $z > 2$ by ground-based 8 meter-class telescopes.

Of course, all of our forecasts assume that the luminosity functions of each supernova type, and the relative frequencies among the supernova types, all remain unchanged at earlier epochs. However, it is entirely plausible and even likely that these properties could evolve, e.g., with metallicity and/or environment. These effects are likely to be crucial in determining the true redshift reach of future sky surveys, and thus predictions such as ours will improve only as real supernova data becomes available with good statistics at ever-increasing redshifts, and one can directly constrain and/or measure evolutionary effects. Moreover, the relatively small sample sizes available to Richardson et al. (2002) could well lead to underestimates of the true range of luminosities of each type. For example, Gezari et al. (2009a) recently report an unusually bright Type II-L event, SN 2008es, with peak magnitude $M_B \simeq -22.2$, far outside of the absolute magnitude range we have adopted for this subtype.

Indeed, the enormous statistics gathered by future surveys will allow for cross-checks and empirical determination of other evolutionary and systematic effects. A major such effect is dust obscuration, to which we now turn.

2.6 Dust Obscuration: Disentangling the Degeneracies and Probing High-Redshift Star-Forming Environments

The loss of some supernovae due to dust obscuration must be understood accurately and quantitatively in order to take full advantage of the large data samples of supernovae which *are* detected. As noted above in §2.4.2, currently we have very limited knowledge of supernova extinction and particularly its evolution, and most of what is reliably known is based on empirical studies of supernova counts. Precisely for this reason, future surveys offer an opportunity to address this problem in great detail by leveraging the enormous numbers of supernovae of all types, seen over a wide range of redshifts and in a wide range of environments. Here we sketch a procedure for recovering this information.

Future surveys will produce well-populated distributions of supernovae; these encode information about extinction and reddening due to dust. Specifically, in redshift bin Δz around z one can measure, often with very high statistical accuracy, the apparent magnitude distribution for each subtype of core-collapse events. These distributions can be made for all bands, but as we have shown, detections and/or light curve information will be most numerous in r and g bands; we will focus on these for the purposes of discussion. Within a redshift bin, the distance modulus μ is fixed, and the light curve and associated K-correction should reflect intrinsic variations within the core-collapse subtype.

Thus, for a given core-collapse subtype and redshift z, one can construct histograms of r and g peak magnitudes. From redshift and supernova type, one can compute the distance modulus and K-correction, and use these to infer, for each event, the dust-obscured peak magnitude $M_{\rm dust} \equiv m_{\rm obs} - \mu(z) - K(z) = M_{\rm peak} + A$ where $M_{\rm peak}$ is the intrinsic peak magnitude for the event, and A is the extinction for this event in its host galaxy. By comparing two passbands we can also evaluate colors, for example $g-r = M_{g,{\rm peak}} - M_{r,{\rm peak}} + E(g-r)$, where $E(g-r)$ is the reddening. In general, within a redshift bin we expect the

A and E to vary on an event-by-event basis, reflecting the properties of dust along the particular line of sight through the particular host galaxy.

Invaluable insight into these issues comes from the Hatano et al. (1998) analysis of extinction in observation of local supernovae. These authors argue that the data are consistent with very strong dependence of extinction with the inclination of the host galaxy; this alone guarantees that A must vary strongly from event to event even within subtypes. Hatano et al. (1998) also argue that the variation of dust column with galactic radius also suggests that extinction is responsible for the paucity of supernovae at small radii. (Shaw, 1979). Finally, Hatano et al. (1998) also point out that core-collapse events are more extincted than Type Ia events because the Ia's have a higher scale height and thus are more likely to occur in less extincted regions.

On an event-by-event basis, intrinsic light curve and color evolution are degenerate with dust evolution. However, the large sample size may allow for a physically motivated empirical approach to lifting this degeneracy. If on theoretical grounds we can assume that at least one core-collapse subtype has negligible intrinsic evolution in its lightcurve, then for that subtype M and K are effectively known and moreover are constant across events in a particular redshift bin. In this case, the apparent magnitude and color distributions can be directly translated into distributions of extinction and reddening. By comparing these distributions (or e.g., their means and variances) across different redshifts, one directly probes dust evolution.

Moreover, if one can use one core-collapse subtype as an approximate "standard distribution" from which to extract dust properties, one might press further by assuming that other core-collapse events will be born in similar environments and thus encounter similar extinction and reddening. One can thus use the empirically determined dust evolution to statistically infer the degree of *intrinsic* lightcurve variation in the other core-collapse subtypes.

If subtype can be firmly established, comparison of magnitude distributions of different

core-collapse subtypes allows for a purely *empirical* approach. Namely, one can compare the evolution of the magnitudes distributions of different subtypes. One could first provisionally treat each supernova subtype as a "standard distribution" with no intrinsic evolution; then for each subtype one would infer dust extinction and reddening at each redshift. It is reasonable to expect that the different subtypes sample the same dust properties, as long as the host environments are not systematically different for the different subtypes (all of which arise in massive-star-forming environments). Indeed, Nugent et al. (2006) have performed such an analysis to use $V - I$ colors of Type II-P events to infer reddening for events out to $z \sim 0.3$.

A comparison of the dust extinction inferred the different subtypes amounts to a test for intrinsic variation. With information from multiple subtypes, it may be possible to isolate dust effects common to all, and intrinsic variation peculiar to each subtype. For example, if one subtype distribution evolves significantly more than another (e.g., one subtype variance grows more than another) then the difference in variance must be intrinsic, and that the lesser variance is an upper limit to the variance due to dust effects.

The ability to empirically measure extinction depends on the intrinsic width of the $A(z)$ distribution, and on surveys' ability to probe this distribution. At low redshift, Hatano et al. (1998) find a wide ($> 1^{\rm mag}$) range of extinctions, much of which they attribute to inclination which will remain an issue at higher redshift. On the other hand, as a given survey pushes to higher redshift, progressively less of the distribution is observable. For the case of LSST, we see in Fig. 2.10 that with $m^{\rm sn}_{\rm lim} = 23^{\rm mag}$ the least obscured events are visible out to redshift $z \sim 1$, while those which have suffered $A_r = 1^{\rm mag}$ of extinction would correspond to the $m^{\rm sn}_{\rm lim} = 22^{\rm mag}$ curves, which reach to about $z \sim 0.5$. Thus over this shallower redshift range, extinction can be probed in detail, but with a narrowing observable range at higher redshift.

If future surveys can empirically determine effects of dust evolution, this would not only remove a major "nuisance parameter" for supernova and cosmology science, but also gain information of intrinsic interest. Namely, we will learn about the cosmic distribution and

evolution of host environments of supernovae and thus of star formation.

2.7 Discussion

The large amount of core-collapse supernovae observed by synoptic surveys will yield a wealth of data and enormous science returns. Here we sketch some of these.

2.7.1 Survey Impact on the Cosmic Supernova and Star Formation Histories

As we have indicated in the previous section, synoptic surveys will determine cosmic core-collapse supernova rate with high precision out to high redshifts. Moreover, with the large number of supernova counts, and with light curves and host environments known, the total cosmic core-collapse redshift history can be subdivided according to environment and/or supernova type. For example, with photometric data alone one can determine to high accuracy correlations between supernova rate and host galaxy luminosity and Hubble type. One can compare supernova rates in field galaxies versus those in galaxy groups and clusters. Using galaxy morphology one can investigate correlations between supernovae and galaxy mergers. With the addition of spectroscopic information one can also search for correlations with host galaxy metallicity.

The CSNR is also tightly related to the cosmic star-formation rate. Therefore with the high precision CSNR, and assuming an unchanging initial mass function, one can make a similarly precise measure of the cosmic star-formation rate. On the other hand, one can test for environmental and/or redshift variations in the initial mass function, by comparing the supernova rates based on direct survey counts with the star-formation rates determined via UV and other proxies.

In addition to core-collapse explosions, synoptic surveys will of course by design also discover a similarly huge number of Type Ia supernovae. Thus the Type Ia supernova rates

can be compared to those for core collapse events. As has been widely noted (e.g., Gal-Yam & Maoz, 2004; Watanabe et al., 1999; Oda & Totani, 2005; Scannapieco & Bildsten, 2005, and references therein) this will yield information about the distribution of time delays between the core-collapse and thermonuclear events. Moreover, one can explore differences in the environmental correlations for the two supernova types (and subtypes).

2.7.2 Survey Supernovae as Distance Indicators: the Expanding Photosphere Method

Type Ia supernovae have become the premier tool for distance determinations at cosmological scales, thanks to their regular light curves, high peak brightnesses, and relatively less dusty environments. Nevertheless, given the importance of the cosmic distance scale, and the ongoing need for systematic crosschecks and calibration, it is worthwhile to consider other methods. Core-collapse events offer just such a method, via the expanding photosphere/expanding atmosphere method.

This method was originally conceived by Baade (1926) and Wesselink (1946) for study of Cephieds; Kirshner & Kwan (1974) applied the Baade-Wesselink method to supernovae. The key to the technique is to exploit the simple kinematics of a newborn supernova remnant: the freely-expanding photosphere grows in size as $R = vt$. Thus, for purely blackbody emission, the luminosity grows with size (i.e., time) as $L = 4\pi R^2 \sigma T^4$. With good sampling to measurements time t since explosion, and spectroscopic inference of v and T, one can recover the luminosity. In principle, therefore, one can use the explosion as a standard candle.

In practice, this method has been slow to mature. Until recently, the agreement with independent distance measures has been only good to within a factor ~ 2 (e.g., Vinkó & Takáts, 2007). The complex (out of local thermodynamic equilibrium) spectra of supernovae has proved difficult to adequately model. However, recently important advances have been made in the radiation transfer modeling of young supernova remnants and its fitting

to spectra of local supernovae (Baron et al., 2004; Dessart & Hillier, 2005, 2008). Because of this, the expanding photosphere (or more properly, expanding atmosphere) method now appears to be reaching consistency with other distance measures; this method now shows agreement approaching the $\sim 10\%$ level. Similar precision now seems possible using a separate, empirical method (Hamuy & Pinto, 2002) which exploits the observed correlation between luminosity and expansion velocity of Type II-P events. This opens up core-collapse supernovae as alternative distance indicators. Indeed, several group (Nugent et al., 2006; Poznanski et al., 2007; Olivares, 2008) have already applied this method to various collections of Type II-P observations, yielding tight Hubble diagrams out to $z \sim 0.3$.

To use this method as it is currently envisioned, follow-up spectroscopy is mandatory for *each* event (see §2.7.5), with photometric surveys identifying the candidates. Obviously, for the largest surveys, in practice only a tiny fraction of core-collapse events could be studied in a (separate) spectroscopic campaign, particularly given that the most common core-collapse types are intrinsically dimmer than Type Ia events and thus require longer exposures to obtain spectra. Followup requirements thus are the limiting factor for the use of core-collapse events as distance indicators.

The situation for Type Ia supernovae is better-studied and also potentially more hopeful. Recent work (Poznanski et al., 2007; Kim & Miquel, 2007; Kunz et al., 2007; Blondin & Tonry, 2007; Wang, 2007; Kuznetsova et al., 2008; Sako et al., 2008) suggests that photometric redshifts of Type Ia events near maximum light could be obtained with sufficient precision (give a low-redshift training set) to provide useful dark energy constraints without spectroscopy. Whether photometric-based distances can be derived for core-collapse events with sufficient accuracy remains to be seen. It nevertheless seems to us a worthy object of further study. In this context it is worth noting that DES plans to do followup spectroscopy on $\sim 25\%$ of Type Ia events (The Dark Energy Survey Collaboration, 2005). We suggest that at least some modest fraction of this follow-up time be dedicated to core-collapse monitoring.

2.7.3 Other Science with Cosmic Supernovae

The physics, astrophysics, and cosmology of cosmic core-collapse supernovae is a fertile topic; with our detectability study in hand, a wide variety of problems present themselves. Here we sketch these out; we intend to return to these in future publications.

The huge harvest of core-collapse events will open new windows onto other aspects of supernova physics. For example, the physics of black hole formation in supernovae, and the neutron-star/black hole divide, remain important open questions. Balberg & Shapiro (2001) have estimated the rates of events with observable signatures of black hole formation; LSST should provide a fertile testing ground for these predictions.

The elaboration of the cosmic history and specific sites of high-redshift supernovae will also offer unique new information about supernova "ecology" – i.e., feedback and cycling of energy, mass, and metals into the surrounding environment. For example, large surveys will offer the opportunity to study supernova rates as a function of host galaxy and galaxy clustering, shedding new light onto large-scale star formation and its connection with galaxy evolution. Moreover, DES and other surveys will discover an enormous number of rich galaxy clusters; the occurrence of both Type Ia and core-collapse events in clusters will offer important new insight into the origin of the very high metallicity of intracluster gas (Maoz & Gal-Yam, 2004; Maoz et al., 2005).

Core-collapse supernovae also are the sources, directly or indirectly, of high-energy radiation of various kinds. For example, supernovae act as accelerators of cosmic rays. These in turn interact with interstellar matter to produce high-energy γ-rays. Pavlidou & Fields (2002) used then-available estimates of the cosmic star-formation rate to show that this γ-ray signal has a characteristic feature, and makes a significant part of the extragalactic γ-ray background around ~ 1 GeV. With the successful launch of the high-energy γ-ray observatory GLAST, this component of the γ-ray background may for the first time be clearly identified. Regardlessly, a sharper knowledge of the cosmic supernova rate (and thus cosmic-ray injection rate) will work in concert with GLAST observations to probe the history of

cosmic rays throughout the universe.

2.7.4 Comparison with Type Ia Survey Requirements

The characteristics of Type Ia supernovae are in general very similar to the core-collapse supernovae. Hence the observational requirements for their identification in synoptic surveys are also very similar. The rest-frame, full-width at half-maximum timescale for Type Ia supernovae is ~ 20 days. Therefore surveys will need a scan cadence of a few days in order to get a well-sampled light curve. For example, the Pan-STARRS strategy for Type Ia discovery is to sample the light curve every 4 days (Tonry et al., 2003; Tonry, 2003). As we have discussed, this sampling frequency is also suitable for the core-collapse supernovae which the time scale of the light curve also last a few weeks.

2.7.5 Redshifts and Typing from Photometry and Followup Spectroscopy

Survey supernovae become scientifically useful only when one can establish, at the very least, their redshift and whether they are core collapse or Type Ia. Since followup spectroscopy will not be possible for the large numbers of future events, photometric redshifts will be needed. For events in which a host galaxy is clearly visible, one can use photometric redshifts of the hosts. Here one is helped by the ability of surveys to stack all of the many (non-supernova) exposures to obtain a much deeper image than those with the supernovae. Once the host redshift is know, the supernova type must be determined. Baysean analysis techniques and software (Dahlén & Goobar, 2002; Poznanski et al., 2007) have been developed to distinguish both Type Ia and core-collapse events. These authors find that type discrimination depends crucially on the accuracy with which the redshift is known. For spectroscopic redshifts, their methods is extremely accurate, and for photometric redshifts the method is still quite good, though in this case misclassifications can reach $15 - 25\%$ depending on $\sigma_{\mathrm{photo}-z}$.

Followup spectroscopy on a subset of events will be essential to calibrate the accuracy of the photometric typing (and host redshifts). In particular, spectroscopy will be invaluable in identifying and quantifying catastrophic failures in the typing algorithms; on the basis of these it may be possible to refine the routines. As noted in the previous section, followup is also required for any events one hopes to use in distance determinations.

For events without clear host galaxies and without followup, one must resort to photometric redshifts and typing based on the supernova light curve itself, in whatever bands are available. It is not clear that this can be done with any reliability on an event-by-event basis. As Poznanski et al. (2007) emphasize, one might make statistical statements about the types and redshifts of the entire class of "hostless" events. Here spectroscopic followup will be essential not only for determining the supernova redshift but also the nature of the underlying host.

2.8 Conclusions and Recommendations for Synopic Surveys

The next ten years will witness a revolution in our observational knowledge of core-collapse supernovae. Synoptic sky surveys will reap an enormous harvest of these events, with tens of thousands discovered in the near future, culminating with of order 100,000 seen annually by LSST. These data will reveal the supernova distribution in space and time over much of cosmic history. The needed observations are naturally a part of the scanning nature of these surveys, and require only that core-collapse events be included in the data analysis pipeline.

The potential science impact of this unprecedented supernova sample is enormous. We have discussed ways in which the photometric supernova data alone will contribute in significant and unique ways to cosmology and astroparticle physics, as well as to studies of core-collapse and supernova evolution themselves. We illustrate one such application by demonstrating how to recover the cosmic supernova rate from the redshift distribution of

supernova counts in synoptic surveys. The large datasets ensure that the statistical error will be very low, and the first large surveys will rapidly determine the CSNR to precision exceeding that of current data based on observation of massive-star proxies.

With the addition of spectroscopic followup observations, the survey-identified core-collapse supernovae can be used as distance indicators. Thanks to recent advances in the phenomenology of supernova spectra and the modelling of their expanding atmospheres, the early light curves provide standardizable candles. This expanding photosphere/atmosphere method could provide a cross-check for the cosmic distance scale as inferred from Type Ia supernovae.

To summarize our recommendations for synoptic surveys, in order to capitalize on this potential:

1. Include core-collapse supernovae (all Type II as well as Types Ib and Ic) in the data analysis pipeline.

2. Include a scanning mode in which the depth $m_{\rm lim}^{\rm sn}$ is as large as possible, in order to maximize the supenova redshift range. Surveys which modes which probe down to $m_{\rm lim}^{\rm sn} = 26^{\rm mag}$ could discover many supernovae (both core-collapse and Type Ia) approaching redshift $z \sim 2$.

3. Adopt scanning cadence of revisits every ~ 4 days, in order to capture core-collapse events at peak brightness, and to obtain a well-sampled lightcurve. This timescale also appropriate for Type Ia events.

4. Allocate some followup spectroscopy to core-collapse events. This will calibrate photometric Type Ia/core-collapse typing and typing among core-collapse subtypes, and will be particularly crucial for probing the nature of events in which a host galaxy is not seen.

We close by re-emphasizing that these recommendations require only modest efforts in analysis, little to no modification of the strategies already in place for Type Ia searches, and

some commitment of followup spectroscopy. Thus a small extra investment of resources will reap handsome scientific rewards as we open our eyes to the incessant rise and fall of these beacons marking massive star death throughout the cosmos.

Acknowledgments It is a pleasure to thank Joe Mohr, Vasiliki Pavlidou, Tijana Prodanovic, Jon Thaler, Yun Wang, David Weinberg, and Michael Wood-Vasey for valuable discussions. We are particularly indebted to Josh Frieman, Avishay Gal-Yam, John Beacom, and David Branch for detailed constructive feedback on an earlier draft, which has greatly improved this paper.

Note: In the final stages of writing this paper we became aware of the work of Young et al. (2008a). These authors discuss core collapse rates in sky surveys, with a focus on events in low-metallicity environments. Where it is possible to compare and when we adopt their parameters (particularly $m_{\rm lim}^{\rm sn}$), our analyses seem to be in broad agreement.

2.9 Supplement I: The Supernova/Star-Formation Connection

The star-formation rate and supernova rate for any astrophysical site are intimately related. Moreover, in many applications such as ours the timescales of interest are much longer than the $\sim$ *few* Myr supernova progenitor lifetimes. In this case, the star-formation rate and supernova rates are proportional. This is expressed above in eq. (2.2). The constant of proportionality can be obtained from the initial mass function $\xi(m)$. In stellar mass range $(m, m+dm)$ the number of new stars is proportional to $\xi(m)\,dm$, while the mass of new stars is $m\,\xi(m)\,dm$. Thus the number of supernovae per unit new star mass–i.e., the conversion between star-formation and supernova rates–is

$$\frac{\mathcal{R}_{\rm SN}}{\dot{\rho}_\star} = \frac{\int_{\rm SN} \xi(m)\ dm}{\int m\ \xi(m)\ dm} = \frac{\int_{\rm SN} \xi(m)\ dm}{\int_{\rm SN} m\ \xi(m)\ dm} \frac{\int_{\rm SN} m\ \xi(m)\ dm}{\int m\ \xi(m)\ dm} = \frac{X_{\rm SN}}{\langle m \rangle_{\rm SN}} \qquad (2.23)$$

where $X_{\rm SN} = \int_{\rm SN} m\,\xi\,dm / \int m\,\xi\,dm$ is the mass fraction of new stars that will go into supernovae, and $\langle m\rangle_{\rm SN} = \int_{\rm SN} m\,\xi(m)\,dm / \int_{\rm SN} \xi(m)\,dm$ is the mean supernova progenitor mass. For illustration, consider a Salpeter IMF $\xi(m) \propto m^{-2.35}$ over mass range $(0.5M_\odot, 100M_\odot)$ and $\xi(m) \propto m^{-1.5}$ for the low mass range $(0.1M_\odot, 0.5M_\odot)$ (Baldry & Glazebrook, 2003, their "Salpeter A" mass function). We also take supernova progenitors to lie in the mass range $m_{\rm SN} \in (8M_\odot, 50M_\odot)$. This gives $X_{\rm SN} = 0.15$,$\langle m\rangle_{\rm SN} \approx 15.95M_\odot$, and thus a star-formation/supernova conversion factor $X_{\rm SN}/\langle m\rangle_{\rm SN} = 0.00914M_\odot^{-1}$. The uncertainty here is significant, probably about a factor of 2.

The cosmic star-formation rate can be estimated from a number of observables tied to massive (i.e., short-lived thus "instantaneous") star-formation. Proxies often adopted are the UV and/or Hα luminosity densities (Madau et al., 1996). Of these, UV light has a more direct connection with massive stars, but is also affected more by the dust extinction than the Hα light (Strigari et al., 2005). Most cosmic star-formation studies find a sharp increase in the rate up to $z = 1$, but there remains a large uncertainty of the star formation rate at higher redshift. In this paper, we adopt the Cole et al. (2001) fitting formula for the cosmic star-formation rate

$$\dot{\rho}_\star^{\rm cole} = \frac{a + bz}{1 + (z/c)^d}\; h\,M_\odot\,{\rm yr}^{-1}\,{\rm Mpc}^{-3} \tag{2.24}$$

where$(a, b, c, d) = (0.017, 0.13, 3.3, 5.3)$, which are one of the best-fitted parameters according to current observing data found by Hopkins & Beacom (2006). Using the conversion factor of Hopkins & Beacom (2006) and our adopted Hubble constant, this gives a local rate of $\mathcal{R}_{\rm SN}(0) = 1.1 \times 10^{-4}$ SNII Mpc^{-3} yr^{-1}. The benchmark CC SNe rate rises to a peak around $z = 2.5$ and then slowly declines at high redshift.

To illustrate the impact of different star formation, we also did all calculations with an alternative CSNR. Here we normalize to the current observed, counting-based CSNR (Botticella et al., 2008b), and take the shape from the a fitting function of the Hippelein et al. (2003) star formation rate. We also lower the rate by 30% because we want the alternative CSNR to be as much different as the benchmark CSNR as possible and Hopkins

& Beacom (2006) suggested that the uncertainty of the normalization of the star formation rate is about 30%. The differences between this and our fiducial rate gives a sense of the current rough but not perfect agreement between the CSNR as inferred indirectly from progenitor light (sometimes reprocessed) and directly from counting.

2.10 Supplement II: Supernova Predictions for Upcoming Synoptic Surveys

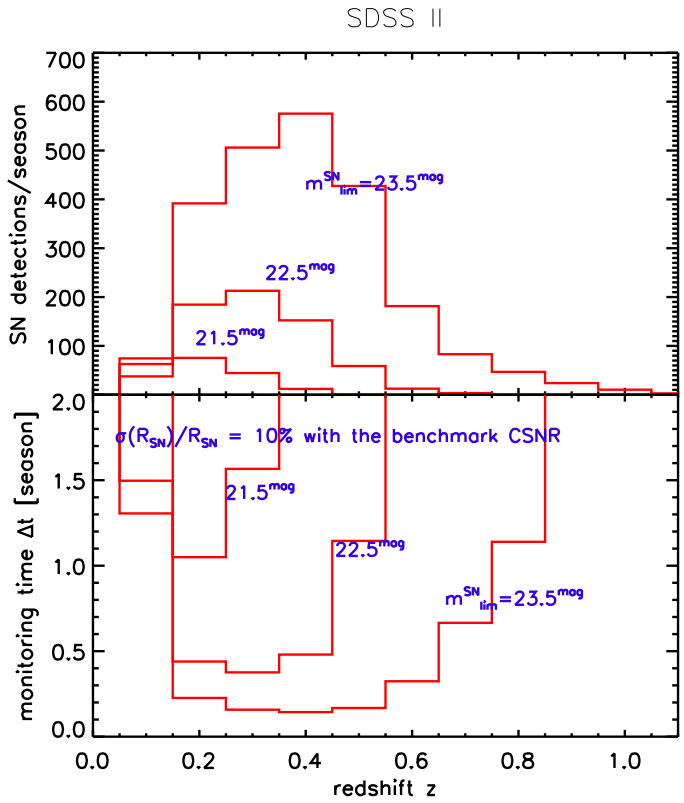

Figure 2.7: Sloan Digital Sky Survey (SDSS-II). All the results plotted here are using the benchmark CSNR. *Top panel:* The number of supernovae observed in one scan season of 3 months per year, in redshift bins of with $\Delta z = 0.1$. Results are shown for a fixed scan sky coverage $\Delta\Omega_{\rm scan} = 300$ deg^2, and the survey depth as labeled. *Bottem panel:* The monitoring time Δt needed in order to determine the cosmic supernova rate to a 10% precision.

Figures 2.7–2.10 show the supernova forecasts for different surveys. For each we show the

expected annual supernova harvest $\Delta N_{\rm obs}(z)$ as a function of redshift, with the sky coverage held fixed to the values in Table 2.1. The count distribution across redshift bins are directly proportional to the differential supernova rate distribution $\Gamma_{\rm SN,obs}(z)$, via eq. (2.18). Thus the shapes the curves follow those of $\Gamma_{\rm SN,obs}(z)$ as seen in Figure 2.4 an explained in the accompanying discussion.

Figures 2.7–2.10 also show the survey scan time required for these data to constrain the cosmic star-formation rate in each redshift bin to within a statistical precision $\sigma(\mathcal{R}_{\rm SN})/\mathcal{R}_{\rm SN} = 10\%$. We have seen (eq. 2.20) that the precision at each bin is inverse with the counts, $\sigma(\mathcal{R}_{\rm SN})/\mathcal{R}_{\rm SN} = 1/\sqrt{\Delta N_{\rm obs}(z)}$. Thus these panels show trends in which monitoring time decreases with the counts per bin. This mirrors the behavior shown in Figure 2.6 and explained in the surrounding discussion.

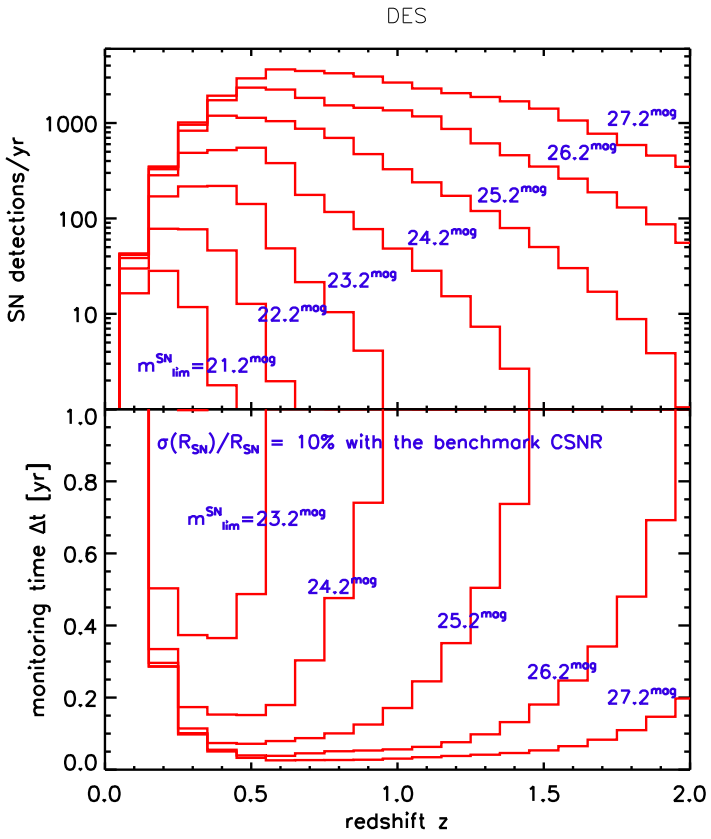

Figure 2.8: As in Figure 2.7, for the Dark Energy Survey (DES). Here results are shown for different $m^{\rm sn}_{\rm lim}$, but for a fixed scan sky coverage $\Delta\Omega_{\rm scan} = 40$ deg^2.

Table 2.3 shows the effect of survey limiting magnitude on redshift range and total supernova harvest in the r-band. We see that each unit increase $\Delta m_{\rm lim}^{\rm sn} = 1^{\rm mag}$ in survey depth yields a large enhancement, in the total supernovae seen. The supernova numbers increase by a factor 4.3 when going from $m_{\rm lim}^{\rm sn} = 21^{\rm mag}$ to $22^{\rm mag}$ to factor of 2.0 when going from $26^{\rm mag}$ to $27^{\rm mag}$. Of course, there is a tradeoff in the needed exposure. For the faintest objects at the highest redshifts, background noise dominates, and monitoring time grows by a factor $(10^{2/5})^2 \sim 6.3$ per magnitude. Thus, including a narrower but deeper survey mode will likely yield fewer supernovae, but if judiciously implemented, this tradeoff may be worth the additional redshift coverage.

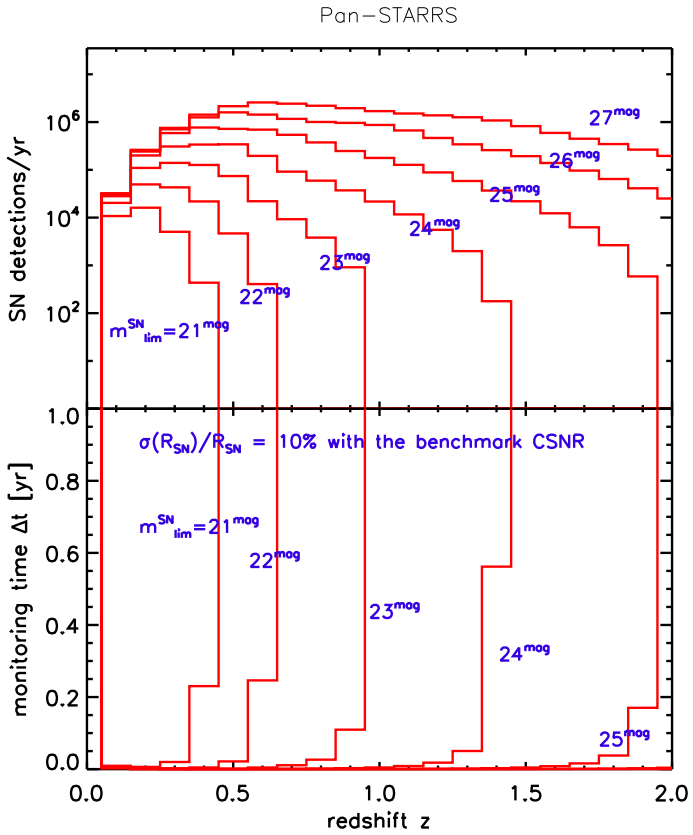

Figure 2.9: As in Figure 2.8, for Pan-STARRS. We hold fixed $\Delta\Omega_{\rm scan} = 30000$ deg^2.

2.11 Supplement III: The K-Correction

The K-correction accounts for redshifting of the supernova spectrum across the passbands in the observer frame. In the context of the Southern inTermediate Redshift ESO Supernova Search, the elegant and instructive analysis of Botticella et al. (2008b) determine K-corrections for the ~ 90 supernova confirmed and candidate events in their survey. They found that the corrections depend strongly on redshift, light curve phase, and on waveband. In particular, the shifts from observed V and R bands to rest-frame B-band both typically have $K < 0$, i.e, a negative correction, particularly at early times most relevant here; this reflects the blue colors of the early phases. The corrections are at early times (within the first three weeks) usually a shift $|K| \lesssim 1^{\rm mag}$, with the largest corrections $K \sim -2^{\rm mag}$. As seen in

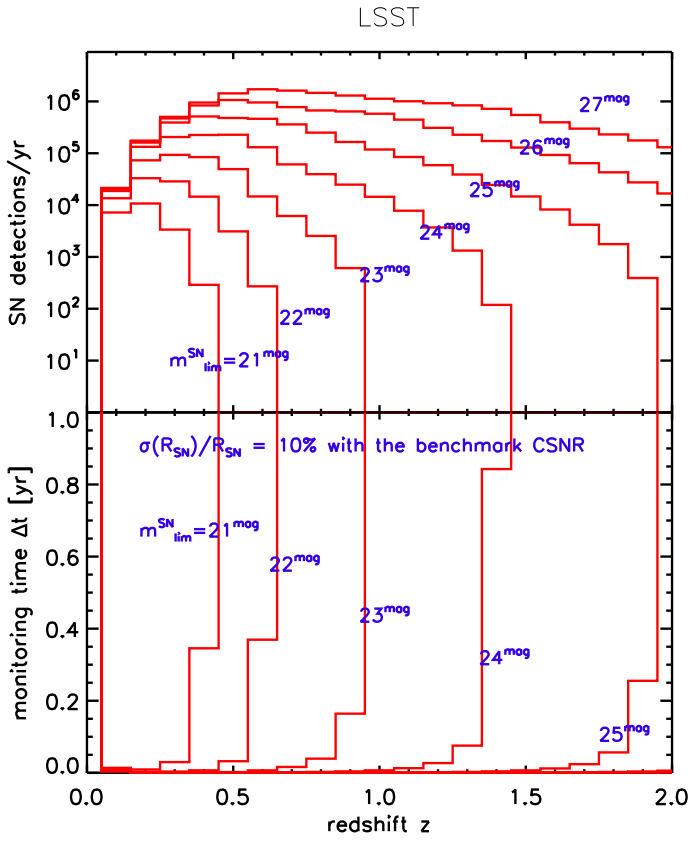

Figure 2.10: As in Figure 2.8, for Large Synoptic Survey Telescope (LSST). We hold fixed $\Delta\Omega_{\rm scan} = 20000$ deg^2.

Table 2.3: Sensitivity to survey depth in r band, for fixed sky coverage.

$m_{\rm lim}^{\rm sn}$	DES		Pan-STARRS		LSST	
[mag]	Total SNe	Redshifts	Total SNe	Redshifts	Total SNe	Redshifts
21	4.32×10^1	$0.081 < z < 0.18$	3.24×10^4	$0.007 < z < 0.36$	2.16×10^4	$0.008 < z < 0.36$
22	1.86×10^2	$0.066 < z < 0.38$	1.40×10^5	$0.007 < z < 0.56$	9.32×10^4	$0.008 < z < 0.56$
23	6.86×10^2	$0.064 < z < 0.66$	5.14×10^5	$0.007 < z < 0.89$	3.43×10^5	$0.008 < z < 0.89$
24	2.19×10^3	$0.063 < z < 1.10$	1.64×10^6	$0.007 < z < 1.34$	1.10×10^6	$0.008 < z < 1.33$
25	6.32×10^3	$0.063 < z < 1.62$	4.74×10^6	$0.007 < z < 1.88$	3.16×10^6	$0.008 < z < 1.88$
26	1.55×10^4	$0.063 < z < 2.17$	1.16×10^7	$0.007 < z < 2.48$	7.73×10^6	$0.008 < z < 2.47$
27	3.17×10^4	$0.063 < z < 2.68$	2.38×10^7	$0.007 < z < 3.08$	1.58×10^7	$0.008 < z < 3.08$

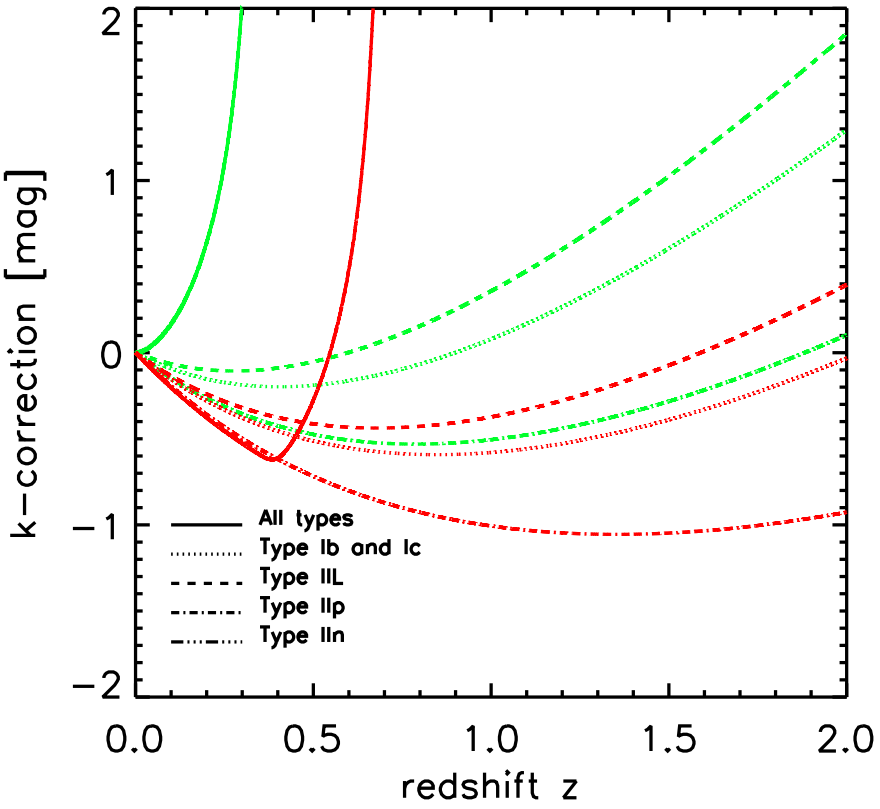

Figure 2.11: K-correction of the four types of supernovae(I-bc,II-L,II-P,II-N) in g and r bands (green lines for g-band and red lines for r-band). The sharp upturn in the Ibc correction reflects a cutoff in the supernova spectrum due to UV line blanketing; see discussion in text.

eq. (2.7), a negative correction would reduce the apparent magnitude and thus *improve* the observability of the supernovae.

In this paper we compute K-corrections following the formalism of Kim et al. (1996) in a single band, and add the color correction term (which described as η_{xB} in Section 2.4.3) to make the corresponding correction when transfer from one band to another. In band x, the K-correction is

$$K_x = 2.5\ \log(1+z)\ +\ 2.5 \log \frac{\int F(\lambda) S_x(\lambda) d\lambda}{\int F(\lambda/(1+z)) S_x(\lambda) d\lambda} \tag{2.25}$$

where $F(\lambda)$ is the unobscured, rest-frame spectral distribution of the supernova, and $S_x(\lambda)$ is the sensitivity of filter x. We included five types of core collapse supernovae: Ib, Ic, II-L, II-P, IIn. For each spectral type, we adopt a rest-frame spectrum $F(\lambda)$ following the prescription of Dahlén & Fransson (1999), who adopt blackbody spectra (sometimes slightly modified) with different temperatures and time evolution. We picked the temperatures which last for about a weak around the peak luminosity and treat them as a constant. Since the surveys we are interested in will have cadence less than a week, this should be a reasonable simplification. For Type Ib and Ic, we choose a 15,000 K blackbody with cutoff at $\lambda < 4000\mathring{A}$ because of UV blanketing. We choose 11,000 K for Type II-L, 10, 000 K for Type II-P, and 14,000 K for Type IIn.

Our resulting K-correction appear in Fig. 2.11, plotted for the g and r bands which we will see are the optimal for supernova discovery. The huge turnoff of the K-correction in Type I-bc is due to the short-wavelength cutoff in its spectrum. A large value is set so that there will be no Type I-bc supernovae observed beyond the cutoff point. Regardless of the turnoff of Type I-bc, for low redshifts the K-correction is in the range of $+2^{\mathrm{mag}}$ to -1.1^{mag} but typically is negative, which is in consistent with Botticella et al. (2008b).

Chapter 3

Synoptic Sky Surveys and the Diffuse Supernova Neutrino Background: Removing Astrophysical Uncertainties and Revealing Invisible Supernovae

This chapter is previously published in The Physical Review D as Lien, A., Fields, B. D., & Beacom, J. F. 2010, Phys. Rev. D, 81, 083001.

3.1 Abstract

The cumulative (anti)neutrino production from all core-collapse supernovae within our cosmic horizon gives rise to the diffuse supernova neutrino background (DSNB), which is on the verge of detectability. The observed flux depends on supernova physics, but also on the cosmic history of supernova explosions; currently, the cosmic supernova rate introduces a substantial ($\pm 40\%$) uncertainty, largely through its absolute normalization. However, a new class of wide-field, repeated-scan (synoptic) optical sky surveys is coming online, and will map the sky in the time domain with unprecedented depth, completeness, and dynamic range. We show that these surveys will obtain the cosmic supernova rate by *direct counting*, in an unbiased way and with high statistics, and thus will allow for precise predictions of the DSNB. Upcoming sky surveys will substantially reduce the uncertainties in the DSNB source history to an anticipated $\pm 5\%$ that is dominated by systematics, so that the observed high-energy flux thus will test supernova neutrino physics. The portion of the universe ($z \lesssim 1$) accessible to upcoming sky surveys includes the progenitors of a large fraction ($\simeq 87\%$) of the expected 10 – 26 MeV DSNB event rate. We show that precision determination of the (optically detected) cosmic supernova history will also make the DSNB into a strong probe

of an extra flux of neutrinos from optically *invisible* supernovae, which may be unseen either due to unexpected large dust obscuration in host galaxies, or because some core-collapse events proceed directly to black hole formation and fail to give an optical outburst.

3.2 Introduction

Core-collapse supernovae are the spectacular outcome of the violent deaths of massive stars. These events, which include Type II, Type Ib, and Type Ic supernovae, are in a real sense "neutrino bombs" in which the production and emission of neutrinos dominates the dynamics and energetics. This basic picture now rests on firm observational footing in light of the detection of neutrinos from SN 1987A (Hirata et al., 1987; Bionta et al., 1987). Thus all massive star deaths – certainly those that yield optical explosions, and even "invisible" events that do not – are powerful neutrino sources. Yet only the very closest events can be individually detected by neutrino observatories, leading to burst rates so small that no new events have been seen in more than two decades.

All core-collapse events within the observable universe emit neutrinos whose ensemble constitutes the diffuse supernova neutrino background (DSNB) [1] (Guseinov, 1967; Bisnovatyi-Kogan & Seidov, 1982; Krauss et al., 1984; Bisnovatyi-Kogan & Seidov, 1984; Domogatskii, 1984; Dar, 1985; Woosley et al., 1986; Totani & Sato, 1995; Malaney, 1997; Hartmann & Woosley, 1997; Kaplinghat et al., 2000; Ando et al., 2003; Fukugita & Kawasaki, 2003; Ando & Sato, 2004; Iocco et al., 2005; Strigari et al., 2005; Lunardini, 2006; Beacom & Strigari, 2006; Aharmim et al., 2006; Wurm et al., 2007; Daigne et al., 2005; Strigari et al., 2004; Yüksel et al., 2006; Lunardini, 2007; Horiuchi et al., 2009). Core-collapse supernovae produce all three active neutrino species (and their antineutrinos), all in roughly equal num-

[1] Type Ia supernovae do not have substantial neutrino emission > 10 MeV, but an intriguing alternative fate of accreting white dwarfs is the accretion-induced collapse (AIC) to a neutron star. Fryer et al. (2009) suggests the AIC events can also produce neutrino emission similar to core-collapse events. If so, AIC events would contribute to the DSNB and to optically visible outbursts. However, these AIC events have not yet been observationally confirmed and the expected AIC rate is much lower than that of core-collapse events. Therefore AIC neutrinos should not greatly change our results.

bers. However, for the foreseeable future only the $\bar{\nu}_e$ flux can be detected above backgrounds present on Earth. Specifically, the DSNB dominates the (anti)neutrino flux at Earth in the $\sim 10-26$ MeV energy range, and has long been a tantalizing signal that has become a topic of intense interest (e.g., Guseinov, 1967; Bisnovatyi-Kogan & Seidov, 1982; Krauss et al., 1984; Bisnovatyi-Kogan & Seidov, 1984; Domogatskii, 1984; Dar, 1985; Woosley et al., 1986; Totani & Sato, 1995; Malaney, 1997; Hartmann & Woosley, 1997; Kaplinghat et al., 2000; Ando et al., 2003; Fukugita & Kawasaki, 2003; Ando & Sato, 2004; Iocco et al., 2005; Strigari et al., 2005; Lunardini, 2006; Beacom & Strigari, 2006; Aharmim et al., 2006; Wurm et al., 2007; Daigne et al., 2005; Strigari et al., 2004; Yüksel et al., 2006; Lunardini, 2007; Horiuchi et al., 2009). Until now no DSNB signal has been detected, which set an upper bound on the DSNB flux. Super-Kamiokande (Super-K) set the upper limit to be $1.2\,\mathrm{cm}^{-2}\,\mathrm{s}^{-1}$ above 19.3 MeV of the neutrino energy (Malek et al., 2003). However, this limit is already close to theoretical prediction and thus Super-K is expecting to detect the first DSNB signal within the next several years.

Recently, Horiuchi et al. (2009) considered a variety of complementary indicators of the cosmic supernova rate, and concluded that the DSNB is no more than a factor $\sim 2-4$ below the 2003 Super-K limit (Malek et al., 2003). Moreover these authors point out that if Super-K is enhanced with gadolinium to tag detector background events (Beacom & Vagins, 2004), the resulting enhanced sensitivity at 10 – 18 MeV should lead to a firm DSNB detection.

In light of the impending DSNB detection it is imperative to quantify the uncertainties in the prediction and to reduce these as much as possible. The predicted flux depends crucially on: (a) supernova neutrino physics, via the emission per supernova; and (b) the cosmic history of core-collapse supernovae, via the cosmic supernova rate (hereafter, CSNR). Our emphasis in the present paper is on the CSNR, which has begun to be measured in a qualitatively new way by "synoptic" surveys. These new campaigns repeatedly scan the sky with a certain fields of view and high sensitivity. Pioneering synoptic surveys are already in hand and have shown the power of this technique. To date, these surveys have reported

the detection of several hundreds of supernovae in total, including both Type Ia and core-collapse events (Miknaitis et al., 2007; Frieman et al., 2008; Sako et al., 2008; Bazin et al., 2009; Palanque-Delabrouille et al., 2010; Dahlen et al., 2004, 2010; Gezari et al., 2009b; Djorgovski et al., 2008; Rau et al., 2009; Drake et al., 2009). Future surveys, such as DES, Pan-STARRS, and LSST, should find $> 10^4$ CCSNe yr^{-1}, eventually with detection rates of $> 10^5$ CCSNe yr^{-1} based on their depths and large fields of view (Lien & Fields, 2009). Current predictions show that these data will provide an absolute measurement of the CSNR to high statistical precision out to $z \sim 1$ (Lien & Fields, 2009; Bernstein et al., 2009). Note that observations seem to suggest that Type IIn supernovae are intrinsically the most luminous core-collapse type (Richardson et al., 2002), and therefore would contribute to most of the detections at $z \gtrsim 0.5$; but as we discuss below, the nature of the bright end of the supernova luminosity function remains uncertain and other rare but bright supernova types (Gezari et al., 2009b; Miller et al., 2009; Gal-Yam et al., 2009; Quimby et al., 2009) might also be important at these large redshifts.

It is important to appreciate that the most crucial input from future synoptic surveys will be the *normalization* of the CSNR. The shape of the CSNR follows from that of the star-formation rate due to the very short lifetimes of all massive star progenitors, and the cosmic star-formation redshift history is already relatively well-known out to $z \sim 1$. However, the CSNR normalization is only known to within $\sim 40\%$. This will be greatly improved by future synoptic surveys, which should measure the CSNR to extremely high precision at $z \sim 0.3$, and therefore dramatically reduce the uncertainties in the CSNR (and hence the DSNB) normalization.

Because our focus is on the interplay between synoptic surveys and neutrino observations, we wish to carefully distinguish different outcomes for massive stars and their resulting optical and neutrino emission. All collapse events produce neutrinos; however, simulations have shown that both the amount and energies of the supernova neutrinos varies with the mass range of the progenitor stars and how they end their lives (Fryer, 1999; Daigne et al.,

2005; Sumiyoshi et al., 2007; Horiuchi et al., 2009; Sumiyoshi et al., 2008; Nakazato et al., 2008, 2009; Lunardini, 2009). Unfortunately, there exists great uncertainty about the fate of massive stars, and the as-yet unresolved physics of the baryonic explosion mechanism may well play an important role in determining the outcomes (Buras et al., 2006; Janka et al., 2007; Mezzacappa et al., 2001; Thompson et al., 2003; Sumiyoshi et al., 2007). Recent work suggests that stars below some characteristic mass (estimated at $\sim 25 M_{\odot}$) do explode, producing optical supernovae and leaving behind neutron stars; on the other hand, stars above some mass scale (estimated at $\sim 40 M_{\odot}$) are expected to collapse directly into massive black holes without optical signals (Fryer, 1999; Heger et al., 2003; Nakazato et al., 2008, 2009). It is possible that between these regimes, a mass range exists (e.g., $25 - 40 M_{\odot}$) that would be a gray area where core-collapses form black holes from fallback while still being able to display some (perhaps dim) optical signals.

In the following sections, we will refer to those massive stars that first undergo regular core collapse and bounce as "core-collapse" events, whether they ultimately leave behind neutron stars or black holes formed from fallback. Those massive stars that collapse directly to black holes we will refer to as "direct-collapse" events. Events that also produce substantial electromagnetic outbursts we refer to as "visible"; those that do not are "invisible." For simplicity, but also following current thinking, we take visible events to be core-collapse events that produce neutron stars and conventional (i.e., SN 1987A-like) neutrino signals. We take invisible events to be direct-collapse events, which have a higher-energy neutrino signal (Nakazato et al., 2008, 2009). "Failed" supernovae should be invisible from our viewpoint, though some may have weak electromagnetic signals that we henceforth ignore (MacFadyen & Woosley, 1999).

The focus of this paper is to quantify how the CSNR determination by future synoptic sky surveys will improve the DSNB prediction, and to point out some of the science payoff of this improvement. After summarizing the DSNB calculations (§3.3), we present our forecasts for the CSNR measurements by synoptic sky surveys (§3.4). Using these, we show the impact

on the DSNB (§3.5). In particular, we discuss present constraints on invisible events, and strategies for DSNB data to probe the fraction of massive star deaths that are invisible (§3.6). We then switch to a extremely conservative viewpoint and discuss the robust lower limit on the DSNB (§3.7). Conclusions are summarized in §3.8.

3.3 DSNB Formalism and Physics Inputs

The neutrino signal from the ensemble of cosmic collapse events is conceptually simple, and is given by the line-of-sight integral of sources out to the cosmic horizon (more precisely, to the redshift where star formation begins; in practice, the result does not change once redshifts of a few are reached). The well-known result is

$$\begin{aligned}\phi_\nu(\epsilon) &= 4\pi I_\nu(\epsilon) = c\frac{dn_\nu}{d\epsilon} \\ &= c\int_0^\infty (1+z)\ \left|\frac{dt}{dz}\right|\ \mathcal{R}_{\rm tot}(z)\ N_\nu[(1+z)\epsilon]\ dz, \end{aligned} \tag{3.1}$$

where $I_\nu(\epsilon)$ is the neutrino intensity (flux per solid angle) of cosmic supernova neutrinos with observed energy ϵ. Because Earth is transparent to neutrinos, detectors see a total (angle-integrated) flux $\phi_\nu(\epsilon)$ from the full sky. Note that neutrinos and their energies are measured individually, so the intensity and fluxes measures particle number, not the energy carried by the particles. Two source terms, $\mathcal{R}_{\rm tot}$ and $N_\nu[(1+z)\epsilon]$, appear in Eq. 3.1. $\mathcal{R}_{\rm tot}$ is the cosmic rate of collapse events, i.e., the number of collapse events per comoving volume per unit time in the rest frame. Each source, i.e., each collapse event, has a neutrino energy spectrum $N_\nu(\epsilon_{\rm emit})$ in its emission frame with rest-frame energy $\epsilon_{\rm emit} = (1+z)\epsilon$; the factor $(1+z)$ accounts for the redshifting of energy into the observer's frame. Because we allow for different neutrino energy spectra for core-collapse (CC) and direct-collapse (DC) events, $N_\nu[(1+z)\epsilon]$ can be expressed as

$$N_\nu[(1+z)\epsilon] = f_{\rm CC}\, N_\nu^{\rm CC}[(1+z)\epsilon] + f_{\rm DC}\, N_\nu^{\rm DC}[(1+z)\epsilon], \tag{3.2}$$

where $f_{\rm DC} = \mathcal{R}_{\rm tot}^{\rm DC}/\mathcal{R}_{\rm tot}$ and $f_{\rm CC} = 1 - f_{\rm DC}$ are the fractions for direct-collapse and core-collapse events, respectively; we assume these to be constants independent of time and thus redshift. Because these fractions are very uncertain, below we will consider a range of possible values. Finally, for the standard ΛCDM cosmology the time interval per unit redshift is

$$\begin{aligned}\left|\frac{dt}{dz}\right| &= \frac{1}{(1+z)H(z)} \\ &= \frac{1}{(1+z)H_0\sqrt{\Omega_{\rm m}(1+z)^3+\Omega_\Lambda}}.\end{aligned} \tag{3.3}$$

Equation 3.1 shows that three inputs control the DSNB: (i) cosmology, via the cosmic line integral and parameters; (ii) supernova neutrino physics, via the source spectrum. (iii) astrophysics, via the CSNR. Of these, the cosmological inputs entering via Eq. 3.3 are very well understood and their error budget is negligible. We adopt the standard ΛCDM model, with parameters from the 5-year WMAP data: $\Omega_{\rm m} = 0.274$, $\Omega_\Lambda = 0.726$, and $H_0 = 70.5$ km s^{-1} Mpc^{-1} (Komatsu et al., 2009). Within this fixed cosmology, DSNB predictions require knowledge of the source spectra and CSNR. The purpose of this paper is to forecast the effects of future improvements on the source rate, but to illustrate these we must adopt source spectra.

Core-collapse neutrino spectra are in principle calculable from detailed supernova simulations, e.g., (Buras et al., 2006; Janka et al., 2007; Mezzacappa et al., 2001; Thompson et al., 2003; Sumiyoshi et al., 2007). In practice, it remains quite difficult to simulate supernova neutrino emission accurately within realistic explosion models (if they explode at all!) and certainly it remains computationally prohibitive to perform such *ab initio* simulations over wide ranges of supernova progenitors. Consequently, in DSNB predictions different groups have taken different approaches in estimating neutrino energy source spectra. Here, we adopt the treatment in the recent DSNB forecasts of Horiuchi et al. (2009). These authors approximated the neutrino energy spectra as Fermi-Dirac distributions with zero chemical

potential:

$$N_\nu(\epsilon) = \mathcal{E}_\nu \frac{120}{7\pi^4} \frac{\epsilon^2}{T_\nu^4} (e^{\epsilon/T_\nu} + 1)^{-1}, \tag{3.4}$$

where $\mathcal{E}_\nu$ is the total energy carried in the electron antineutrino flavor and T_ν is the effective electron antineutrino temperature. Neutrino flavor change effects are absorbed into the choices of $\mathcal{E}_\nu$ and T_ν. Following Horiuchi et al. (2009), we assume the total energy is equally partitioned between each neutrino flavor for both core-collapse and direct-collapse events, i.e. $\mathcal{E}_\nu = \mathcal{E}_{\nu,\rm tot}/6$ for individual neutrino flavor, where $\mathcal{E}_{\nu,\rm tot}$ is the total (all-species) energy output. The variation in neutrino emission from different core-collapse progenitor stars is in general expected to be small because neutrinos come from newly-formed neutron stars. We adopt $\mathcal{E}_{\nu,\rm tot} = 3\times10^{53}$ erg per core-collapse event. Horiuchi et al. (2009) finds that the average temperature after neutrino mixing is constrained to lie in the range $T_\nu \sim 4 - 8$ MeV. We choose $T_\nu = 4$ MeV as our benchmark temperature, which is close to the empirically-derived spectrum of SN 1987A (Yüksel & Beacom, 2007).

For the direct-collapse events, hydrodynamic simulations show that the neutrino spectra are sensitive to the progenitor masses and nuclear equation of states, with models giving total neutrino energy outputs ranging from 1.31×10^{53} to 5.15×10^{53} erg and different neutrino average energies ranging from $\epsilon_\nu^{\rm avg} = 18.6$ to 23.6 MeV (Sumiyoshi et al., 2007, 2008; Nakazato et al., 2008, 2009). We choose the model with higher energy so it will create a greater difference for comparison. That is, we take $\mathcal{E}_{\nu,\rm tot} = 5.2 \times 10^{53}$ erg, and $T_{\bar{\nu}_e} = \epsilon_\nu^{\rm avg}/3.15 = 7.5$ MeV.

In what follows, we first take all supernovae to be core-collapse events (thus visible) as the fiducial case, and then we will examine the impact of the direct collapse (invisible) supernova scenario. Since the emission from the direct-collapse events is taken to be larger, this will increase the DSNB detection rates. Cosmic supernova neutrinos will be detected mainly via inverse beta decay $\bar{\nu_e} + p \to n + e^+$ interactions with protons in a liquid water or scintillator detector. This reaction is endoergic with the threshold energy of 1.8 MeV. To a good approximation, the nucleon remains at rest, so that $\epsilon_{e^+} \simeq \epsilon - \Delta$, where ϵ_{e^+} is the

positron total energy, ϵ is the $\bar{\nu}_e$ energy, and $\Delta = m_n - m_p = 1.295$ MeV. The expected differential event rate, per unit time and energy, is

$$\frac{dR_{\rm detect}}{d\epsilon} = N_p \; \sigma_{\nu p}(\epsilon) \; \phi_\nu(\epsilon) \quad . \tag{3.5}$$

The well-known inverse beta decay cross section $\sigma_{\nu p}(\epsilon)$ (Vogel & Beacom, 1999; Strumia & Vissani, 2003), taken here at lowest order, and which increases with energy roughly as ϵ^2. Thus the event rates give larger weight to the high-energy neutrino flux, which, as we will see is the regime best probed by supernova surveys. The total event rate in a detector sensitive to neutrino energies ϵ is thus $R = \int_{\epsilon_{\rm min}}^{\epsilon_{\rm max}} dR/d\epsilon \; d\epsilon$. The factor N_p in Eq. 3.5 gives the number of free protons (those in hydrogen atoms) in the detector; in our calculations, we use the value corresponding to 22.5 kton of pure water for Super-K.

The upper panel of Fig. 3.1 shows the neutrino event rate – the integrand of Eq. (1) with $T_\nu = 4$ MeV – with respect to redshift at certain fixed observed energies. Because of redshift, neutrinos with low observed energies are more likely to come from high redshift supernovae, while neutrinos with high observed energies are more likely to come from low redshift supernovae.

A measurement of DSNB neutrinos and their energy spectrum will thus provide unique new insights into the physics of massive-star death. But for the DSNB to usefully probe the neutrino emission from supernova interiors, the cosmic source rates must be known. It is to this that we now turn.

3.4 DSNB Astrophysics Input

The CSNR not only controls the DSNB flux, but also is of great intrinsic interest, and has a direct impact on numerous problems in cosmology and particle astrophysics. The stellar progenitors of both core-collapse and direct-collapse events are very short-lived; consequently the CSNR is closely related to the cosmic *star-formation* rate, which has been intensively

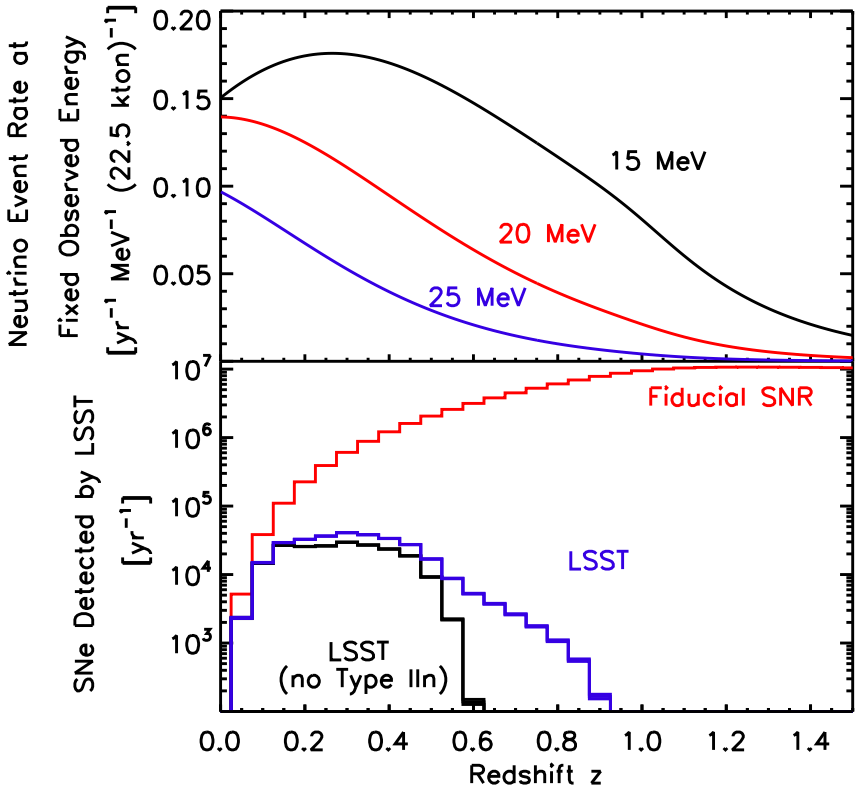

Figure 3.1: DSNB and synoptic survey redshift distributions. *Upper Panel*: The integrand of Eq. 3.1 as a function of redshift for different choices of observed neutrino energies; this shows the redshift distribution of sources that contribute to the DSNB signal at these energies. Here we assume all the supernovae are core-collapse events, as defined in §3.2. *Bottom Panel*: The blue curve is the supernova detection rate by LSST in r-band as a function of redshift, with survey depth $m_{\rm lim}^{\rm sn} = 23^{\rm mag}$ and sky coverage of 6.1 sr (20,000 deg^2). The black curve is a more conservative estimation of the LSST supernova detection rate by excluding Type IIn supernovae, which seem to be the most luminous based on the small sample of current data. The red curve is the fiducial supernova rate for comparison, which is the full-sky supernova rate without considering dust extinction or survey depth. The curves have bin size $\Delta z = 0.05$, and the band thickness (which are in most cases thinner than the curve width) represent the statistical uncertainty $1/\sqrt{N}$.

studied for the past decade (Madau et al., 1996; Hopkins, 2004, 2007; Hopkins & Beacom, 2006). From the present epoch back to $z \sim 1$, the cosmic star-formation rate increases by an order of magnitude. At higher redshifts, $z \gtrsim 1$, the cosmic star-formation rate becomes less certain, but the $z \lesssim 1$ regime is responsible for a large fraction of the observable DSNB

signal. On the other hand, while the *shape* of the cosmic star-formation rate is relatively secure, the absolute *normalization* remains harder to pin down. Recent estimates using multiwavelength proxies for the star-formation rate indicate a $\pm 20\%$ uncertainty at $z = 0$ and a larger uncertainty at higher redshift, producing an average of $\pm 40\%$ uncertainty on the DSNB detection rate (Horiuchi et al., 2009). For the direct supernova rate data reported in Horiuchi et al. (2009), here we adopt a $\pm 40\%$ uncertainty at $z = 0$, double that on the star-formation rate itself (this should not be confused with the 40% above).

Fortunately, a new generation of powerful sky surveys are poised to offer a new, high-statistics measure of the CSNR. These surveys have wide fields of view and large collecting areas, in order to produce deep scans of large portions of the sky. These synoptic surveys are designed to repeatedly scan a large portion of the sky every few nights with limiting single-exposure magnitudes of $\sim 21^{\mathrm{mag}}$ to $\sim 24^{\mathrm{mag}}$, and possibly deeper in several passbands. Relatively more modest prototype synoptic surveys have already been completed, e.g., SDSS-II (Frieman et al., 2008; Sako et al., 2008) and SNLS (Bazin et al., 2009; Palanque-Delabrouille et al., 2010), or are underway, e.g., the Pan-STARRS 1 prototype telescope has already seen first light (Tonry, 2003), and the Palomar Transient Factory already reported their first results (Rau et al., 2009). Large-scale planned surveys include DES (The Dark Energy Survey Collaboration, 2005), LSST (The Large Synoptic Survey Telescope Collaboration, 2007; Tyson, 2002), SkyMapper (Keller et al., 2007), and the full-scale Pan-STARRS.

These synoptic surveys will repeatedly scan the sky with revisit times ("cadences") of $\sim$ few days. The cadence timescale is ideally suited for following supernova light curves and detecting events near maximum brightness. Indeed, the SNLS have reported 289 confirmed Type Ia events and 117 confirmed core-collapse supernovae out to $z \sim 0.4$ (Bazin et al., 2009; Palanque-Delabrouille et al., 2010). SDSS-II also reported 403 spectroscopically confirmed events (Frieman et al., 2008; Sako et al., 2008) (most of which were Type Ia), and 15 confirmed Type IIp events that are potentially capable of being used as standardized candles (D'Andrea et al., 2010). The Palomar Transient Factory has already found (Quimby

et al., 2009) three events which are among the most luminous core-collapse events ever found, and which appear to be pulsational pair-instability explosions of ultramassive stars. Finally, Pan-STARRS 1 has reported its first confirmed supernova (Tonry, 2003).

Note that these surveys are *unbiased* in that they cover a large portion of the sky regions systematically and thus do not pre-select galaxy types or redshifts or luminosities for supernova monitoring, whereas most of the past supernova surveys monitored pre-selected galaxies so that the results were biased, though attempts have been made to correct for that.

Currently, most of the design efforts for synoptic surveys focus on Type Ia supernovae, because these events are a crucial cosmological distance indicator at large redshifts. However, the survey requirements for Type Ia supernova detection are also well-matched to collapse events, and therefore surveys that are tuned for Type Ia supernovae will automatically observe collapse events also. With their proposed properties, these surveys are expected to discover $\sim 10^5$ collapse events per year out to redshift $z \sim 1$ (Young et al., 2008b; Lien & Fields, 2009). Due to the large sample size, spectroscopic followup is unfeasible for most events, so photometric redshifts of the host galaxies (for which deep co-added fluxes will be available) or of the supernovae themselves will be needed, just as in the case of Type Ia events (Zheng et al., 2008).

Lien & Fields (Lien & Fields, 2009) give detailed predictions for the supernova harvest by synoptic surveys; here we summarize the key factors important for the DSNB. Within the 5-color SDSS *ugriz* bandpass system, the r and g bands provide the largest supernova harvest, due largely to high detector efficiency for these wavelengths. Moreover, distant intrinsically blue collapse events are redshifted into these bands. Detection of a supernova is done by differencing exposures of the same field of view. To determine if a transient is a supernova and to establish its type, one must follow the supernova through the rise and fall of its light curve. Consequently the peak flux must be brighter than the minimum flux for point source detections, and following Lien & Fields (2009) we set a supernova limiting magnitude $m_{\rm lim}^{\rm sn} = m_{\rm lim} - 1^{\rm mag}$ that is brighter by $1^{\rm mag}$ than the single-visit point-source limit

$m_{\rm lim}$. Finally, for a given scan cadence timescale, a survey must trade off scan area $\Delta\Omega_{\rm scan}$ and exposure depth $m_{\rm lim}^{\rm sn}$. Surveys with large scan area, such as Pan-STARRS and LSST, are planned to have survey depth $m_{\rm lim}^{\rm sn} = 23^{\rm mag}$.

The blue curve in the lower panel of Fig. 3.1 plots the expected collapse event rate detected by LSST in r-band. One can see from the plot that in one year, LSST will have more than 100 supernova detections in each $\Delta z = 0.05$ redshift bin out to redshift $z \sim 0.9$, and for $z \simeq 0.1 - 0.5$, LSST will be able to detect more than 10^4 supernovae in each bin. Lien & Fields (2009) shows that Type IIn supernovae contribute to most of the detections for $z \gtrsim 0.5$ based on the luminosity functions provided in Richardson et al. (2002). Since this higher end of the detection redshift range is highly affected by the small sample of Type IIn in Richardson et al. (2002), we also plot the black curve for reference to show a more conservative estimation that excludes Type IIn supernovae. One can see that the detection would reach $z \sim 0.6$ in this case. The thickness of the blue and black curve represent the statistical uncertainty ($1/\sqrt{N}$), which in most cases are thinner than the curve width because the uncertainty is very small due to the large number of supernovae. The full-sky fiducial supernova rate based on Horiuchi et al. (2009) is also plotted for comparison. The difference between the fiducial supernova rate and the LSST detection rate is mainly due to survey depth (magnitude/flux limit), sky coverage and to a lesser extent dust obscuration.

A high precision measurement of the CSNR can therefore be done via direct counting of the enormous number of collapse events versus redshift. While a measurement of the CSNR *shape* will test the consistency with results inferred from other methods, such as the star-formation history, the real power of synoptic surveys will be the high-statistics determination of the CSNR *normalization*. Note that this can in principle be determined by precision measurement of the CSNR at a *single* redshift bin, where the counts are the largest. For a large survey like LSST, this should occur around $z \sim 0.3$, which is set by the tradeoff of survey volume and limiting magnitudes (Lien & Fields, 2009). In general, LSST is expected to probe the CSNR out to redshift $z \sim 0.9$ to $1/\sqrt{N} \sim 10\%$ statistical precision

within one year of observation.

As mentioned earlier, detections in the $z \sim 0.5 - 0.9$ range will be dominated by the most luminous core-collapse events. In a study of the core-collapse luminosity function based on relatively sparse and inhomogeneously taken data, the relatively rare Type IIn events were found to be the most intrinsically luminous (Richardson et al., 2002); and ultraluminous Type IIn events have been found (Smith et al., 2007; Drake et al., 2010; Rest et al., 2011). Recent observations, including those by the synoptic Palomar Transient Factory and by ROTSE-III/Texas Supernova Search, show that other core-collapse types can also lead to ultraluminous explosions; of these, the newly-discovered pair-instability outbursts are particularly intriguing and encouraging because this entire class of events has likely gone unnoticed until now (Gezari et al., 2009b; Miller et al., 2009; Gal-Yam et al., 2009; Quimby et al., 2009). There is clearly much more to be learned about the bright end of the supernova luminosity function. As more data of these ultraluminous events become available, the redshift reach of synoptic surveys will come into a much better focus.

3.5 Impact of Synoptic Surveys on the DSNB

We are now in a position to assess the synoptic survey impact on the DSNB. Our viewpoint is to envision the situation several years from now, when synoptic surveys have been running in earnest, and when the DSNB signal has been at last detected. Of course, real surveys will miss core-collapse events for a variety of reasons, yet following Lien & Fields (2009) we believe there is good reason to expect that these losses can be calibrated, empirically or semi-empirically, and thus the absolute CSNR can be obtained out to $z \lesssim 1$; this should verify the already well-determined shape of the cosmic star-formation rate in this regime. Furthermore, surveys will definitely measure the low-redshift *normalization* of the CSNR to high precision via *direct counting*.

To be sure, it will be far from trivial to arrive at the understanding we presuppose. There

will be formidable astrophysical challenges in extracting from survey data the supernova properties of interest, most importantly the event type, redshifts, and obscuration; less crucially for our purposes one would like as well the intrinsic luminosity. Lien & Fields (2009) discusses some reasons for optimism in the face of these challenges, and we also remind the reader that these issues are crucial not only for studies of the DSNB but also are central for other key topics in astrophysics and cosmology. Most notably, the problems of obtaining supernova type, redshift, and obscuration are at least as pressing (and in some respects more challenging) when one uses supernovae as cosmological distance indicators and thus as probes of dark energy. Put differently, if survey supernovae are understood well enough to do dark energy cosmology, then we expect that the star-formation rate should be well-understood enough to give the DSNB source history out to $z \sim 1$, and the CSNR normalization to high precision.

We now explore the impact of a CSNR determination of this kind. That is, we assume that one can use synoptic surveys to infer the absolute normalization and shape of the CSNR out to some redshift $z_{\rm max}$. In particular, Lien & Fields (2009) showed that all core-collapse types should be visible out to $z_{\rm max} \gtrsim 0.5$, and the very bright Type IIn events should extend to $z_{\rm max} \gtrsim 1$ (Smith et al., 2007; Drake et al., 2010; Rest et al., 2011; Cooke, 2008). Thus we will take the CSNR *shape* to be directly known from surveys to $z = 1$, and following Lien & Fields (2009) we assume that the *normalization* will be very well-determined statistically, and so we will anticipate a measurement good to $\delta\mathcal{R}_{\rm tot}/\mathcal{R}_{\rm tot} = 5\%$; this error would be dominated by systematic uncertainties at the most relevant redshifts.

Referring again to Fig. 3.1, we compare the redshift reach of synoptic surveys with the redshift distribution of the DSNB sources. We see that the two are well matched. That is, within the detection energy range ($\sim 10-26$ MeV positron energy), the neutrino sources peak within the redshift range of upcoming supernova surveys. Quantitatively, the detection rate is about 1.8 neutrinos/year within the detector energy range of 10 – 26 MeV positron energy for neutrinos from all redshifts (i.e., $z_{\rm max} = 6$). Of this total rate, events within redshift

$z = 1$ contribute 1.5 (87%) neutrinos/year, and events within redshift $z = 0.5$ contribute 1.0 (54%) neutrinos/year. Our results are in good agreement with the numbers shown in Horiuchi et al. (2009) and Ando (2004). Therefore a large fraction of the observable neutrinos come from events within $z \sim 1$, which is about the same redshift range as the upcoming supernova surveys.

We thus see that using supernovae to directly infer the CSNR allows us to robustly predict a large fraction of the detectable neutrino events. A high precision measurement of the CSNR would therefore put a better constraint on the DSNB flux, which encodes knowledge of supernova neutrino physics. For example, one would then be able to distinguish the difference between neutrino models with different effective temperatures, as demonstrated in Fig. 3.2.

Figure 3.2 plots the neutrino detection rates estimated based on models with different neutrino effective temperatures ($T_\nu = 4$, 6, 8 MeV, respectively) versus neutrino energy in the observer's frame. The upper panel shows the current $\delta\mathcal{R}_{\rm tot}/\mathcal{R}_{\rm tot} = 40\%$ uncertainty in the cosmic supernova rate normalization. The bottom panel shows the future normalization uncertainty of $\delta\mathcal{R}_{\rm tot}/\mathcal{R}_{\rm tot} = 5\%$ (dominated by systematics), which would be achieved within one year observation of the upcoming supernova surveys. One can see that it is not easy to distinguish different neutrino models with the current 40% uncertainty. However, with a future 5% precision, it would be certainly possible to distinguish the differences between each models and therefore provide a way to study supernova neutrino physics by combining neutrino detections and supernova surveys.

Moreover, after several years of exposure, one might hope to attain statistics sufficient to measure the *difference* between the observed flux and the contributions from lower-redshift epochs sampled by survey supernovae. This difference encodes a wealth of interesting physics and astrophysics.

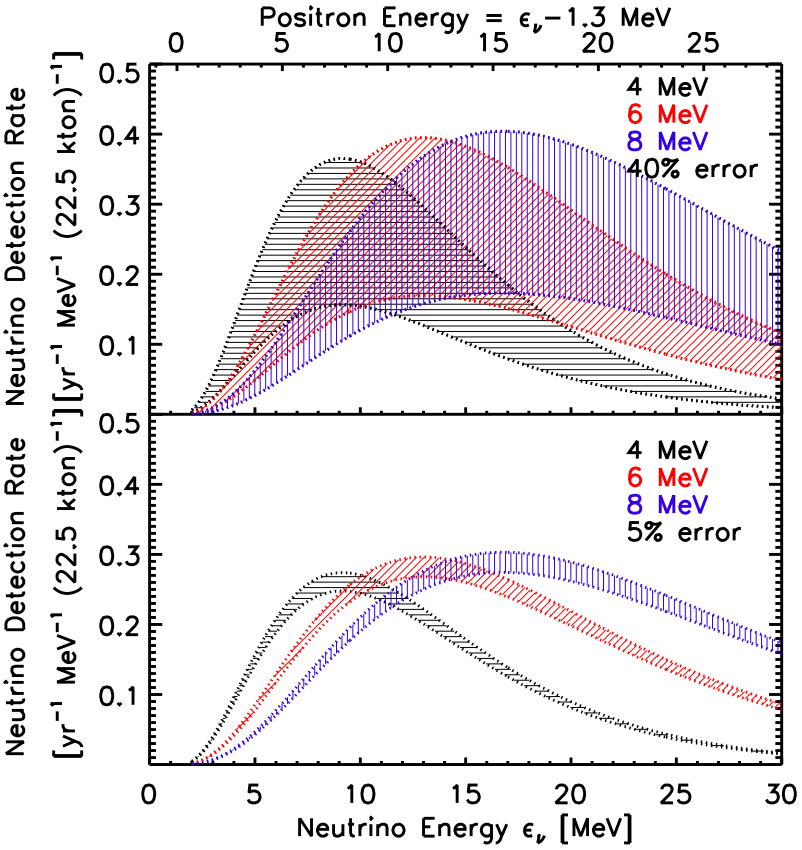

Figure 3.2: *Upper Panel*: Neutrino detection rate as a function of neutrino observed energy, with different neutrino effective temperatures are plotted for comparison (curves from left to right represent 4, 6, 8 MeV, respectively). The band thickness of the curves represent a $\delta\mathcal{R}_{\rm tot}/\mathcal{R}_{\rm tot} = 40\%$ uncertainty in the current CSNR normalization. *Bottom Panel*: Same as the upper panel, but with a 5% normalization uncertainty instead, which is the uncertainty expected from upcoming supernova surveys with one year observations.

3.6 Invisible Supernovae Revealed

The most dramatic possibility for a mismatch between the neutrino and optical supernova measures would reflect a real lack of optical explosions due to "invisible" supernovae. As mentioned in Section 3.3, even in the context of conventional models there is a great uncertainty about whether stars with masses between 25 to 40 $M_\odot$ explode or not. A Salpeter initial mass function $dN_\star/dm \propto m^{-2.35}$ (Salpeter, 1955), dictates that for collapse events in the $8 - 100M_\odot$ range, $\sim 90\%$ are core-collapse events (masses $\lesssim 40M_\odot$), which in our

assumption make optically luminous explosions even for those that form black holes from fallback, and $\sim 10\%$ are direct-collapse events ($\gtrsim 40 M_{\odot}$) that are optically invisible, but have larger neutrino emission with greater total energy $\mathcal{E}_{\nu,\mathrm{tot}}$ and higher neutrino average temperature T_{ν}. A relatively conservative case, which has recently been studied by Lunardini (Lunardini, 2009), would then assume that around 10% of collapse events failed to explode, hence one would expect that the neutrino flux from neutrino detectors would at least be $\sim 10\%$ higher than neutrino flux from supernova surveys.

However, there remain large uncertainties in our *qualitative* understanding of massive star death, not to mention even larger quantitative uncertainties in neutrino and photon outputs. If, as expected, the neutrino emission is larger for these events than for ordinary supernovae, then the signal increase in the detectors can be significantly larger (Daigne et al., 2005; Lunardini, 2007; Sumiyoshi et al., 2007; Horiuchi et al., 2009; Sumiyoshi et al., 2008; Nakazato et al., 2008, 2009; Lunardini, 2009). Given these substantial uncertainties it is entirely possible that the invisible fraction is much higher than 10%. For example, one possible scenario is that supernovae that form black holes from fallback might actually belong to the invisible events category. Fryer (2009) predicts the light curves of these fallback events with peak magnitudes around $V = -13$ to -15, which correspond to luminosities several orders of magnitude lower than ordinary core-collapse events. These authors also suggest that the total neutrino emission from the fallback events can be larger than normal supernovae (Fryer, 2009). Thus if we treat the fallback supernovae as invisible events with larger neutrino emission, the invisible fraction will be higher than current estimates would suggests (Lunardini, 2009). Therefore we will take the invisible fraction as an *a priori* free parameter, and explore constraints based on neutrinos and other observables.

Fig. 3.3 shows several constraints on the visible supernova rate $\mathcal{R}_{\mathrm{vis}}$ and invisible supernova rate $\mathcal{R}_{\mathrm{invis}}$ at $z = 0$. These constraints are estimated based on current data with the assumption that the *shape* of the CSNR is known, and we adopt the fiducial model described in Horiuchi et al. (2009). Blue regions in the plot represent the allowed regions;

the gray region represents the explicit exclusion from the non-observation of neutrinos; and white regions represent areas that are disallowed implicitly, that is, they lie outside of current allow regions but are not banned directly based on current limits.

One way to constrain $\mathcal{R}_{\rm tot}$ is using the current *observed cosmic star-formation rate*. The ratio of massive star counts per unit mass into all stars depends only on the choice of initial mass function; we take this ratio to be $0.007/M_\odot$ assuming the Salpeter Initial Mass Function (IMF) (Salpeter, 1955). With the uncertainty $\sim 20\%$ in the cosmic star-formation rate normalization (Horiuchi et al., 2009), the upper and lower limit of current star formation rate at $z = 0$ correspond to $\mathcal{R}_{\rm tot}(0) = 1.25 \pm 0.25 \times 10^{-4}\,{\rm yr}^{-1}\,{\rm Mpc}^{-3}$. respectively, which set the darker blue region in Fig. 3.3. Also, the present *observed CSNR* with $\sim 40\%$ uncertainty in its normalization is plotted as the light-blue region in Fig. 3.3, which correspond to the value of $\mathcal{R}_{\rm tot}(0) = 1.25 \pm 0.50 \times 10^{-4}\,{\rm yr}^{-1}\,{\rm Mpc}^{-3}$.

The *DSNB limit* in Fig. 3.3 shows the constraint estimated from the current non-detection of the supernova neutrino background, which sets an upper bound of the total core-collapse supernova rate $\mathcal{R}_{\rm tot} = \mathcal{R}_{\rm vis} + \mathcal{R}_{\rm invis}$. Yüksel et al. (2006) points out that the upper limit on the neutrino flux set by Super-K in 2003 corresponds to an upper limit of 2 events per year for a 22.5 kton detector in the energy range of 18 – 26 MeV (see also Lunardini & Peres (2008) for the temperature dependence of the Super-K limits in terms of flux instead of event rate). For the benchmark $T_\nu = 4$ MeV case, this limit allows the current $\mathcal{R}_{\rm tot}$ to be 4.7 times larger than current fiducial value if we assume all neutrino emission comes from visible events. On the other hand, the Super-K limit implies a current $\mathcal{R}_{\rm tot}$ that is 0.64 times smaller than our fiducial value if all neutrino emission comes from invisible events. Note that these two factors are not the same because there is more neutrino emission per invisible event.

The DSNB constraint has substantial uncertainties from both the visible and invisible supernova contributions. The neutrino emission from visible events depends on the neutrino emission spectrum, i.e., temperature. To illustrate how this would change the DSNB limit,

we also plotted the DSNB limit when assuming visible events have $T_\nu = 6$ MeV instead of 4 MeV. The 6 MeV line intersects the $\mathcal{R}_{\rm vis}$ axis at 1.9 instead of 5.8 for the 4 MeV line. While the uncertainty in the neutrino emission from visible events would affect where the DSNB limit intersect with the $\mathcal{R}_{\rm vis}$ axis, the uncertainty in the neutrino emission from invisible events would change where the limit intersects with the $\mathcal{R}_{\rm invis}$ axis. In this paper we adopt the highest-energy case for the neutrino emission from invisible events; however, if we choose the lowest-energy case in Nakazato et al. (2008, 2009), then the limit would intersect with the $\mathcal{R}_{\rm invis}$ axis at 4.6 and the whole region shown in Fig. 3.3 would be allowed by this limit and thus would give a weaker constraint.

In addition to constraints based on current observational data, Kochanek et al. proposed new method of probing invisible supernovae (Kochanek et al., 2008). These authors suggested monitoring a million supergiants, in galaxies within 10 Mpc. Because the supergiant phase lasts $\sim 10^6$ years, every year about one monitored supergiant will end its life. While some events will result in an ordinary optically bright supernovae, if any events lack optical outbursts – and are thus invisible by our definition – they will simply *disappear* in sight. Considering that the local cosmic star-formation rate is about two times higher than the cosmic average, the lowest invisible event rate that predicts one disappearing event in the proposed five years observation is around $\mathcal{R}_{\rm invis} = 0.25 \times 10^{-4}\,{\rm yr}^{-1}\,{\rm Mpc}^{-3}$. This line is shown as the horizontal line labeled as *sensitivity to stellar disappearance* in Fig. 3.3.

Despite the preliminary nature of some of the constraints in Fig 3.3, several interesting trends already emerge. The allowed region for invisible supernovae is nonzero, but it is bounded and cannot be arbitrarily large. Future observations will severely restrict the allowed region for visible supernovae. Obviously, the mere demonstration that $\mathcal{R}_{\rm invis}$ is nonzero would immediately offer novel and unique insight into supernova physics. Moreover, any quantitative determination of the absolute value of $\mathcal{R}_{\rm invis}$ or the ratio $\mathcal{R}_{\rm invis}/\mathcal{R}_{\rm vis}$ would give detailed insight into the explosion mechanism over the full range of core-collapse events.

Also, Fig. 3.3 allows a larger invisible fraction than the $f_{\rm invis} = 10\%$ predicted from

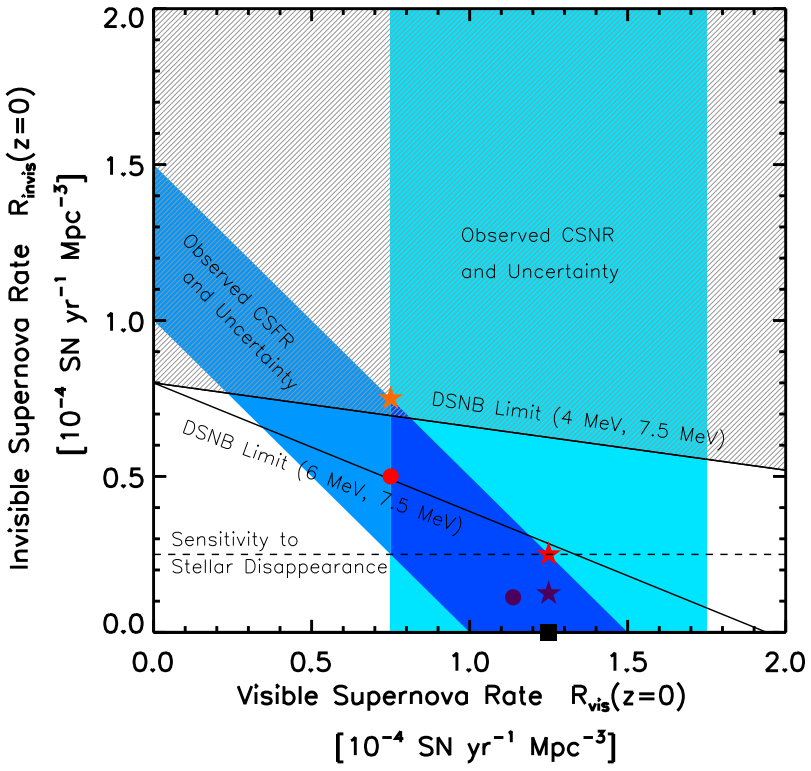

Figure 3.3: Summary of current and future constraints on the invisible supernova rate $\mathcal{R}_{\rm invis}$ (i.e. the direct-collapse event rate in our assumption) and the visible supernova rate $\mathcal{R}_{\rm vis}$ (i.e. the core-collapse event rate in our assumption). Blue regions are those allowed by current observed cosmic star-formation rate (CSFR) and CSNR and their uncertainties. The grey-lined region is disallowed based on the non-detection of the DSNB by Super-K with the assumption that $T_\nu = 4$ MeV for visible events and 7.5 MeV (and also a higher total energy) for invisible events. Another DSNB limit with $T_\nu = 6$ MeV instead of 4 MeV is also plotted for comparison. The horizontal dashed line shows the sensitivity to stellar disappearance, which will directly probe the invisible supernova rate (Kochanek et al., 2008). Note circles explored in Fig. 3.4 and stars in Fig. 3.5. Square marks a baseline shown in Fig. 3.4 and 3.5.

current theory. We marked several possible invisible fractions that we will discuss more in the figures below. The square represents a baseline, with invisible fraction $f_{\rm invis} = 0\%$. Circles mark possible $f_{\rm invis}$ assuming the total CSNR is fixed to the fiducial number of $\mathcal{R}_{\rm tot} = 1.25 \times 10^{-4}\,{\rm yr}^{-1}\,{\rm Mpc}^{-3}$. The purple circle is the conservative case with $f_{\rm invis} = 10\%$, and red circle marked the highest invisible fraction ($f_{\rm invis} = 40\%$) one can reach with $\mathcal{R}_{\rm tot}$

fixed. The corresponding changes in the DSNB detection are shown in Figure 3.4, where we see that when error in $\mathcal{R}_{\rm vis}$ drops to 5%, it will become possible to tell the difference between these three cases in the detectable neutrino energy range. The energy dependence of the fraction traces back to the higher energy of the neutrino flux from black hole forming supernovae. Therefore invisible events contribute a larger fraction of the neutrino flux at higher neutrino energy.

Another set of key points in Fig. 3.3 are marked with stars. In choosing these points, we allow for the uncertainties in $\mathcal{R}_{\rm vis}$ in order to explore even higher possible $f_{\rm invis}$ values while staying within current limits. If the visible event rate is fixed to the fiducial number of $\mathcal{R}_{\rm vis} = 1.25\times10^{-4}\,{\rm yr}^{-1}\,{\rm Mpc}^{-3}$, then the purple star marks the point with $f_{\rm invis} = 10\%$ adding to current fiducial $\mathcal{R}_{\rm vis}$, and the red star marks the point with $f_{\rm invis} = 17\%$, which is the highest $f_{\rm invis}$ one can reach with $\mathcal{R}_{\rm vis}$ fixed. However, the visible event rate is quite uncertain and could fall substantially below our fiducial value. Including this uncertainty, the highest $f_{\rm invis}$ that is allowed by current limit is around the point marked by the orange star with $f_{\rm invis} = 50\%$. Note that this point seems to lie just outside the DSNB constraint, however, one should keep in mind that the DSNB constraint is very sensible to theoretical assumption of the supernova neutrino emission and hence has its own uncertainty, as discussed earlier.

The DSNB detections corresponding to the points marked by stars are shown in Figure 3.5. Note that the black curve with $f_{\rm invis} = 0\%$ represents the neutrino detections from the visible events, and thus is the one that would be estimated by supernova surveys; the purple and red curves include different fractions of invisible events on top of the visible events, which represent those that would be detected by neutrino detectors. Therefore Fig. 3.5 illustrates how the differences between DSNB from neutrino detectors and supernova surveys would encode information of the fraction of invisible events. Again, the band thickness in this figure indicates the expected 5% uncertainty in $\mathcal{R}_{\rm vis}$, and it is clear that these three cases will be distinguishable. The DSNB detections for the very extreme case with $f_{\rm invis} = 50\%$ is plotted as the orange curve for comparison.

A 50% invisible event fraction would lead to a significant difference between flux from neutrino detectors and supernova surveys. We find that neutrinos due to invisible events within $z \sim 1$ would contribute around 75% of the event rate in the detectable energy range. For comparison, we expect the neutrinos associated with dust-obscured supernovae to be about $\sim 20\%$ of the signal. Thus, if the invisible event fraction approaches current limits, the neutrino census of supernovae should be able to rapidly and strongly point to the large contribution from these events. Additionally, an invisible event fraction of 50% could push the mass limit of the direct-collapse events to as low as $\sim 14\ M_{\odot}$ with the Salpeter IMF. However, theories about supernova progenitors remain quite uncertain and therefore the lower mass limit implied by the invisible fraction is also not necessarily well-defined. Once the upcoming surveys put better constraints on the invisible fraction, one can hope to learn more about the mass limit of direct-collapse events.

3.7 Astrophysical Challenges and Payoffs

Our discussion until now has taken a point of view that by the time synoptic surveys are well under way, the loss of supernova detections from dust and survey depth can be corrected, either using the survey data themselves or from followup observations. In this section, we change our viewpoint from this optimistic, wide-ranging anticipation of future progress to a more restricted focus on the power of the survey-detected supernovae alone.

For real surveys, some of the collapse events must be lost from detection mainly due to three factors: survey limiting magnitude, dust obscuration, and the invisible events without optical explosions. On the other hand, neutrino detection will be unaffected by any of these issues. Therefore, neutrino flux from neutrino detectors should exceed that estimated from supernova surveys.

Supernova surveys thus provide a totally empirical, model-independent method to estimate the *extreme lower limit* to the DSNB by simply adding up the neutrino contribution

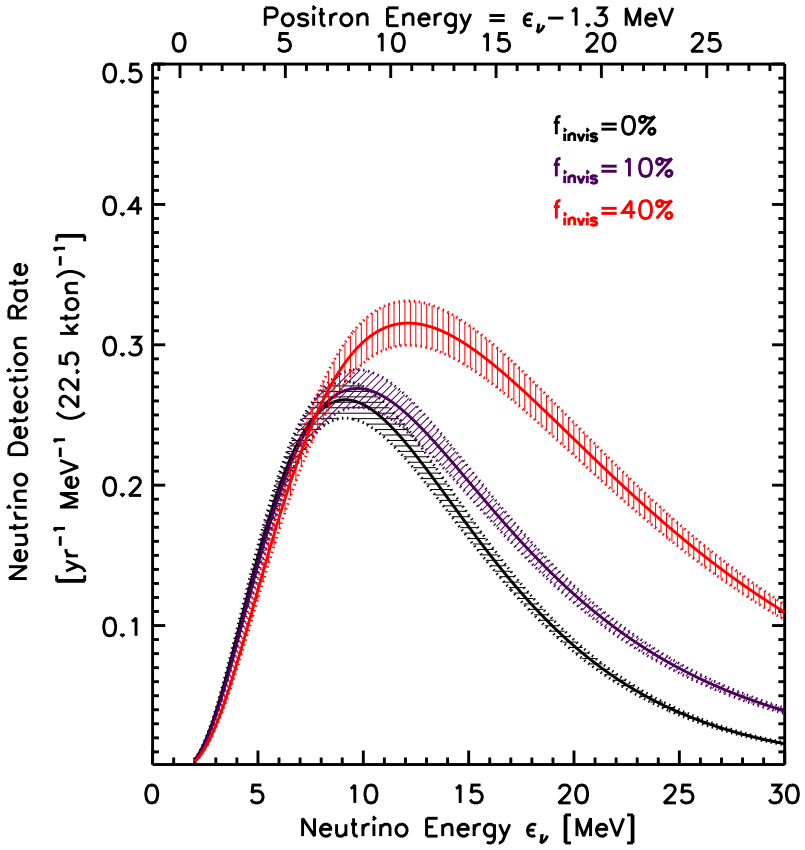

Figure 3.4: One year neutrino detection as a function of neutrino observed energy. Three different fractions of the invisible events are plotted with $\mathcal{R}_{\rm tot}$ fixed to the fiducial number. Curves with different colors correspond to the square/circles with the same color in Fig. 3.3,i.e., red (top) curve represents $f_{\rm invis} = 40\%$, purple (middle) curve represents $f_{\rm invis} = 10\%$, and black (bottom) curve represents $f_{\rm invis} = 0\%$. The band thickness of the curves represent 5% uncertainty expected from upcoming supernova surveys.

from each supernova detected. The resulting lower bound to the DSNB flux is

$$\phi_\nu^{\rm min}(\epsilon) \equiv \phi_\nu^{\rm survey}(\epsilon) = \frac{4\pi}{\Delta\Omega_{\rm scan}\Delta t} \sum_{i=1}^{\rm survey\ SNe} \frac{N_\nu[(1+z_i)\epsilon]}{4\pi D_L(z_i)^2} \tag{3.6}$$

where each term in the sum is the flux contributed by each supernova observed in the survey, and the prefactor includes a correction for the fraction $\Delta\Omega_{\rm scan}/4\pi$ of the sky covered by the survey. The fluxes depend on the luminosity distance $D_L(z)$, which is fixed by precisely known cosmological parameters. Notice that in this equation, only the neutrino energy

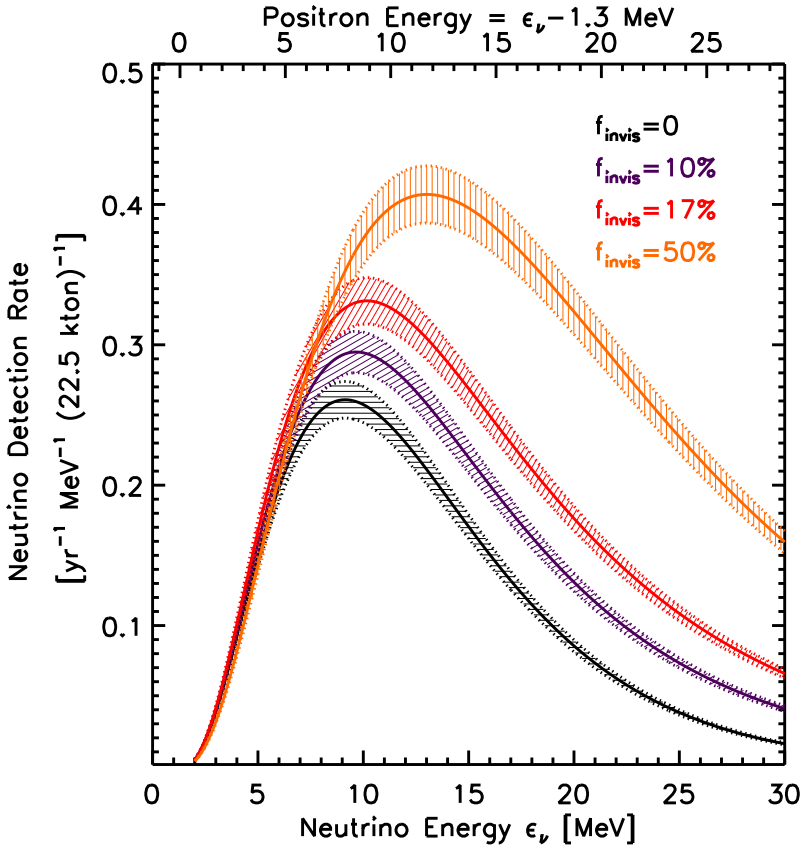

Figure 3.5: Similar to Fig. 3.4. However, we allow larger numbers for $\mathcal{R}_{\rm tot}$. Curves with different colors correspond to square/stars in Fig. 3.3, i.e., Curves with different colors correspond to square/stars in Fig. 3, i.e., orange (top) curve represents $f_{\rm invis} = 50\%$, red (second top) curve represents $f_{\rm invis} = 17\%$, purple (third top) curve represents $f_{\rm invis} = 10\%$, and black (bottom) curve represents $f_{\rm invis} = 0\%$. The band thickness of the curves represent 5% uncertainty expected from upcoming supernova surveys.

spectrum $N_\nu[(1+z_i)\epsilon]$ depends on supernova and neutrino physics.

This "what you see is what you get" approach is robust but conservative. Namely, the result $\phi_\nu^{\rm survey}(\epsilon)$ will be an extreme lower bound for the DSNB flux. More detailed and quantitative discussion can be found in Supplement 3.10.

Once the DSNB is detected, the *difference* between the detected flux and the survey-based lower bound provides a unique measure of the events unseen by surveys. For example, it is conceivable that the survey predictions could *exceed* the DSNB detection (or upper

limit!). This result would be very surprising and thus extremely tantalizing, as it would challenge our assumptions related to supernova physics and neutrino physics. In other words, this would mean that one or both terms in Eq. 3.6, the luminosity distance D_L and/or the supernova neutrino emission spectrum $N_\nu[(1+z_i)\epsilon]$, might be wrong. But the physics behind D_L rests on well-established Friedmann-Robertson-Walker cosmology, and depends only on well-determined cosmological parameters. Thus a "DSNB deficit" would much more likely point to problems in the supernova emission spectrum $N_\nu(\epsilon)$. Therefore, if the lower bound estimation $\phi_\nu^{\rm survey}(\epsilon)$ turn out to be higher than the actual neutrino detections, we would be driven to rethink supernova neutrinos in a way to substantially reduce the observable signal.

The more likely and certainly more conventional expectation is that when the DSNB is detected, its flux will be higher than the supernova survey lower bound $\phi_\nu^{\rm survey}(\epsilon)$. In this case, the *sign* of the difference would be unsurprising, but the *magnitude* of the detected versus survey excess would still encode valuable new information, such as the invisible fraction as discussed in the previous section.

One might also hope for the possibility to combine survey supernovae and the DSNB to probe events that *are* optically visible but are lost due to dust obscuration; this could give insight into the nature and evolution of cosmic dust. To see how $\phi_\nu^{\rm survey}$ would change with different dust models, we examine with two extreme cases: (1) model with extremely low dust obscuration by assuming constant dust obscuration as those at local universe mentioned in Mannucci et al. (2007); and (2) a model with very high dust obscuration by doubling the dust evolution with redshift compares to the model suggested in Mannucci et al. (2007). We find that with $m_{\rm lim}^{\rm sn} = 23$, the neutrino detection rate estimated from uncorrected supernova surveys changes by only $\sim 7\%$ when comparing these two models. That is, dust models (1) and (2) give 0.34 to 0.31 events per year, respectively. Therefore the neutrino detection rate estimated from supernova survey is insensitive to the dust models and hence it will be difficult to use the DSNB to distinguish different dust models with the expected survey precisions.

3.8 Conclusions

With the next generation synoptic surveys coming online, a high precision measurement of the CSNR via *direct counting* will be achieved, and thus greatly reduce the uncertainty in the DSNB to a few percent. An interlocking set of strategies suggest themselves, by which one can leverage survey supernovae and the DSNB to probe neutrino physics as well as the astrophysics of cosmic supernovae. For example, the high-precision DSNB prediction based on supernova surveys would be able to distinguish supernova neutrino models with different neutrino temperatures.

As we have shown, the $z \lesssim 1$ DSNB contribution comprises most of signal at high energy $\gtrsim$ 10 MeV, and so a comparison of the high-energy predictions and observations would measure the amount of events unseen by surveys. One of the exciting possibilities is using the DSNB to probe the fraction of invisible events. With the current uncertainties, the observed cosmic star-formation rates and the CSNR already suggests possible ranges for the invisible fraction. Indeed, limits from present observables allows a substantial invisible events to up to $\sim 50\%$, which is much higher than the fraction suggests by current supernova theories ($\sim 10\%$). Once the upcoming synoptic surveys begin and provide high precisions on the CSNR and the cosmic star-formation rate, one can hope to reveal the fraction of invisible events.

The current non-detection of the DSNB flux also limits the total supernova rate. However, this limit is sensitive to the theoretical assumptions of the total neutrino energy $\mathcal{E}_{\nu,\mathrm{tot}}$ and neutrino temperature T_ν. Therefore the high precision of the DSNB prediction inferred from upcoming supernova surveys will make this limit stronger by providing knowledge of supernova neutrino physics.

While it is unknown whether and to what degree truly invisible supernovae occur, it is certain that survey depth and dust obscuration will also hide supernovae from detections. To interpret the supernova data physically demands that we distinguish between these factors. While the loss from survey depth is likely to be corrected by knowledge of supernova lumi-

nosity function, to entangle the degeneracy between dust obscuration and invisible events will be challenging. However, we believe it is not impossible to discriminate the two. For example, there are observables across multiple wavelengths that can be used to estimate dust extinction. If we can constrain the amount of dust to a higher precision by combining all different ways of measuring dust, then the dust effects can be modeled out [2]. Hence, the only left main unknown would be the fraction of invisible events and we could learn this fraction by comparing the neutrino flux from neutrino detectors and supernova surveys.

On the other hand, even without any extrapolations to the original observational data, precision measurement of the CSNR will be achieved by upcoming surveys, and thus will infer a robust lower limit of the DSNB flux by simply adding up the neutrino contribution from each supernova.

We conclude by again underscoring the happy accidents that large-scale synoptic sky surveys will come online just at the time that large neutrino experiments should first discover the DSNB, and that the redshift reach of the two are comparable. By exploiting the interconnections among the results from these observatories, we have a real hope of shedding new light into particle physics and particle astrophysics.

3.9 Acknowledgments

We are pleased to thank Avishay Gal-Yam and Jim Rich for enlightening discussion of supernova discovery by synoptic surveys and the challenges and opportunities these present. We are grateful to the anonymous referee for helpful comments that have improved this paper. We would also like to thank the Theoretical Physics Institute at the University of Minnesota, and to the Goddard Space Flight Center for their hospitality while some of this work was done. J.F.B. was supported by NSF CAREER Grant PHY-0547102.

[2] A possible cross-check here are Type Ia events. These are due to an older stellar population than core-collapse events and thus should not be preferentially obscured in their immediate locations; however, those in spiral galaxies will still suffer obscuration by host-galaxy disk material that happens to lie along the line of sight. Thus Type Ia obscuration and reddening should set lower limits to the effects suffered by core-collapse events.

3.10 Supplement: Surveys Set a Model-Independent Lower Bound to the DSNB

As mentioned in Section 3.7, a conservative and robust lower bound of the DSNB flux can be predicted by upcoming supernova surveys. Figure 3.6 shows our estimations for the *lower bounds* to the neutrino flux inferred from the core-collapse events detected in the r-band by a synoptic survey. We keep $\Delta\Omega_{\rm scan}$ fixed for simplicity, but show dependence on $m_{\rm lim}^{\rm sn}$ to illustrate the sensitivity to this parameter. Planned surveys have sophisticated scan strategies using a variety of cadences; for reference, the largest scan areas of Pan-STARRS and LSST are planned to have a sensitivity of $m_{\rm lim}^{\rm sn} \approx 23^{\rm mag}$ in the bandpasses of interest.

The upper panel shows the predicted neutrino detection rate from the observed core-collapse events versus neutrino energy. Results for the neutrino detection rate from core-collapse events observed with different limiting magnitude (from $m_{\rm lim}^{\rm sn} = 23^{\rm mag} - 26^{\rm mag}$) are plotted. Additionally, the highest black curve plots the detection rate from *all* core-collapse events within the horizon (i.e., with no limiting magnitude applied) for comparison. The second highest black curve, also shows the detection rate for infinite survey limiting magnitude, but shows an estimate of the effect of dust extinction in the host galaxy. The middle panel shows the integrated neutrino detection rate $\phi_\nu^{\rm survey}(>\epsilon)$ above energy ϵ. In other words, this is the energy-integrated version of the upper panel. The lowest panel shows the fraction of the neutrino detection rate from the observed supernovae over the events from all supernovae in the universe, that is, the corresponding middle-panel red/blue curve divided by the highest black curve.

The difference between the two black curves in Fig. 3.6 gives an indication of the neutrino contribution from dust-obscured supernovae. We see that an even larger effect is the loss of supernovae due to finite survey limiting magnitude. Note that when adding dust effects and limiting magnitudes, the reductions of detection rates are more severe at low neutrino energies. This is because observed neutrinos are redshifted, and as a result, a larger portion

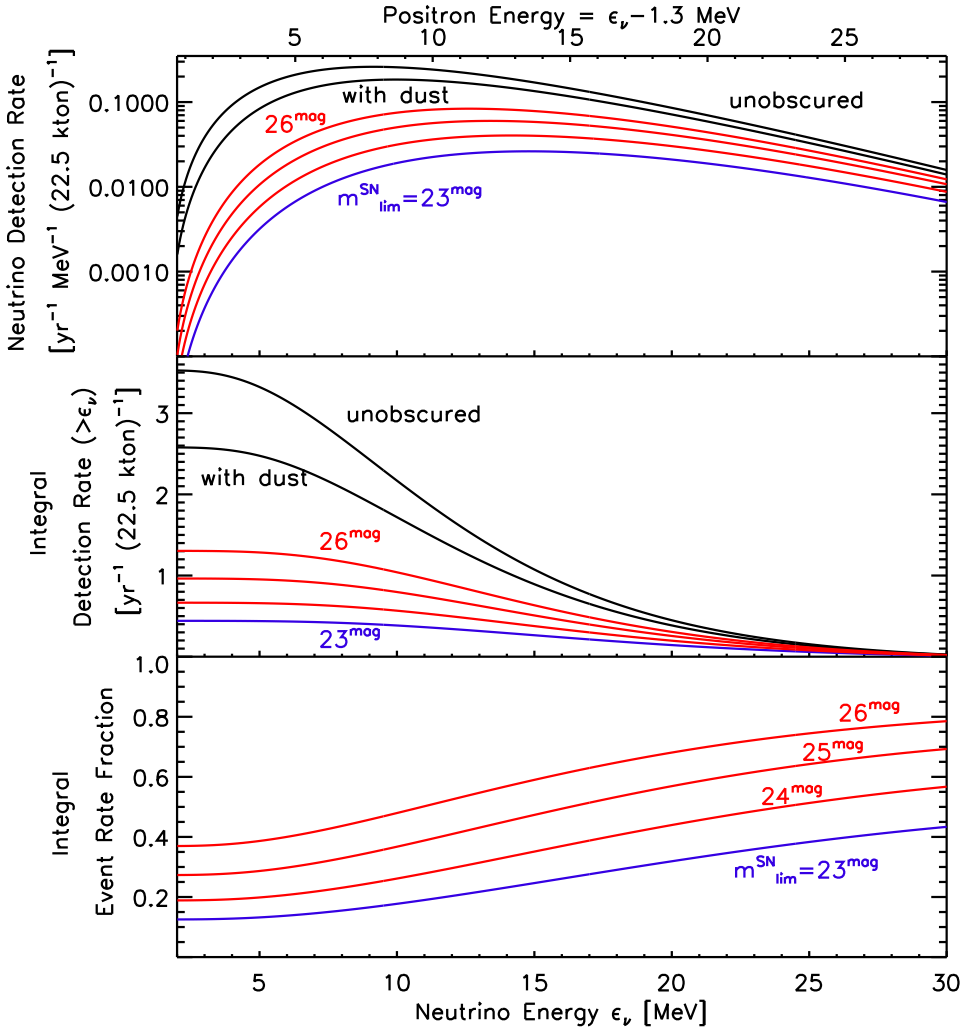

Figure 3.6: *Upper Panel*: Extreme *lower bounds* to the DSNB detection rate obtained by summing supernovae observed by surveys with different limiting magnitudes, the blue curve is the limiting magnitude proposed by LSST and Pan-STARRS. The blue and red curves represent a lower limit because they apply no correction for supernovae that are too dim or too obscured to be seen in surveys. The two black curves are shown for comparison: Top black curve is the DSNB flux from all core-collapse events in the universe out to redshift z $\sim$ 6. Second top black curve is the DSNB flux from core-collapse events after considering dust obscuration but with infinite survey limiting magnitude. Results assume $T_\nu = 4$ MeV. *Middle Panel*: The integrated DSNB detection rate, i.e. the detection rate above a certain antineutrino energy and integrated out to $\epsilon_\nu = 30$ MeV. The colors indicate the same features as in the top plot. *Lower Panel*: The fraction of the DSNB detection rate from the observed core-collapse events over those from the total collapse events. That is, a middle-panel red/blue curve divided by the highest black curve. Note that in this figure the x-axis starts at 2 MeV because no events can be detected below the threshold energy of 1.8 MeV.

of low-energy neutrinos come from higher redshift where dust obscuration is more severe and supernova apparent magnitudes are dimmer because of larger distances.

The observability of this energy dependence is to be understood in the context of the energy threshold of the neutrino detectors. For example, Super-K in its present form can discriminate from atmospheric backgrounds, and thus detect, cosmic neutrinos in the $\sim 18 - 26$ MeV range. If Super-K is enhanced with gadolinium (Beacom & Vagins, 2004), background rejection would be sufficiently improved in the 10 – 18 MeV range to open this crucial window onto the DSNB.

One sees more directly from the lower panel what portion of the total neutrino events detected by neutrino detector come from the observed core-collapse events with certain survey limiting magnitudes. This panel shows that $\sim 18\%$ of the neutrino events detected above 10 MeV are contributed by core-collapse events observed by surveys with a $23^{\rm mag}$ limiting magnitude.

We could thus estimate the *extreme lower limit* to the DSNB to be $\approx 15\%$ of the total detection events in the 10 – 18 MeV range, and $\approx 29\%$ of the total events in the 18 – 26 MeV range, assuming surveys with $m_{\rm lim}^{\rm sn} \approx 23^{\rm mag}$. Surveys including deeper scans will see larger fractions, e.g., approaching $\approx 54\%$ of the event rate within 18 – 26 MeV for $m_{\rm lim}^{\rm sn} \approx 25^{\rm mag}$. Notice that the numbers we showed above might be slightly lower than the percentages read directly from the lower panel of Fig. 3.6, since the numbers above are integrated only through the detectable energy range to reflect the best of what neutrino detectors would observe, while in Fig. 3.6, the numbers are integrated out to 30 MeV.

Chapter 4

Radio Supernovae in the Great Survey Era

This chapter is accepted for publication in The Astrophysical Journal and is co-authored with Nachiketa Chakraborty, Brian D. Fields, and Athol Kemball.

4.1 Abstract

Radio properties of supernova outbursts remain poorly understood despite longstanding campaigns following events discovered at other wavelengths. After ~ 30 years of observations, only ~ 50 supernovae have been detected at radio wavelengths, none of which are Type Ia. Even the most radio-loud events are $\sim 10^4$ fainter in the radio than in the optical; to date, such intrinsically dim objects have only been visible in the very local universe. The detection and study of radio supernovae (RSNe) will be fundamentally altered and dramatically improved as the next generation of radio telescopes comes online, including EVLA, ASKAP, and MeerKAT, and culminating in the Square Kilometer Array (SKA); the latter should be $\gtrsim 50$ times more sensitive than present facilities. SKA can repeatedly scan large ($\gtrsim 1\,\mathrm{deg}^2$) areas of the sky, and thus will discover RSNe and other transient sources in a new, automatic, untargeted, and unbiased way. We estimate SKA will be able to detect core-collapse RSNe out to redshift $z \sim 5$, with an all-redshift rate ~ 620 events yr^{-1} deg^{-2}, assuming a survey sensitivity of 50 nJy and radio lightcurves like those of SN 1993J. Hence SKA should provide a complete core-collapse RSN sample that is sufficient for statistical studies of radio properties of core-collapse supernovae. EVLA should find ~ 160 events yr^{-1} deg^{-2} out to redshift $z \sim 3$, and other SKA precursors should have similar detection rates. We also pro-

vided recommendations of the survey strategy to maximize the RSN detections of SKA. This new radio core-collapse supernovae sample will complement the detections from the optical searches, such as the LSST, and together provide crucial information on massive star evolution, supernova physics, and the circumstellar medium, out to high redshift. Additionally, SKA may yield the first radio Type Ia detection via follow-up of nearby events discovered at other wavelengths.

4.2 Introduction

Supernovae are among the most energetic phenomena in the universe, and are central to cosmology and astrophysics. For example, core-collapse supernovae are explosions arising from the death of massive stars and hence are closely related to the cosmic star-formation rate and to massive-star evolution; they are responsible for the energy and baryonic feedback of the environment (Madau et al., 1998). Type Ia supernovae show uniform properties in their lightcurves and play a crucial role as cosmic "standardizable candles" (Phillips, 1993b; Riess et al., 1996).

Our knowledge of the *optical* properties of supernovae, is increasing rapidly with the advent of prototype "synoptic"–i.e., repeated scan–sky surveys, such as SDSS-II (Frieman et al., 2008; Sako et al., 2008) and SNLS (Bazin et al., 2009; Palanque-Delabrouille et al., 2010). These campaigns are precursors to the coming "Great Survey" era in which synoptic surveys will be conducted routinely over very large regions of sky, e.g., LSST (The Large Synoptic Survey Telescope Collaboration, 2007; Bernstein et al., 2009) and Pan-STARRS (Tonry, 2003). The number of detected supernovae will increase by several orders of magnitude in this era (Bernstein et al., 2009; Lien & Fields, 2009).

In contrast to this wealth of optical information, properties of supernovae in the radio remain poorly understood, fundamentally due to observational limitations. Radio supernovae (RSNe) have primarily been discovered by follow-up observations of optical outbursts,

and only very rarely by accident. To date, only ~ 50 core-collapse outbursts have radio detections, and no Type Ia explosion has ever been detected in the radio (Weiler et al., 2004; Panagia et al., 2006). The core-collapse subtype Ibc has been a focus of recent study in the radio, because some Type Ibc events are associated with long Gamma-Ray Bursts (GRBs) (Galama et al., 1998; Kulkarni et al., 1998; Soderberg, 2007; Berger et al., 2003).

Current radio interferometers are scheduled primarily around targeted observations proposed by individual principal investigators. This stands in contrast to future radio interferometers planned for the coming "Great Survey" era. These include the Square Kilometer Array (SKA[1]) and its precursor prototype arrays (for example, ASKAP[2] and MeerKAT[3]). These telescopes will operate primarily as wide-field survey instruments focusing on several key science projects (Carilli & Rawlings, 2004). As synoptic telescopes, they will be far better suited to study all classes of transient and time-variable radio sources, including RSNe. Gal-Yam et al. (2006) already pointed out the power of synoptic radio surveys for detecting radio transients of various types, including supernovae and GRBs, in an unbiased way. Here we quantify the prospects for RSNe.

In this paper we explore this fundamentally new mode of *untargeted* RSN discovery and study. We adopt a forward-looking perspective, and consider the new science enabled by RSNe observations in an era in which the full SKA is operational. Our focus is mainly on core-collapse supernovae, the type for which some radio detections already exist. However, we will also discuss the possibility of Type Ia radio discovery based on current detection limits. We will first summarize current knowledge of radio core-collapse supernovae (§4.3), and the expected sensitivity of SKA (§4.4). Using this information, we forecast the radio core-collapse supernovae harvest of SKA (§4.5), and consider optimal survey strategies (§4.6). We conclude by anticipating the RSN science payoff in this new era (§4.7). We adopt a standard flat ΛCDM model with $\Omega_{\rm m} = 0.274$, $\Omega_\Lambda = 0.726$, and $H_0 = 70.5\,{\rm km\,s^{-1}\,Mpc^{-1}}$ (Komatsu

[1]http://www.ska-telescope.org
[2]http://www.atnf.csiro.au/projects/askap
[3]http://www.ska.ac.za/meerkat

et al., 2009) throughout.

4.3 Radio Properties of Supernovae

Several key properties of RSNe have been established, as a result of the longstanding leadership of the NRL-STScI group (recently reviewed in Weiler et al., 2009; Stockdale et al., 2007; Panagia et al., 2006) and of the CfA group and others (summarized in Soderberg, 2007; Berger et al., 2003). We summarize these general RSN characteristics, which we will use to forecast the RSN discovery potential of synoptic radio surveys.

4.3.1 Radio Core-Collapse Supernovae

Observed core-collapse RSNe have luminosities spanning $\nu L_\nu \sim 10^{33} - 10^{38}$ erg s^{-1} at 5 GHz, and thus are $\gtrsim 10^4$ times less luminous in the radio than in the optical. Their intrinsic faintness has prevented RSN detection in all but the most local universe. Even within a particular core-collapse subtype, radio luminosities and lightcurves are highly diverse, e.g., two optically similar Type Ic events might be radio bright in one case and undetectable in the other (Munari et al., 1998; Nakano & Aoki, 1997; Stockdale et al., 2006) [4]. Additionally, core-collapse RSNe spectral shapes strongly evolve with time; lightcurves peak over days to months depending on the frequency. RSN emission can be understood in terms of interactions between the blast, ambient relativistic electrons, and the circumstellar medium (Chevalier, 1982b,a, 1998).

To model RSN emission as a function of frequency and time, we adopt the semi-empirical form derived by Chevalier (1982b) and extended in Weiler et al. (2002),

$$L(t,\nu) = L_1 \left(\frac{\nu}{5\,\mathrm{GHz}}\right)^{\alpha} \left(\frac{t}{1\,\mathrm{day}}\right)^{\beta} e^{-\tau_{\mathrm{external}}} \left(\frac{1-e^{-\tau_{\mathrm{CSM_{clumps}}}}}{\tau_{\mathrm{CSM_{clumps}}}}\right) \left(\frac{1-e^{-\tau_{\mathrm{internal}}}}{\tau_{\mathrm{internal}}}\right) \quad . \quad (4.1)$$

[4] New Radio Supernova Results (Stockdale et al., 2006) are available online at: http://rsdwww.nrl.navy.mil/7213/weiler/sne-home.html

We follow the notation of Weiler et al. (2002). $L(t,\nu)$ is the supernova luminosity at frequency ν and time t after the explosion. Optical depths from material both outside ($\tau_{\rm external}$, $\tau_{\rm CSM_{clumps}}$) and inside ($\tau_{\rm internal}$) the blast-wave front are taken into account (see Weiler et al., 2002).

Parameters embedded in each optical depth term are those for SN 1993J, one of the best studied RSNe (Weiler et al., 2007). Radio emission from SN 1993J is dominated by the clumped-circumstellar-medium (clump-CSM) term, and hence

$$L(t,\nu) \sim \frac{1-e^{-\tau_{\rm CSM_{clumps}}}}{\tau_{\rm CSM_{clumps}}}, \tag{4.2}$$

where $\tau_{\rm CSM_{clumps}} = 4.6\times10^5\ (\frac{\nu}{5\ {\rm GHz}})^{-2.1}\ (\frac{t}{1\ {\rm day}})^{-2.83}$, for SN 1993J. At small t, $\tau_{\rm CSM_{clumps}}$ is large and $L(t,\nu) \sim 1/\tau_{\rm CSM_{clumps}} \propto \nu^{2.1}\ t^{2.83}$, so luminosity grows as a power law at early times. With all optical depth parameters fit to SN 1993J, the peak luminosity is controlled by the prefactor L_1.

Our main focus will be on RSN discovery, and thus it is most important to capture the wide variety of peak radio luminosities, which correspond in our model to a broad distribution for L_1. Figure 4.1 shows a crude luminosity function (not-normalized) based on the sample of 20 core-collapse supernovae (15 Type II and 5 Type Ibc) that have a published peak luminosity at 5 GHz (Weiler et al., 2004; Stockdale et al., 2003, 2007; Papenkova et al., 2001; Stockdale et al., 2006; Baklanov et al., 2005; Pooley et al., 2002). We use 5 GHz data to construct our luminosity function because the most RSNe have been observed at this frequency. However, our predictions will span a range of frequencies, based on this luminosity function and eq. (4.2). The data are divided into four luminosity bins of size $\Delta\log_{10}(L) = 1$. The black curve in Fig. 4.1 is the best-fit Gaussian, with average luminosity $\log_{10}(L_{\rm avg}/{\rm erg\,s^{-1}\,Hz^{-1}}) = 27.3$, a standard deviation $\sigma = 1.25$, and $\chi^2 = 0.18$. SN 1987A is marked in Fig. 4.1, but was not used in the fit to avoid possible bias due to its uncommonly low luminosity. The fitted luminosity function might be biased towards the brighter end,

because of the current survey sensitivity and the small and incomplete nature of the sample.

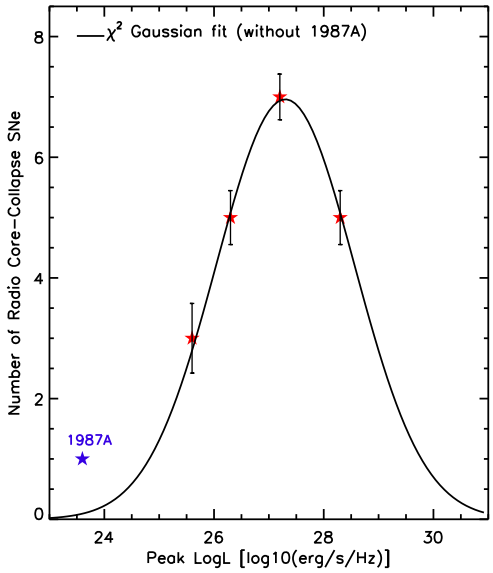

Figure 4.1: Radio luminosity function (not-normalized) at 5 GHz of core-collapse supernovae showing core-collapse supernovae count as a function of $\log_{10}(L)$, where L is the peak radio luminosity. Data are binned to $\Delta \log_{10}(L) = 1$. The black curve shows the χ^2-fitted Gaussian to the underlying data (red stars).

4.3.2 Radio Type Ia Supernovae

All searches to date have failed to detect radio emission from Type Ia supernovae. Panagia et al. (2006) reported the radio upper limits of 27 Type Ia supernovae from more than two decades of observations by the Very Large Array (VLA). The weakest limit on a Type Ia event is 4.2×10^{26} erg s^{-1} Hz^{-1} at 1.5 GHz for SN 1987N, which is around one order of magnitude lower than the average luminosity of radio-detected core-collapse supernovae (see §4.3.1). The strongest limit on Type Ia radio emission is even tighter, 8.1×10^{24} erg s^{-1} Hz^{-1} at 8.3 GHz for SN 1989B. Additionally, the $z \sim 0$ cosmic Type Ia supernova rate is around 1/4.5 of the core-collapse supernova rate (Bazin et al., 2009). The intrinsic faintness in radio and their smaller rate make detecting Type Ia in radio observations especially hard.

4.4 Next-Generation Radio Telescopes: Expected Sensitivity

Radio detections of supernovae to date have been restricted both by the limiting sensitivity of contemporary radio interferometers and the need for dedicated telescope time for transient followup. This situation will change drastically with SKA's unprecedented sensitivity and particularly by its ability to repeatedly scan large regions of the sky at this great depth.

Current SKA specifications adopt a target sensitivity parameter $A_{\rm eff}/T_{\rm sys} = 10^4$ m^2 K^{-1} at observing frequencies in the low several GHz, including $z = 0$ HI observations at 1.4 GHz. $A_{\rm eff}$ is the effective aperture, and $T_{\rm sys}$ is the system temperature. We will adopt this value of $A_{\rm eff}/T_{\rm sys}$, which yields a 1-σ rms thermal noise limit in total intensity of

$$\sigma_I = 0.15\ \mu{\rm Jy}\ (\Delta\nu/{\rm GHz})^{-1/2}\ (\delta{\rm t}/{\rm hr})^{-1/2}, \tag{4.3}$$

for a bandwidth $\Delta\nu$ and observation duration δt. The SKA will therefore reach a thermal noise limit of several nJy in deep continuum integrations ($\delta t \sim 1000$ hr) (SKA Design Reference Mission, 2009) [5]. We define the associated survey sensitivity $S_{\rm min}$ (the minimum flux density threshold) as $S_{\rm min} = 3\sigma_I$. In common with other radio interferometers, SKA will accumulate sensitivity in targeted deep fields, including transient-monitoring fields, by accumulating integration time over multiple individual observing tracks. We therefore will adopt a fiducial SKA supernova sensitivity of $S_{\rm min} = 50$ nJy in 100 hours of observation, but we will show how our results are sensitive to other choices of $S_{\rm min}$.

It is anticipated that transient fields will be revisited with a cadence appropriate to the variability timescales under study and that interferometric inverse imaging methods will include source models with time variability. Survey optimization for interferometric transient detection is an active area of current SKA research. The technical details are beyond the intent and scope of this paper, but will be influenced by science goals for transient source

[5] http://www.skatelescope.org/PDF/DRM_v1.0.pdf

study in general, including pulsars, GRBs, and supernovae (as considered in this paper), as well as the as-yet undiscovered transient population.

4.5 Radio Supernovae for SKA

With its unprecedented sensitivity, SKA will be capable of synoptic search for core-collapse RSNe and open new possibilities in radio astronomy. In this section, we predict the RSN detections of SKA based on current knowledge to demonstrate how the RSN survey can be done.

4.5.1 Core-Collapse Supernovae

The detection rate $\Gamma_{\rm detect} = dN_{\rm SN}/(dt_{\rm obs}\, d\Omega\, dz)$ for a given RSN survey is

$$\Gamma_{\rm detect} = f_{\rm survey}\ f_{\rm radio}\ f_{\rm ISM}\ \Gamma_{\rm SN} \quad , \tag{4.4}$$

and is set by several observability factors f that modulate the total rate of all supernovae

$$\Gamma_{\rm SN}(z) = \frac{dN_{\rm SN}}{dV_{\rm comov}\, dt_{\rm em}}\ \frac{dt_{\rm em}}{dt_{\rm obs}}\ \frac{dV_{\rm comov}}{d\Omega\, dz} = \mathcal{R}_{\rm SN}(z)\, r^2_{\rm comov}(z)\, c \left|\frac{dt}{dz}\right| \tag{4.5}$$

within the cosmic volume out to redshift z (Madau et al., 1998; Lien & Fields, 2009).

We see that the total cosmic supernova rate $\Gamma_{\rm SN}$ depends on cosmology via the volume element and the time dilation terms. Because ΛCDM cosmological parameters are now known to high precision, these factors have a negligible error compared to the other ingredients in the calculation. The other factor in $\Gamma_{\rm SN}$ is the cosmic core-collapse supernova rate density $\mathcal{R}_{\rm SN}(z) = dN_{\rm SN}/(dV_{\rm comov}\, dt_{\rm emit})$. Some direct measurements of this rate now exist out to $z \sim 1$, but the uncertainties remain large (Cappellaro et al., 1999; Dahlen et al., 2004; Cappellaro et al., 2005; Hopkins & Beacom, 2006; Botticella et al., 2008a; Dahlen et al., 2008a; Kistler et al., 2008a; Bazin et al., 2009; Smartt et al., 2009; Dahlen et al., 2010; Li

et al., 2011a; Horiuchi et al., 2011). However, core-collapse events are short-lived, and so the cosmic core-collapse rate is proportional to the cosmic star-formation rate $\dot{\rho}_\star$, which is much better-determined and extends to much higher redshifts. We thus derive $\mathcal{R}_{\rm SN}$ from the recent Horiuchi et al. (2009) fit to the cosmic star-formation rate. The proportionality follows from the choice of initial mass function; we apply the Salpeter initial mass function (Salpeter, 1955) and assume the mass range of core-collapse SNe progenitors to be $8M_\odot - 50M_\odot$; this gives $\mathcal{R}_{\rm SN} = (0.007\, M_\odot^{-1})\, \dot{\rho}_\star$

Several effects reduce the total rate $\Gamma_{\rm SN}$ to the observed rate $\Gamma_{\rm detect}$ in eq. (4.4). Due to finite survey sensitivity, only a fraction $f_{\rm survey}$ of events are bright enough to detect, and only some fraction $f_{\rm radio}$ of supernovae will emit in the radio. We neglect interstellar extinction and assume $f_{\rm ISM} \sim 1$ at the radio wavelengths considered.

The term $f_{\rm radio}$ in eq. (4.4) contains the greatest uncertainty due to the relatively small sample of RSNe observed to date, and the unavoidable incompleteness of the sample (K. Weiler, private communication 2010). The only published fraction available is for Type Ibc supernovae. Using VLA for radio follow-up, Berger et al. (2003) suggests that $f_{\rm radio,Ibc} \sim 12\%$ after surveying 33 optically-detected Type Ibc supernovae. For the purpose of demonstration, we will adopt $f_{\rm radio} = 10\%$ for the calculations presented in this paper, which we believe is rather conservative.

An order-of-magnitude calculation provides a useful estimate of the expected core-collapse RSN rate. As discussed in §4.4, we adopt a fiducial SKA sensitivity of $S_{\rm min} = 50$ nJy. Hence SKA will be able to detect supernovae with average radio luminosity ($L \sim 10^{27}$ erg s^{-1} Hz^{-1}) to a distance $D_L = \sqrt{L/4\pi S_{\rm min}} \sim 4$ Gpc, which for a ΛCDM cosmology corresponds to $z \sim 1$. This will give a detectable volume of $V_{\rm detect} \sim (4/3)\pi D_L^3 \sim 2.85 \times 10^{11}$ Mpc^3. Observations show that the core-collapse supernova rate $R_{\rm SN} \sim 10^{-3}$ yr^{-1} Mpc^{-3} at $z \sim 1$ (Dahlen et al., 2008a, 2010). Assuming the fraction of the total core-collapse supernovae that display the adopted average radio luminosity to be $f_{\rm radio} \sim 10\%$ (Berger et al., 2003), the all-sky detection rate $dN_{\rm SN}/dt \sim R_{\rm SN} \times f_{\rm radio} \times V_{\rm detect} \sim 2.85 \times 10^7$ yr^{-1}. This corresponds

to a areal detection rate $dN_{\rm SN}/(dt\,d\Omega) \sim 700$ yr^{-1} deg^{-2}. As we now see, a more careful calculation confirms this estimate.

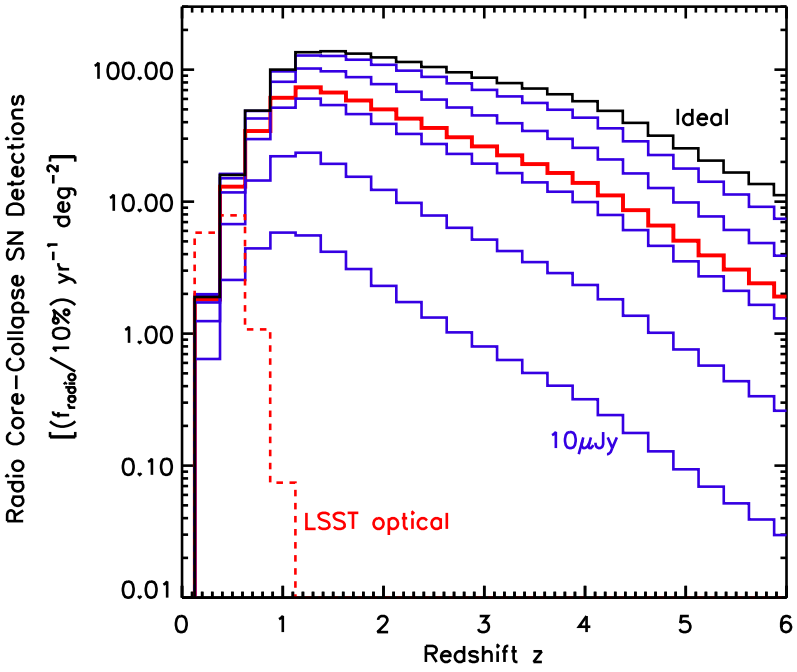

Figure 4.2: Estimated radio core-collapse supernova detection rate as a function of redshift at 1.4 GHz, assuming $f_{\rm radio} = 10\%$. Predictions are shown for different survey sensitivities: $S_{\rm min} = \{10\ \mu$Jy (blue), 1 μJy (blue), 100 nJy (blue), 50 nJy (thick red), 10 nJy (blue), 1 nJy (blue)$\}$ from bottom to top solid curves, respectively. We adopt 50 nJy as our benchmark sensitivity hereafter. For comparison, the red-dashed curve shows the LSST optical supernova detection rate per year per deg^2 (Lien & Fields, 2009). Also, the top solid curve (black) plots the ideal core-collapse RSN rate for comparison.

A careful prediction involves detailed calculation of $f_{\rm survey}(z)$. The fraction $f_{\rm survey}(z)$ of observable radio-emitting events depends on adopted survey sensitivity, and on the normalized supernova luminosity function $\Phi_{\rm 5GHz}(\log L)$, which is measured at a peak luminosity at 5 GHz (derived in § 4.3). In this paper we will only consider whether a supernova is detectable at its peak luminosity at each corresponding frequency. The peak radio luminosity should be reached earlier at higher frequencies because of preferential absorption at lower frequencies (Weiler et al., 2002). At different redshift, the peak flux density $S_{\rm min}^{\rm peak}$ in the

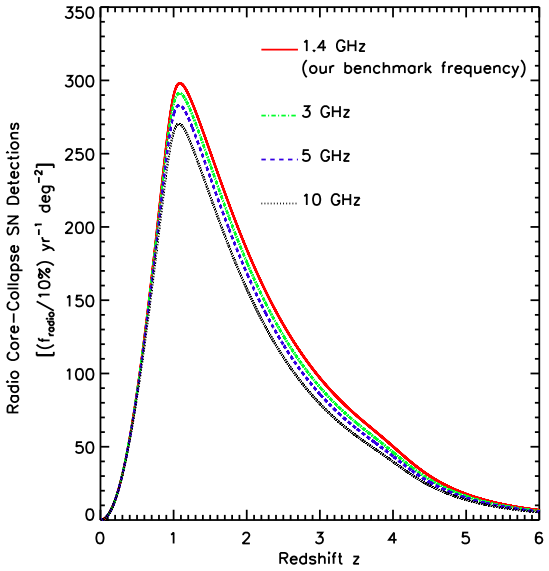

Figure 4.3: Estimated radio core-collapse supernova detection rate as a function of redshift for different frequency bands, for $f_{\rm radio} = 10\%$, and an adopted survey sensitivity $S_{\rm min} = 50$ nJy.

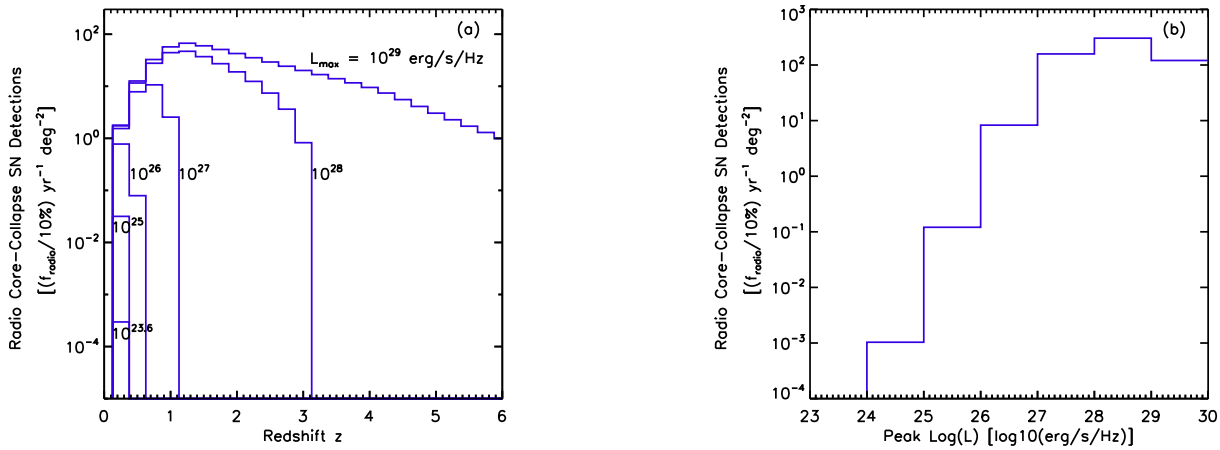

Figure 4.4: Core-collapse detection sensitivity to supernova radio luminosity, at 1.4 GHz, and for survey sensitivity $S_{\rm min} = 50$ nJy. (a)*Left Panel*: Supernova distribution over redshift, for different cutoffs for the luminosity function. (b)*Right Panel*: Supernova distribution in luminosity bins, integrated over all redshifts.

observed frequency ν can be tied to the corresponding luminosity threshold $L_{\rm min}^{\rm peak}$ by

$$L_{\rm min}^{\rm peak}(z;\nu_{\rm emit}) = \frac{4\pi D_L^2(z)}{(1+z)} S_{\rm min}^{\rm peak}(\nu_{\rm obs}), \tag{4.6}$$

where the luminosity distance is $D_L(z) = (1+z)\, c/H_0 \int_0^z dz' \, [\Omega_{\rm m}(1+z')^3+\Omega_\Lambda]^{-1/2}$. However, because the luminosity function we used is based on the peak luminosity at 5 GHz, we must find the corresponding luminosity threshold at this frequency by applying corrections based on the radio spectrum,

$$L^{\rm peak}_{\rm min,5GHz} = L^{\rm peak}_{\rm min} \, \frac{\int_{\rm 5GHz\ band} S^{\rm peak}(\nu_{\rm em})\ d\nu_{\rm em}}{\int_{\rm obs\ band} S^{\rm peak}[(1+z)\nu_{\rm obs}]\ d\nu_{\rm obs}}. \tag{4.7}$$

The detectable fraction resulting from survey sensitivity can therefore be estimated as

$$f_{\rm survey} = \int_{\log L^{\rm peak}_{\rm min,5GHz}} \Phi_{\rm 5GHz}(\log L)\, d\log L. \tag{4.8}$$

Figure. 4.2 plots the results of our predicted core-collapse RSN detection rate for different target survey sensitivities, $S_{\rm min}$. We adopt a benchmark frequency of 1.4 GHz because this will be one of the first major bands SKA deploys to observe neutral hydrogen. The related instantaneous field-of-view at 1.4 GHz of current SKA designs based on dish reflectors is approximately 1 deg^2, which we adopt. Fig. 4.2 plots the ideal core-collapse supernova rate for comparison (assuming infinite sensitivity but $f_{\rm radio} = 10\%$). One can see that the detection rate at 1 nJy is very close to the ideal rate in the universe.

Results for our fiducial SKA flux limit $S_{\rm min} = 50$ nJy are highlighted in Fig. 4.2. At this sensitivity, we see that we can expect that radio supernovae will be discovered (event rates > 5 RSN yr^{-1} deg^{-2}) over the enormous redshift range $z \simeq 0.5$ to 5. The total rate of RSNe expected in this entire redshift range is

$$\frac{dN_{\rm SN}}{dt\, d\Omega}(> 50 \text{ nJy}) \approx 620 \text{ RSNe yr}^{-1} \text{ deg}^{-2} \quad , \tag{4.9}$$

in good agreement with our above order-of-magnitude estimate. This sample size is large enough to be statistically useful and to allow for examination of the redshift history of RSNe. Moreover, out to $z \sim 1$, SKA will detect almost all cosmic RSNe in the field of view, while

at higher redshift the detections still comprise $> 10\%$ of the underlying ideal cosmic rate. For comparison, we also see that LSST will detect optical supernovae out to $z \lesssim 1$. Thus SKA will be complementary to LSST as a unique tool for cosmic supernova discovery.

Figure. 4.3 shows how core-collapse RSN detections vary for different observing frequencies, fixing a common survey sensitivity $S_{\rm min} = 50$ nJy and bandwidth $\Delta\nu = 1$ GHz. Results show similar numbers of detections at different bands, which is caused by a relatively flat spectrum shape at peak luminosities. Because SKA will be able to detect core-collapse RSNe out to high redshift $z \sim 5$, the frequency-redshift and time-dilation effects are significant. Weiler et al. (2002) noted that RSNe peak when the optical depth $\tau \sim 1$. Since the optical depth depends both on frequency and time with similar power index (Weiler et al., 2002), the frequency-redshift and time-dilation effects approximately cancel, so that a fixed observed frequency, the peak time is nearly redshift-independent.

As mentioned above, our luminosity function is likely biased toward the available bright events in a small and incomplete sample. To explore how this bias could affect our results, Fig. 4.4 shows how the detection rate with $S_{\rm min} = 50$ nJy at 1.4 GHz depends on core-collapse RSN luminosity. Fig. 4.4(a) shows that RSN with peak luminosities greater than 10^{27} erg s^{-1} Hz^{-1} contribute all of the detections beyond redshift $z \sim 1$, and RSN need to peak brighter than 10^{28} erg s^{-1} Hz^{-1} to be seen beyond $z \sim 3$. Fig. 4.4(b) similarly shows that the all-redshift detection rate becomes substantial for explosions peaking $> 10^{26}$ erg s^{-1} Hz^{-1}.

Type Ibc supernovae are of particular interest given their association with long gamma-ray bursts (GRBs; Galama et al., 1998; Woosley, 1993; Heger et al., 2003). Fig. 4.5 shows our predictions for Type Ibc detections of SKA per year per deg^2 at 1.4 GHz with a survey sensitivity of 50 nJy. The red curve shows the radio Type Ibc detections, assuming that Type Ibc represents 25% of core-collapse events (Li et al., 2011b), and $f_{\rm radio,Ibc} = 12\%$ with luminosity $\sim 10^{27}$ erg s^{-1} Hz^{-1} [6] (Berger et al., 2003). The blue curve shows the possible detections of the sub-class of Type Ibc supernovae that display extreme radio emission

[6]Here we simply assume a Gaussian distribution for the luminosity function centered at the specified luminosity with $\sigma = 1$.

and hence might be powered by central engines and related to GRBs. We assume that 0.5% of all Type Ibc supernovae are powered by central engines and have luminosities of $\sim 10^{29}$ erg s^{-1} Hz^{-1} (Berger et al., 2003). We adopted the spectrum of SN 1998bw, which is a Type Ic supernova (Weiler et al., 2002). Under these assumptions the SKA will be able to make unbiased, untargeted detections of ~ 130 radio Type Ibc supernovae per year per deg^2, and ~ 20 Type Ibc supernovae that might be connected to GRBs.

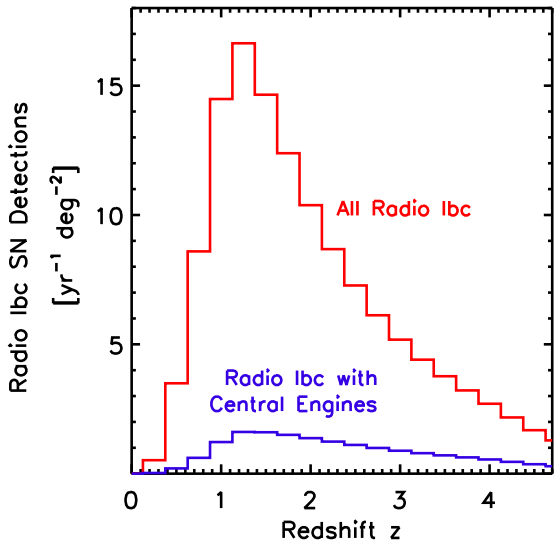

Figure 4.5: Predicted detection rate of Type Ibc supernovae as a function of redshift. In this plot we assume the sensitivity for SKA is $S_{\rm min} = 50$ nJy. The red curve shows all of the radio Ibc detections, assuming $f_{\rm radio,Ibc} = 12\%$ (Berger et al., 2003). The blue curve shows only the detection rate for Radio Ibc with central engines, assuming 0.5% of all of the Type Ibc RSNe are powered by central engines.

Finally, we turn to SKA precursors. The EVLA[7], a current leading-edge radio interferometer operating at centimeter wavelengths, is anticipated to reach a 1-σ rms noise of $\sigma_I \sim 1$ μJy or less in 10 hours, while SKA is expected to reach $\sigma_I \sim 50$ nJy in 10 hours. With data accumulated over repeated scans spanning over 1000 hours, an rms $\sigma_I \sim 5$ nJy may be reached. In synoptic surveys, we would expect EVLA to detect core-collapse events

[7]http://www.aoc.nrao.edu/evla

at a rate ~ 160 RSNe yr^{-1} deg^{-2} over a redshift range $z = 0.5$ to 3 (Fig. 4.2). A sample of this size over this redshift range will already mark a major advance in the study of cosmic RSNe, and further motivate the full SKA. ASKAP and MeerKAT are expected to have sensitivities comparable to that of EVLA (Johnston et al., 2009; de Blok et al., 2010), hence we would expect these to detect RSNe with similar rates and redshift reach.

4.5.2 Type Ia Supernovae

If all Type Ia RSNe are dimmer than the weakest limit presented in §4.3.2, the expected SKA detection rate is essentially zero. For example, if a typical Type Ia has a radio luminosity equal to the lowest published limit, $L = 8.1 \times 10^{24}$ erg s^{-1} Hz^{-1}, this can be seen with a sensitivity $S_{\rm min} = 50$ nJy out to a luminosity distance ~ 300 Mpc ($z \sim 0.08$). While ~ 3900 cosmic Ia events should occur per year out to this distance over the entire sky, $\ll 1$ events are expected in the SKA field of view. More optimistically, imagine a typical Type Ia radio luminosity is $L = 10^{26}$ erg s^{-1} Hz^{-1}, which is below $L = 4.2 \times 10^{26}$ erg s^{-1} Hz^{-1}, the highest published limit (Panagia et al., 2006); here the luminosity distance increases to ~ 1400 Mpc ($z \sim 0.28$). In this case, we find an SKA Type Ia detection rate ~ 0.5 yr^{-1} deg^{-2}, based on the local cosmic Type Ia rate derived from SDSS-II optical data (Dilday et al., 2010), $S_{\rm min} = 50$ nJy, and $f_{\rm radio} = 10\%$.[8] We see that even optimistically, we expect fewer than one event per SKA field-of-view per year. Even with $f_{\rm radio} = 100\%$, the detection rate is still only ~ 5 yr^{-1} deg^{-2}. Therefore we conclude that SKA will make few, if any, blind detections of Type Ia supernovae.

Targeted radio observations to follow up from nearby optical detections will probably be the best way to search for such events. For example, we expect 10 Type Ia events/year in the LSST sky within ~ 60 Mpc ($z \sim 0.015$). Type Ia (or core collapse!) events within this distance observed with $S_{\rm min} = 50$ nJy, would be detectable at luminosities $L \gtrsim 3.0 \times 10^{23}$ erg s^{-1} Hz^{-1}. Amusingly, this is close to the radio luminosity of SN 1987A.

[8] This also is implied by Fig. 4.4, which is for core-collapse events that have a higher cosmic rate.

4.6 Radio Survey Recommendations

A key requirement for detecting weak radio emission from CSM-supernovae interactions is improved radio interferometer sensitivity. High angular resolution – below an arcsecond at 1.4 GHz, (Weiler et al., 2004) – is also required to avoid natural confusion and to help identify supernovae against background galaxies. This is similar to the maximum EVLA angular resolution at 1.4 GHz. For comparison, the maximum anticipated SKA baseline length of 3000 km, producing angular resolution of 0.014 arcsecond at 1.4 GHz, is sufficient to distinguish different galaxies and also to resolve galaxies as extended sources within the observable universe with rms confusion limit of $<$ 3 nJy at 1.4 GHz (Carilli & Rawlings, 2004).

A key science goal of the SKA is to detect transient radio sources, both known (e.g. pulsars, GRBs), and as-yet unknown. This requires sophisticated transient detection and classification algorithms very likely running commensally with other large surveys planned by the SKA, such as the HI spectroscopic survey and deep continuum fields. We assume here that SKA transient detection algorithms will encompass automated detection of RSNe. For example, current parameterized models (Weiler et al., 1986, 1990; Montes et al., 1997; Chevalier, 1982b,a) based on available data predict patterns of spectral index evolution characteristic of supernovae in general, and supernova sub-types in particular. This information could be exploited for RSN detection, even potentially against a background of unrelated source variability. Broad frequency coverage is important in this regard (Weiler et al., 2004).

The SKA intrinsically is a high dynamic-range instrument, given the sensitivity implied by the large collecting area. The most demanding SKA science applications will require a dynamic range of 10^7:1. The detection of faint RSNe will require a dynamic range that falls within that envelope.

Although the lightcurves of RSNe show great diversity, the luminosities of core-collapse supernovae usually change much slower in radio than in optical. RSN lightcurves typically evolve on timescales of weeks to years; a useful lightcurve compilation appears in Stockdale

et al. (2007). Thus the minimum survey cadence (revisit periodicity) need not be any more frequent than this. Also, we have shown that core-collapse RSNe can be found out to high redshift with surveys pushing down to $S_{\rm min} = 50$ nJy. For SKA this corresponds to about 100 hours of exposure, in line with planned deep field exposures which are part of the key science. Thus, SKA as currently envisioned is well-suited to core-collapse discovery.

On the other hand, SKA probably will not have sufficient survey sensitivity for a volumetric search for Type Ia events, based on our current knowledge of the cosmic Type Ia rate and the upper limits in their luminosities set by the non-detection of these events. Follow-up observations from other wavelengths will likely be the best way to search for Type Ia RSNe.

The small volume of the local universe will limit nearby *untargeted* SKA detections of low-redshift core-collapse RSNe. We estimate only ~ 2 core-collapse RSN detections per year per square degree within redshift $z \sim 0.5$ (assuming a 50 nJy sensitivity at 1.4 GHz and $f_{\rm radio} = 10\%$). Unless SKA has large sky coverage comparable to those of optical surveys, it will be hard to get statistical information from such a small sample. Therefore, *targeted* radio followup of optically-confirmed nearby supernovae will be crucial to build a core-collapse RSN "training set" database needed for refining automatic identification and classification techniques.

With detection methods optimized based on low-z radio data for optically-identified events, radio surveys can then be used to independently detect core-collapse RSNe at high redshift based only on their radio emission. As shown in Fig. 4.2, supernova searches at high redshift ($z \gtrsim 1$) will largely rely on radio synoptic surveys, the inverse of the strategy proposed above for low-redshift domain. Surveys for core-collapse RSNe will likely not be synoptic all-sky surveys due to operational limitations, but will likely proceed in a limited set of sub-fields, visited over an hierarchical set of cadences to cover a range of time-scales for general transient phenomena and multiple commensal science objectives. It is also important to match core-collapse RSNe survey sky coverage and cadence to that used in complementary optical surveys. LSST will repeatedly scan the whole sky every ~ 3 days. Thus a cadence

~ 1 week for RSNe sub-fields will be preferred for an SKA core-collapse supernova survey.

4.7 Discussion and Conclusions

SKA's capability for unbiased synoptic searches over large fields of view will revolutionize the discovery of radio transients in general and core-collapse RSNe in particular (Gal-Yam et al., 2006). The unprecedented sensitivity of SKA could allow detection of core-collapse RSNe out to a redshift $z \sim 5$. These detections will be *unbiased* and *automatic* in that they can occur anywhere in the large SKA field of view without need for targeting based on prior detection at other wavelengths. With SKA, the core-collapse RSN inventory should increase from the current number of several dozen to ~ 620 yr^{-1} deg^{-2}. EVLA should detect ~ 160 yr^{-1} deg^{-2}, and other SKA precursors should reap similarly large RSN harvests. In contrast, intrinsically dim RSNe such as Type Ia events and 1987A-like core-collapse explosions are unlikely to be found blindly. However, the SKA (and precursor) sensitivities will offer the possibility of detecting these events via *targeted* followup of discoveries by optical synoptic surveys such as LSST.

The science payoff of large-scale RSNe searches touches many areas of astrophysics and cosmology. We conclude with examples of possible science applications with the new era of RSN survey. However, the true potential of untargeted radio search is very likely beyond what we mention.

Non-prompt RSN emission requires the presence of circumstellar matter, so such surveys will probe this material and the pre-supernova winds producing it. For core-collapse supernovae, pre-supernova winds should depend on the metallicities of the progenitor stars (Leitherer et al., 1992; Kudritzki & Puls, 2000; Vink et al., 2001; Mokiem et al., 2007), and should be weaker in metal-poor environments with lower opacities in progenitor atmospheres. This effect should lead to correlations between RSN luminosity and host metallicity, as well as an evolution of the RSN luminosity function towards lower values at higher redshifts. For

Type Ia supernovae, the mass-loss rate from the progenitors depends on the nature of the binary system, i.e., single or double degenerate (Nomoto et al., 1984; Iben & Tutukov, 1984; Webbink, 1984). Radio detection of Type Ia supernovae will probe the mass and density profile of the surrounding environment and hence be valuable for studying Type Ia physics (Eck et al., 1995; Panagia et al., 2006; Chomiuk et al., 2011).

Large-scale synoptic RSNe surveys will complement their optical counterparts. While optical surveys such as LSST will provide very large supernova statistics at $z \lesssim 1$, radio surveys will be crucial for detections at higher redshifts. The nature and evolution of dust obscuration presents a major challenge for optical supernova surveys and supernova cosmology. Current studies suggest dust obscuration increases rapidly with redshift, but uncertainties are large. Mannucci et al. (2007) estimate that optical surveys may miss $\sim 60\%$ of core-collapse supernovae and $\sim 35\%$ of Type Ia supernovae at redshift $z \sim 2$. RSN observations, in contrast, are essentially unaffected by dust. Thus, high-redshift supernovae could be detected at radio wavelengths but largely missed in counterpart optical searches. Comparing supernova detections in both optical and radio will provide a new and independent way to measure dust dependence on redshift. In particular, SKA will be a powerful tool to directly detect supernovae in dust-obscured regions at large redshift, and therefore offer what may be the only means to study the total supernovae rate, star-formation, and dust behavior in these areas.

Additionally, radio surveys will reveal rare and exotic events. For example, some Type Ibc supernovae are linked to long GRBs (Galama et al. 1998; and see reviews in Woosley & Bloom, 2006; Gehrels et al., 2009), probably via highly relativistic jets powered by central engines and will manifest themselves in extremely luminous radio emission (Woosley, 1993; Iwamoto et al., 1998; Li & Chevalier, 1999; Woosley et al., 1999; Heger et al., 2003). Thus one might expect radio surveys to preferentially detect more Type Ibc supernovae than other supernova types. An unbiased sample of Type Ibc RSNe will provide new information about the circumstellar environments of these explosions and thus probe the mass-loss effects

believed to be crucial to the Ibc pre-explosion evolutionary path (Price et al., 2002; Soderberg et al., 2004, 2006a; Crockett et al., 2007; Wellons & Soderberg, 2011); in addition, a large sample of Ibc RSNe will allow systematic study of the differences, if any, between those which do an do not host GRBs (Berger et al., 2003; Soderberg et al., 2006b; Soderberg, 2007).

Furthermore, radio surveys give unique new insight into a possible class of massive star deaths via direct collapse into black holes, with powerful neutrino bursts but no electromagnetic emission (MacFadyen & Woosley, 1999; Fryer, 1999; MacFadyen et al., 2001; Heger et al., 2003). These "invisible collapses" can be probed by comparing supernovae detected electromagnetically and the diffuse background of cosmic supernova neutrinos (Lien et al., 2010, and references therein). By revealing dust-enshrouded SNe, radio surveys will make this comparison robust by removing the degeneracy between truly invisible events and those which are simply optically obscured. Indeed, direct collapse events without explosions but with relativistic jets are candidates for GRB progenitors. A comparison among RSNe, optical supernovae, GRBs, and neutrino observations will provide important clues to the physics of visible and invisible collapses, and their relation with GRBs.

We thus believe that a synoptic survey in radio wavelengths will be crucial in many fields of astrophysics, for it will bring the first complete and unbiased RSN sample and systematically explore exotic radio transients. SKA will be capable of performing such an untargeted survey with its unprecedented sensitivity. Our knowledge of supernovae will thus be firmly extended into the radio and to high redshifts.

Acknowledgments We thank Kurt Weiler, Christopher Stockdale, and Shunsaku Horiuchi for encouragement and illuminating conversations. We are also grateful to Joseph Lazio for helpful comments that have improved this paper.

Chapter 5

The Diffuse Gamma-ray Background from Supernovae

This chapter describes work in progress, co-authored with Brian D. Fields.

5.1 Abstract

The origin of the diffuse extragalactic gamma-ray background (EGB) has been intensively studied but remains unsettled. Current popular source candidates include unresolved star-forming galaxies, starburst galaxies, and blazars. In this paper we provide estimations of the EGB from the interactions of cosmic rays accelerated by Type Ia supernovae in both star-forming and quiescent galaxies. In the case of star-forming galaxies, we generalize earlier work that has only included core-collapse supernovae. We find that consistently including Type Ia events makes little change to the EGB prediction, so long as both supernova types have the same cosmic-ray acceleration efficiencies in star-forming galaxies. Turning to Type Ia supernovae in quiescent galaxies lacking star formation, we find the large reservoirs of hot gas in these objects provide abundant targets for cosmic rays. We also find the resulting EGB contribution of Type Ia supernovae in these objects is very sensitive to the cosmic-ray acceleration efficiency of supernovae and the cosmic-ray confinement. If we assume similar efficiency and cosmic-ray confinement for both quiescent and star-forming galaxies, quiescent galaxies can also be an important source of the EGB. In this case, star-forming galaxies and quiescent galaxies together will dominate the EGB and leave little room for other sources. If other sources like blazars and starburst galaxies are also predicted to have major contributions to the EGB, the cosmic-ray acceleration efficiency or the cosmic-ray

confinement in quiescent galaxies must be significantly lower than in star-forming galaxies. In any case, the EGB will provide important constraints on the cosmic-ray production efficiency as well as the cosmic-ray confinement in quiescent galaxies. Additionally, we discuss the impact of the supernova observations from large synoptic (repeated-scan) surveys, such as the LSST, to the EGB analysis.

5.2 Introduction

Direct measurements of the diffuse extragalactic gamma-ray background (EGB) are difficult due to the dominating foreground emission from our Galaxy (e.g., Hunter et al., 1997). The accuracy of the EGB measurement thus greatly depends on our understanding of the Galactic emission. The first EGB observation was reported by the SAS-2 satellite (Fichtel et al., 1977, 1978). Recently, the *Fermi Gamma-ray Space Telescope* updated the EGB measurements from the Energetic Gamma-ray Experiment Telescope (EGRET) (Sreekumar et al., 1998) and provided the most reliable EGB observations so far (Abdo et al., 2009a). Despite the difficulty in its observation, the EGB encodes important information about the highest-energy environments in the cosmos.

The EGB arises from a combination of all the unresolved extragalactic gamma-ray sources, such as matter and antimatter annihilation (Stecker et al., 1971), annihilation from exotic particles like dark matter (Silk & Srednicki, 1984; Rudaz & Stecker, 1991), massive black holes at redshifts of $z \sim 100$ (Gnedin & Ostriker, 1992), primordial black hole evaporation (Page & Hawking, 1976), and other unresolved point sources like galaxies and AGNs. Current candidates for the dominate unresolved point sources of the EGB include star-forming galaxies, starburst galaxies, and blazars (those AGNs that have their relativistic jets pointing at us) (e.g., Pavlidou & Fields, 2001; Prodanović & Fields, 2006; Fields et al., 2010; Makiya et al., 2011; Thompson et al., 2007; Stecker, 2007; Stecker & Venters, 2010; Venters & Pavlidou, 2011; Padovani et al., 1993; Stecker et al., 1993; Pavlidou & Venters,

2008; Mukherjee & Chiang, 1999; Inoue & Totani, 2009). Star-forming galaxies are galaxies with smaller star-formation rates than those of the starburst galaxies. We follow the criterion adopted in Fields et al. (2010) to distinguish star-forming and starburst galaxies. Due to the larger uncertainty in the cosmic-ray propagation in starburst galaxies (e.g., Thompson et al., 2007; Lacki et al., 2010), we will not consider the EGB contribution from starburst galaxies in this paper. However, we will estimate the EGB contribution from quiescent galaxies, which contain little or no star formation and hence have not been included in EGB estimations. Quiescent galaxies usually include all elliptical galaxies and some S0 galaxies. The important factor for the EGB estimation is not the galaxy type but the amount of star formation. Therefore we will discuss galaxies with the following terminologies, star-forming galaxies and quiescent galaxies, and assume no star formation in quiescent galaxies.

Recent studies suggest that the gamma-ray emission in galaxies comes from interaction between cosmic rays and the interstellar medium (ISM). The dominant mechanism for gamma-ray production in such environments is the pion-decay process: $p_{\rm cr}+p_{\rm ISM} \rightarrow p+p+\pi^0$, and $\pi^0 \rightarrow \gamma+\gamma$, in which a cosmic-ray proton $p_{\rm cr}$ interacts with an ISM proton $p_{\rm ISM}$ and produces a neutral pion that quickly decays into gamma rays (Stecker, 1971; Abdo et al., 2009a; Strong et al., 2000; Pohl, 1993, 1994).

Supernovae (SNe) are the most favored possibility of the cosmic-ray production sites in galaxies. Many groups have studied the EGB emission from cosmic rays accelerated by SNe in star-forming galaxies (e.g., Dar & Shaviv, 1995; Prodanović & Fields, 2006; Fields et al., 2010; Stecker & Venters, 2010; Makiya et al., 2011). Some estimations suggest that star-forming galaxies can be the dominant source of the EGB (Fields et al., 2010), while other groups predict that a major contribution of the EGB comes from blazars (Stecker & Venters, 2010; Makiya et al., 2011; Inoue & Totani, 2009). However, there exist large uncertainties from the source inputs. Most of the analyses regarding star-forming galaxies focused on the EGB contribution from cosmic rays accelerated by core-collapse supernovae (CC SNe) and implicitly assume that *only* these events accelerate cosmic rays. We extend the analysis

of the EGB from star-forming galaxies in Fields et al. (2010) to include Type Ia SNe as accelerators in the Milky Way and in other galaxies.

CC SNe arise in massive stars with short lifetimes, and thus trace ongoing star formation. In contrast, Type Ia supernovae result from thermonuclear runaway of white dwarfs accreting mass from their companion stars and hence are related to star formation with some delay time. For this reason, observations have shown that Type Ia SNe exist in both star-forming galaxies and quiescent galaxies, while CC SNe are rarely seen in quiescent galaxies (Filippenko, 2001; Mannucci et al., 2005). Observations have suggested that the intrinsic cosmic CC SN rate is about 4.5 times higher than the intrinsic cosmic Ia SN rate at redshift $z < 0.4$ (Bazin et al., 2009). Also, studies suggest that the Ia rate in a star-forming galaxy is much larger than that in a quiescent galaxy (Mannucci et al., 2005; Sullivan et al., 2006),

The efficiency of cosmic-ray acceleration by SNe remains poorly understood but is crucial for understanding cosmic-ray acceleration physics as well as supernova energy feedback. Theories propose that cosmic rays are produced by diffusive shock acceleration in the blast waves from SN explosions (e.g., Schlickeiser, 1989; Berezhko & Ellison, 1999). Current studies suggest that $\sim 30\%$ of the initial kinetic energy from a supernova needs to be transferred to cosmic-ray acceleration if we assume that supernovae are the dominate sources for cosmic-ray production and the nucleosynthesis of Be^6, Li^6, and B in the Milky Way (Fields et al., 2001). Also, some theoretical predictions expect the cosmic-ray acceleration efficiency in quiescent galaxies is much lower than in star-forming galaxies. Dorfi & Voelk (1996) suggest that only $\lesssim 1\%$ of the total explosion energy goes into cosmic-ray energy.

Understanding the supernova rate and their efficiency in producing cosmic rays is critical for studying the EGB contributions from these galaxies. Our knowledge about SNe will increase significantly when the next generation optical survey telescope, the Large Synoptic Survey Telescope (LSST), comes online during the next decade. LSST is planning to scan the whole available sky, repeated every $\sim$ 3 days, with unprecedented survey sensitivity (Ivezic et al., 2008). The project will observe $\sim 10^5$ CC SNe per year out to redshift $z \sim 1$

(Lien & Fields, 2009) and $\sim 5 \times 10^4$ Type Ia events out to redshift $z \sim 0.8$ (Bailey et al., 2009). The cosmic SN rate can thus be measured via *direct counting* to high redshift with extremely low statistical uncertainty.

In this paper, we will first describe the general formalism of estimating the EGB from cosmic rays accelerated by supernovae in both star-forming and quiescent galaxies (§ 5.3). We will then discuss the cosmic Type Ia rate in each galaxy classification that will be used in our EGB analysis (§ 5.4). The estimations of the EGB contribution from Type Ia SNe in star-forming and quiescent galaxies are presented in § 5.5 and § 5.6, respectively. Additionally, we discuss the uncertainties in the EGB predictions in § 5.7. Finally, we summarize the results in § 5.8.

5.3 General Formalism

Integration of the gamma-ray contributions from each unresolved extragalactic source over the line of sight to the cosmic horizon gives the well-known formalism of the EGB intensity,

$$\frac{dI}{dE} = \frac{c}{4\pi} \int \mathcal{L}_\gamma[E_{\rm em}, z](1+z) \left| \frac{dt}{dz} \right| dz, \tag{5.1}$$

where $\mathcal{L}_\gamma[E_{\rm em}, z]$ is the comoving luminosity density (or emissivity) at rest-frame energy $E_{\rm em}$, and $|dt/dz| = [(1+z)H(z)]^{-1} = [(1+z)H_0\sqrt{\Omega_m(1+z)^3+\Omega_\Lambda}]^{-1}$ for the standard ΛCDM cosmology. We use $\Omega_m = 0.274$, $\Omega_\Lambda = 0.726$, and $H_0 = 70.5$ km s^{-1} Mpc^{-1} from the five-year WMAP data (Komatsu et al., 2009).

Because the pionic gamma-ray emission is produced from the interaction between cosmic rays and the hydrogen atoms in the ISM, the pionic gamma-ray luminosity from a specific

galaxy can be written as

$$\mathrm{L}_\gamma(\mathrm{E}_{\mathrm{em}}) = \int \Gamma_{\pi^0\to\gamma\gamma}(E_{\mathrm{em}})\ n_H\ dV_{\mathrm{ism}} \tag{5.2}$$

$$= \Gamma_{\pi^0\to\gamma\gamma}(E_{\mathrm{em}})\ N_H \tag{5.3}$$

where $\Gamma_{\pi^0\to\gamma\gamma}(E_{\mathrm{em}})$ represents a spatial average of the gamma-ray production rate per interstellar hydrogen atom. $N_H = \int n_H\ dV_{\mathrm{ism}}$ is the total number of hydrogen atoms in the galaxy obtained by integrating the number density of hydrogen atom n_H over the ISM volume. N_H is proportional to the total mass of gas in the galaxy M_{gas} and can therefore be estimated by $N_H = X_H\ M_{\mathrm{gas}}/m_p$, where X_H is the mass fraction of hydrogen atoms and m_p is the mass of a proton.

If the entire pionic gamma-ray production rate $\Gamma_{\pi^0\to\gamma\gamma}(E_{\mathrm{em}})$ from a galaxy originates from the cosmic-ray flux Φ_{cr} accelerated by supernovae, we can simply assume $\Gamma_{\pi^0\to\gamma\gamma}(E_{\mathrm{em}}) \propto \Phi_{\mathrm{cr}} \propto\ \Lambda_{\mathrm{esc}}\ R_{\mathrm{SN,eff}}$, where $R_{\mathrm{SN,eff}}$ is the effective supernova rate weighted by the cosmic-ray acceleration efficiency ϵ, and Λ_{esc} is the escape path length of the cosmic ray, which quantifies the cosmic-ray confinement, and we assume the value to be universal and unchanging. $\Gamma_{\pi^0\to\gamma\gamma}(E_{\mathrm{em}})$ can thus be estimated via normalization to the gamma-ray emission of a known galaxy, which would be the Milky Way in our case,

$$\frac{\Gamma_{\pi^0\to\gamma\gamma}(E_{\mathrm{em}})}{\Gamma^{\mathrm{MW}}_{\pi^0\to\gamma\gamma}(E_{\mathrm{em}})} = \frac{\Phi_{\mathrm{cr}}}{\Phi^{\mathrm{MW}}_{\mathrm{cr}}} = \frac{R_{\mathrm{SN,eff}}}{R^{\mathrm{MW}}_{\mathrm{SN,eff}}}. \tag{5.4}$$

The pionic gamma-ray luminosity of a particular galaxy can thus be estimated as

$$\mathrm{L}_\gamma(\mathrm{E}_{\mathrm{em}}) = \Gamma^{\mathrm{MW}}_{\pi^0\to\gamma\gamma}(E_{\mathrm{em}})\ \frac{R_{\mathrm{SN,eff}}}{R^{\mathrm{MW}}_{\mathrm{SN,eff}}}\ X_H\ M_{\mathrm{gas}}/m_p, \tag{5.5}$$

Eq. 5.5 also implies that we assume the same gamma-ray energy spectrum as that of the Milky Way. This pionic gamma-ray spectrum always has a peak at $E \sim m_{\pi^0}/2$, at which the two gamma-ray photons inherit the same rest-mass energy of the decayed π^0. At large

energy, the spectrum shows the same asymptotic index as that of the cosmic-ray spectrum, which we take to be 2.75 as in Fields et al. (2010).

Theoretically, both CC SNe and Type Ia events produce cosmic rays and hence pionic gamma rays. Therefore the effective supernova rate $R_{\rm SN,eff}$ in Eq. 5.5 is a combination of the effective Type Ia rate $R_{\rm Ia,eff} \equiv \epsilon_{\rm Ia}\ R_{\rm Ia}$ and the effective CC SN rate $R_{\rm CC,eff} \equiv \epsilon_{\rm CC}\ R_{\rm CC}$, where $\epsilon_{\rm Ia}$ and $\epsilon_{\rm CC}$ are the cosmic-ray production efficiencies of Type Ia and CC SNe, respectively. There exist slightly different definitions of the cosmic-ray acceleration efficiency in current literature. For example, some studies present the efficiency as the fraction of the total cosmic-ray production energy out of the total kinetic energy output from a supernova (e.g., Dorfi & Voelk, 1996; Fields et al., 2001; Helder et al., 2010), while other studies define the parameter as the percentage of the energy flux that becomes relativistic particles after crossing the shock (e.g., Ellison et al., 2007). Most of these definitions describe the fraction of the supernova explosion energy that become cosmic rays. Therefore, if we assume all supernovae have the same explosion energy and the produced cosmic rays have the same energy spectrum, the cosmic-ray acceleration efficiency will be proportional to the total cosmic-ray production in a galaxy over the supernova rate in that galaxy, i.e., $\epsilon \propto \Phi_{\rm cr}/(\Lambda_{\rm esc}\ R_{\rm SN})$. Since we normalized our prediction to the gamma-ray production in the Milky Way (Eq. 5.5), the important factor in the calculation is not the absolute value of ϵ, but the difference between the acceleration efficiency ϵ in different supernova types (Ia and CC) and galaxy classes (quiescent and star-forming). In other words, it is important to know the fractions $\epsilon_{\rm Ia}/\epsilon_{\rm CC}$ and $\epsilon_{\rm Q}/\epsilon_{\rm S}$. Unfortunately, these two fractions are poorly known. Thus for our fiducial numerical results, we will take $\epsilon_{\rm Ia}/\epsilon_{\rm CC} = 1$ and $\epsilon_{\rm Q}/\epsilon_{\rm S} = 1$. However, we will keep the notations of the acceleration efficiencies in our formalism to keep in mind that the efficiencies might depend on supernova types and galaxy environments. Further possibilities of choosing different cosmic-ray acceleration efficiencies will be discussed in § 5.6.

Star-forming galaxies contain both Type Ia and CC SNe. Therefore their pionic gamma-

ray luminosity density $\mathcal{L}_{\gamma,\mathrm{S}}$ can be calculated by averaging over te galaxy density n_{galaxy},

$$\mathcal{L}_{\gamma,\mathrm{S}} = \frac{\Gamma^{\mathrm{MW}}_{\pi^0\to\gamma\gamma}(E_{\mathrm{em}})}{(\epsilon_{\mathrm{Ia,MW}}\ R^{\mathrm{MW}}_{\mathrm{Ia}} + \epsilon_{\mathrm{CC,MW}}\ R^{\mathrm{MW}}_{\mathrm{CC}})}\ \frac{X_H}{m_p}\ (\langle M_{\mathrm{gas}}\ \epsilon_{\mathrm{Ia,S}} R_{\mathrm{Ia,S}}\ n_{\mathrm{galaxy}}\rangle + \langle M_{\mathrm{gas}}\ \epsilon_{\mathrm{CC}} R_{\mathrm{CC}}\ n_{\mathrm{galaxy}}\rangle). \tag{5.6}$$

In quiescent galaxies, there is almost no star formation. We will assume the star-formation rate (and thus the CC SN rate) to be zero in a quiescent galaxy. However, Type Ia SNe do exist in quiescent galaxies because these events can form after some delay time since the star formation. The pionic gamma-ray luminosity density in quiescent galaxies $\mathcal{L}_{\gamma,\mathrm{Q}}$ only comes from Type Ia events, and therefore

$$\mathcal{L}_{\gamma,\mathrm{Q}} = \frac{\Gamma^{\mathrm{Q0}}_{\pi^0\to\gamma\gamma}(E_{\mathrm{em}})}{\epsilon_{\mathrm{Ia}}\ R^{\mathrm{Q0}}_{\mathrm{Ia}}}\ \frac{X_H}{m_p}\ \langle M_{\mathrm{gas}}\ \epsilon_{\mathrm{Ia,Q}}\ R_{\mathrm{Ia,Q}}\ n_{\mathrm{galaxy}}\rangle. \tag{5.7}$$

$\Gamma^{\mathrm{Q0}}_{\pi^0\to\gamma\gamma}(E_{\mathrm{em}})$ and $R^{\mathrm{Q0}}_{\mathrm{SN}}$ are the gamma-ray production rate and Type Ia event rate in a standard quiescent galaxy Q0 for normalization. However, since no gamma-ray emission from a quiescent galaxy has ever been measured, we will still adopt the values of the Milky Way and estimate the gamma-ray luminosity density for quiescent galaxies as

$$\mathcal{L}_{\gamma,\mathrm{Q}} = \frac{\Gamma^{\mathrm{MW}}_{\pi^0\to\gamma\gamma}(E_{\mathrm{em}})}{(\epsilon_{\mathrm{Ia,MW}}\ R^{\mathrm{MW}}_{\mathrm{Ia}} + \epsilon_{\mathrm{CC,MW}}\ R^{\mathrm{MW}}_{\mathrm{CC}})}\ \frac{X_H}{m_p}\ \langle M_{\mathrm{gas}}\ \epsilon_{\mathrm{Ia,Q}}\ R_{\mathrm{Ia,Q}}\ n_{\mathrm{galaxy}}\rangle. \tag{5.8}$$

Note that since the gamma-ray production from the Milky Way comes from both Type Ia and CC SNe, $\Gamma^{\mathrm{MW}}_{\pi^0\to\gamma\gamma}(E_{\mathrm{em}})$ needs to be normalized to the total SN rate in the Milky Way instead of just the Type Ia rate.

The total pionic gamma-ray luminosity density will be a combination of emissions from both star-forming and quiescent galaxies, that is, $\mathcal{L}_{\gamma,\mathrm{tot}} = \mathcal{L}_{\gamma,\mathrm{S}} + \mathcal{L}_{\gamma,\mathrm{Q}}$. The EGB contributions from cosmic rays accelerated by CC SNe has been carefully examined in Fields et al. (2010) and by many other groups (e.g., Stecker & Venters, 2010; Makiya et al., 2011). Here we will focus on the EGB contributions related to Type Ia events. In our calculation, we do not include the intergalactic EGB absorption $\gtrsim 30$ GeV (Salamon & Stecker, 1998).

5.4 The Cosmic Type Ia Supernova Rate in Star-forming and Quiescent Galaxies

Type Ia SNe do not trace immediate star formation because these events have different origins from CC SNe. The prevailing scenarios for Type Ia SN origin include merging of two white dwarfs (double degenerate, Webbink, 1984), or a white dwarf accreting from mass-overflow of its supergiant companion (single degenerate, Nomoto et al., 1984; Iben & Tutukov, 1984). Both of these scenarios involve white dwarfs merging in a binary system, and thus Type Ia SNe are delayed from the formation of the progenitor stars. For this reason, Type Ia SNe are found in all galaxies, including the quiescent galaxies where there is no longer star-forming activity. A complete account of the Type Ia SN contribution to the EGB must therefore include contributions from events in star-forming and quiescent galaxies.

We adopt the comoving cosmic Ia rate density $\mathcal{R}_{\rm Ia} = dN_{\rm Ia}/(dV_{\rm com}\ dt)$ as a function of redshift fitted directly from observational data in the SDSS (Dilday et al., 2010). However, this fitting function is only appropriate out to redshift $z \sim 1$, based on current measurements. The cosmic Ia SN rate beyond redshift $z \sim 1$ remains very uncertain. However, we do know that the cosmic Ia rate should decrease at high redshift. Some of the measurements at high redshift suggest the turn over might happen around redshift $z \sim 1-2$. In our simplified model here, we adopt a decreasing Gaussian function $\mathcal{R}_{\rm Ia} \propto \exp[-(z-1)^2/(2\sigma^2)]$ after the peak at redshift $z = 1$, where $\sigma = 0.6$ and the function is normalized to match the $\mathcal{R}_{\rm Ia}$ value at $z = 1$. Additionally, we place an artificial cutoff of the Ia rate at redshift $z = 2$. The reason is that at $z = 2$, the Type Ia rate in quiescent galaxies, which we take to be a constant, starts to exceed the rate in star-formation galaxies, which is contrary to the theoretical expectation. More detailed explanation can be found in § 5.6, where we discuss the Ia SN rate in quiescent galaxies.

Fig. 5.1 shows the adopted cosmic Ia SN rate as a function of redshift. Although the uncertainty in the rate increases significantly at higher redshift, most of the EGB from Type

Ia SNe arises from events at lower redshift ($z \lesssim 1$) (Ando & Pavlidou, 2009). Therefore the choice of the Type Ia rate at $z \gtrsim 1$ only has a small effect on the final estimation of the EGB. The black curve plots the total cosmic Ia SN rate in both star-forming and quiescent galaxies. The red curve shows the cosmic Ia SN rate in only quiescent galaxies. We adopted a constant rate for quiescent galaxies, for the reason explained in § 5.6. The blue curve represents the cosmic Ia SN rate in only star-forming galaxies, which we calculated by subtracting the total rate from the rate in quiescent galaxies.

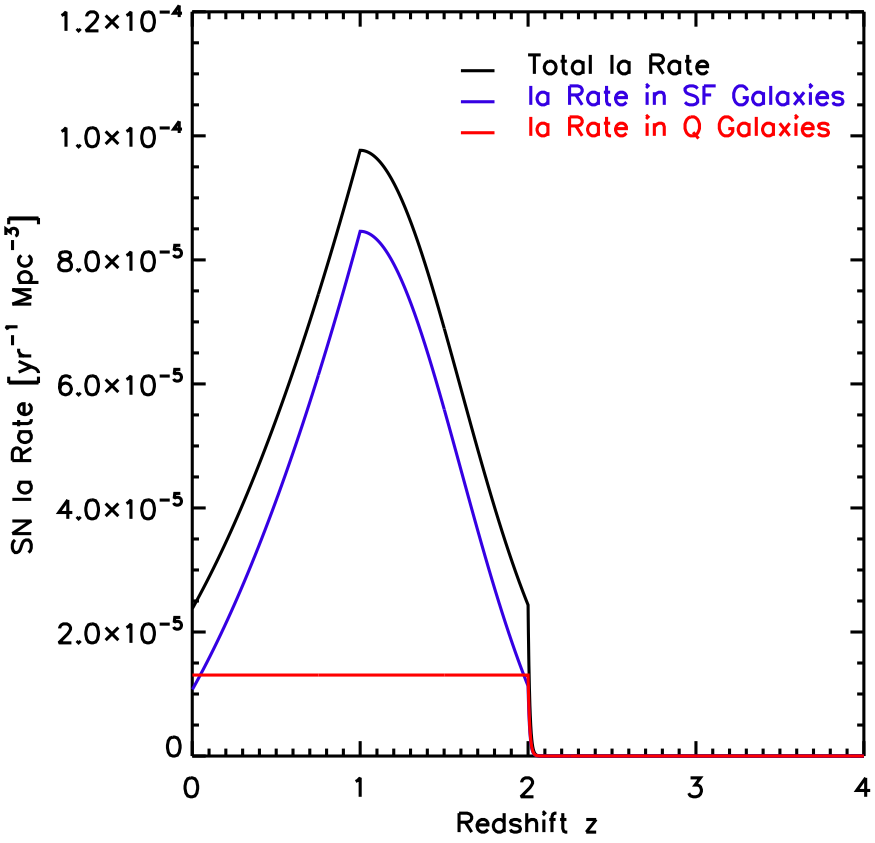

Figure 5.1: The adopted Type Ia SN rate. The black curve plots the total cosmic Type Ia rate; blue curve plots the cosmic Ia rate in star-forming galaxies; red curve plots the cosmic Ia rate in quiescent galaxies.

5.5 The Extragalactic Gamma-ray Background from Type Ia Supernovae in Star-forming Galaxies

As described in § 5.3, the EGB luminosity density $\mathcal{L}^{\rm Ia}_{\gamma,{\rm S}}$ is dominated by two physics inputs: the supernova rate in a galaxy, which is associated with the amount of cosmic rays, and the total gas mass of that galaxy, which accounts for the total hydrogen targets that interact with the cosmic rays. To reflect these two physics inputs, we follow the approach adopted in Fields et al. (2010) and rewrite the EGB contribution from Type Ia events (the first term in Eq. 5.6) as below,

$$\mathcal{L}^{\rm Ia}_{\gamma,{\rm S}} = \frac{\epsilon_{\rm Ia,S}\ \Gamma^{\rm MW}_{\pi^0\to\gamma\gamma}(E_{\rm em})}{(\epsilon_{\rm Ia,MW}\ R^{\rm MW}_{\rm Ia} + \epsilon_{\rm CC,MW}\ R^{\rm MW}_{\rm CC})}\ \frac{X_H}{m_p}\ \langle M_{\rm gas,S}\rangle\ \mathcal{R}_{\rm Ia,S}, \tag{5.9}$$

where

$$\langle M_{\rm gas,S}\rangle \equiv \frac{\langle M_{\rm gas,S}\ \ R_{\rm Ia,S}\ n_{\rm galaxy,S}\rangle}{\langle R_{\rm Ia,S}\ n_{\rm galaxy,S}\rangle} \tag{5.10}$$

$$= \frac{\int dL_{\rm H_{\alpha,z}}\ M_{\rm gas,S}(L_{\rm H_\alpha},z)\ R_{\rm Ia,S}(L_{\rm H_\alpha},z)\ \frac{dn}{dL_{\rm H_{\alpha,z}}}}{\int dL_{\rm H_{\alpha,z}}\ R_{\rm Ia,S}(L_{\rm H_\alpha},z)\ \frac{dn}{dL_{\rm H_{\alpha,z}}}}, \tag{5.11}$$

and $\mathcal{R}_{\rm Ia,S} \equiv \langle R_{\rm Ia,S}\ n_{\rm galaxy,S}\rangle$ is the cosmic Type Ia rate in star-forming galaxies, as shown in Fig. 5.1. In a star-forming galaxy, the galaxy gas mass $M_{\rm gas,S}$ and the galaxy Type Ia rate $R_{\rm Ia}$ can be related to the star-formation rate in that galaxy, which can be connected to the observable H_α luminosity $L_{\rm H_{\alpha,z}}$ of the galaxy by $\psi(L_{\rm H_\alpha},z)/(1\ M_\odot\ \ {\rm yr}^{-1}) = {\rm L_{H_{\alpha,z}}}/(1.26\times 10^{34}$ W) (Hopkins, 2004). Therefore we express the gas mass $M_{\rm gas,S}$ and the Type Ia rate $R_{\rm Ia}$ in terms of $L_{\rm H_{\alpha,z}}$. The corresponding galaxy luminosity function at this wavelength can be expressed by the Schechter function (Nakamura et al., 2004).

At a specific redshift, the gas mass in star-forming galaxies $M_{\rm gas,S}$ and the star-formation

rate can be connected by

$$M_{\rm gas,S} = 2.8 \times 10^9 \ M_\odot \ (1+z)^{-\beta} \ \left(\frac{\psi}{1 \ M_\odot \ {\rm yr}^{-1}} \right)^{\omega}, \tag{5.12}$$

with $\beta = 0.571$ and $\omega = 0.714$, as shown in Fields et al. (2010). The Type Ia rate in a galaxy can be linked to the star-formation rate via some delay-time distribution $\Delta(\tau)$,

$$R_{\rm Ia}(z) \propto \int_0^{t(z)} \ \psi(t-\tau) \ \Delta(\tau) \ d\tau, \tag{5.13}$$

where $t(z)$ is the corresponding cosmic age at redshift z. The delay-time distribution $\Delta(\tau)$ gives the probability that a Type Ia SN explodes a time τ after the progenitor's birth. More detailed discussion about the delay-time distribution can be found in the Supplement. The galaxy luminosity function at a certain redshift for star-forming galaxies in the H_α band can be presented in the form of a Schechter function of

$$\frac{dn}{dL_{\rm H_{\alpha,z}}} = \frac{n_{\star,z}}{L_{\star,z}} \ (\frac{L_{\rm H_{\alpha,z}}}{L_{\star,z}})^{-\alpha} \ e^{-L_{\rm H_{\alpha,z}}/L_{\star,z}} \tag{5.14}$$

with $\alpha = 1.43$ (Nakamura et al., 2004).

In general, it is hard to know how the galaxy luminosity $L_{\rm H_{\alpha,z}}$ evolves with redshift. However, we can investigate the evolution in two simplified cases: pure luminosity evolution and pure density evolution. Pure luminosity evolution assumes that galaxy luminosities evolve with redshift, while galaxy density stays unchanged, i.e., $L_{\star,z}$ in Eq. 5.14 has redshift dependence and $n_{\star,z}$ does not. Pure density evolution assumes that galaxy density evolves with redshift, while galaxy luminosity remains constant, i.e., $n_{\star,z}$ in Eq. 5.14 depends on redshift and $L_{\star,z}$ does not. The real situation should be bracketed by these possibilities.

5.5.1 Pure Luminosity Evolution

In the case of pure luminosity evolution, there is no evolution of the galaxy density. Therefore, evolution of the star-formation rate in each galaxy, and hence the evolution of the galaxy H_α luminosity $L_{\mathrm{H}_{\alpha,z}}$, must trace the general evolution of the cosmic star-formation rate $\dot{\rho}_\star$. Under this assumption, we can show that $\langle M_{\mathrm{gas,S}} \rangle$ is independent of the choice of the delay-time function (see derivation in the Supplement). When adopting the Schechter function for $\frac{dn_{\mathrm{galaxy,S}}}{dL_{\mathrm{H}_{\alpha,z}}}$, one will find that $\langle M_{\mathrm{gas,S}} \rangle \propto (1+z)^{-\beta}\ (L_{\star,z})^{\omega} \propto (1+z)^{-\beta}\ (\frac{\dot{\rho}_\star(z)}{\dot{\rho}_\star(z=0)})^{\omega}$, with a local value of $\langle M_{\mathrm{gas,S}} \rangle_{z=0} = 6.8 \times 10^9\ M_\odot$ (see detailed calculation in the Supplement).

The predicted EGB from Type Ia SNe in star-forming galaxies is plotted as the solid blue line in the left panel of Fig. 5.2. For comparison, the dashed blue line shows the EGB contribution from CC SNe in star-forming galaxies. The shape of the dashed blue lines trace the results in Fields et al. (2010). However, the normalization of the CC SN curves is lower by the fraction of the CC SN rate over the total SN rate (~ 0.82 from Bazin et al., 2009), which is due to the fact that Fields et al. (2010) have implicitly assumed that CC SNe produce all of the gamma-ray emission in galaxies. Our estimation shows that the EGB from Type Ia SNe is around an order-of-magnitude lower than those from CC SNe, which is due to the lower Type Ia rate in star-forming galaxies. The black curve in Fig. 5.2 presents the total EGB emission from both Type Ia and CC SNe in star-forming galaxies. Note that even though we added the EGB contribution from Type Ia SNe, we also lower the EGB emission from CC events by the corresponding CC SN fraction. The Ia to CC fraction does not change much within $z \sim 1$, which is the redshift range where most of the EGB signals originate. Therefore the total EGB emission from star-forming galaxies turns out to be very similar to the prediction in Fields et al. (2010), in which the authors assumed that all of the EGB contribution comes from the CC events.

The shape of the EGB curves in Fig. 5.2 trace the general features of the pionic gamma-ray energy spectrum. This is because the observed EGB intensity at a specific energy originated from a combination of sources at different redshifts, as described in Eq. 5.1. Therefore, the

redshift evolution of the unresolved sources is smeared out in the energy plot and mostly affects the normalization of the EGB intensity but not the spectral shape.

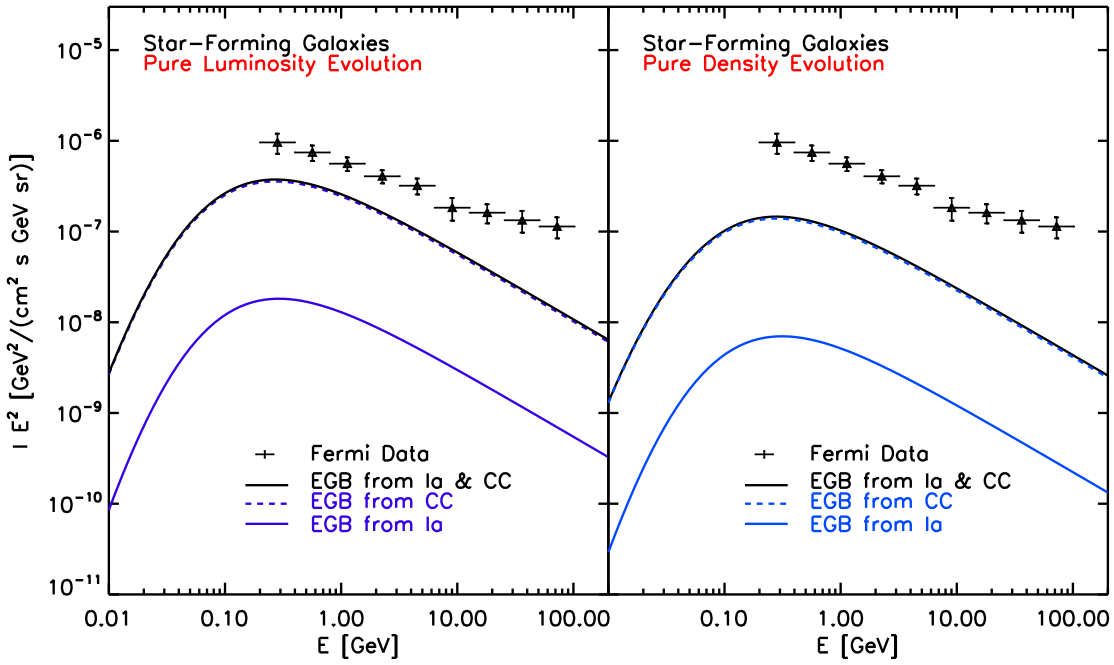

Figure 5.2: The EGB from SNe in star-forming galaxies. Results in the left panel assume pure luminosity evolution. Results in the right panel assume pure density evolution. The dashed blue line shows the contribution from CC SNe; the solid blue line shows the contribution from Ia SNe; and the black line plots the total contribution from both CC and Ia SNe. The *Fermi* data are obtained from Abdo et al. (2009a).

5.5.2 Pure Density Evolution

For pure density evolution, only the galaxy density evolves with redshift while the galaxy luminosity does not. Therefore, the star-formation rate ψ in a galaxy also remains constant, and the evolution in the cosmic star-formation rate will purely depend on the growth of the galaxy density. Hence, in the case of pure density evolution, $L_{\mathrm{H}_{\alpha,z+\Delta z}} = L_{\mathrm{H}_{\alpha,z}}$. With similar calculations as those in the case of pure luminosity evolution (see the Supplement for details), one can find that $\langle M_{\mathrm{gas,S}} \rangle$ is also independent of the choice of the delay-time

function. Also, $\langle M_{\rm gas,S}\rangle \propto (1+z)^{\beta}$ in the case of pure density evolution.

Results for the case of pure density evolution are shown in the right panel of Fig. 5.2. Again, the solid blue line and the dashed blue line represent the EGB from Type Ia and CC, respectively. The black line shows the combined gamma-ray contribution from both Type Ia and CC events. Similar to the results of pure luminosity evolution, the EGB from Type Ia SNe is lower than that from CC events because of the lower Type Ia rate. Additionally, the predicted EGB emission is slightly lower if we assume pure density evolution instead of pure luminosity evolution.

5.6 The Extragalactic Gamma-ray Background from Type Ia Supernovae in Quiescent Galaxies

Following a similar procedure to § 5.5, we will now discuss the EGB from cosmic rays accelerated by Type Ia SNe in quiescent galaxies. We again express the EGB luminosity density $\mathcal{L}^{\rm Ia}_{\gamma,{\rm Q}}$ (Eq. 5.8) in the following form to describe the physics inputs from the average gas mass $\langle M_{\rm gas,Q}\rangle$ and the cosmic Ia rate in quiescent galaxies $\mathcal{R}_{\rm Ia,Q}$,

$$\mathcal{L}^{\rm Ia}_{\gamma,{\rm Q}} = \frac{\epsilon_{\rm Ia,Q}\ \Gamma^{\rm MW}_{\pi^0\rightarrow\gamma\gamma}(E_{\rm em})}{(\epsilon_{\rm Ia,MW}\ R^{\rm MW}_{\rm Ia} + \epsilon_{\rm CC,MW}\ R^{\rm MW}_{\rm CC})}\ \frac{X_H}{m_p}\ \langle M_{\rm gas,Q}\rangle\ \mathcal{R}_{\rm Ia,Q}, \tag{5.15}$$

where

$$\langle M_{\rm gas,Q}\rangle \equiv \frac{\langle M_{\rm gas,Q}\ R_{\rm Ia,Q}\ n_{\rm galaxy,Q}\rangle}{\langle R_{\rm Ia,Q}\ n_{\rm galaxy,Q}\rangle} \tag{5.16}$$

$$= \frac{\int dM_{\star,{\rm Q}}\ M_{\rm gas,Q}(M_{\star,{\rm Q}},z)\ R_{\rm Ia,Q}(M_{\star,{\rm Q}},z)\ \frac{dn}{dM_{\star,{\rm Q}}}}{\int dM_{\star,{\rm Q}}\ R_{\rm Ia,Q}(M_{\star,{\rm Q}},z)\ \frac{dn}{dM_{\star,Q}}}, \tag{5.17}$$

Unlike the star-forming galaxies, where both $\langle M_{\rm gas,S}\rangle$ and $\mathcal{R}_{\rm Ia,S}$ can be related to the observable H_α luminosity, it is easier to connect both $\langle M_{\rm gas,Q}\rangle$ and $\mathcal{R}_{\rm Ia,Q}$ to the total stellar mass $M_{\star,{\rm Q}}$ in a quiescent galaxy.

For the cosmic Type Ia rate in quiescent galaxies, we adopt the estimation from Sullivan et al. (2006), which can be linked to $M_{\rm gas,Q}$ directly. These authors assume a bimodal delay-time distribution and decompose the Ia rate into two groups: the long-delay time and short-delay time. In their model, the short-delay time group simply traces the star-formation rate, while the long-delay time group has a constant probability for all delay times, i.e., $\Delta(\tau) = {\rm A} = {\rm constant}$. Therefore the Type Ia rate in a galaxy can be written as

$$R_{\rm Ia} = A\ M_{\star,{\rm Q}} + B\ \psi. \tag{5.18}$$

$\psi \sim 0$ in a quiescent galaxy, thus $R_{\rm Ia,Q} = A\ M_{\star,{\rm Q}}$, where $M_{\star,{\rm Q}}$ is the total stellar mass created throughout the star-formation history in the quiescent galaxy. Sullivan et al. (2006) estimated $A = 5.1 \times 10^{-14}$ yr^{-1} M$_{\odot}^{-1}$ in quiescent galaxies based on measurements of the Type Ia rate in the Supernova Legacy Survey (SNLS).

Although quiescent galaxies have almost no active star formation, the bulk of their baryonic content is in diffuse hot gas that can be seen in X-ray. Observations have suggested that the $M_{\rm gas}/M_{\rm baryon}$ fraction in quiescent galaxies is typically larger than that in star-forming galaxies (e.g., Dorfi & Voelk, 1996; Mathews & Brighenti, 2003; Jiang & Kochanek, 2007). The existence of the large amount of hot gas in quiescent galaxy is crucial for the EGB prediction. Since most of the studies show the galaxy gas mass in different galaxy types and quiescent galaxies is dominated by early-type galaxies, we will use the estimation of the gas mass in early-type galaxies as the amount of gas in quiescent galaxies. Jiang & Kochanek (2007) found that the average stellar mass fraction of the total halo mass in early-type galaxies is $M_{\star}/M_{\rm tot} \sim 0.026$ or 0.056 based on different assumptions of the halo mass dynamics. Both of these numbers are significantly lower than the cosmological baryon-to-mass ratio $\Omega_b/\Omega_m \sim 0.176$ measured by WMAP (Spergel et al., 2007). If we assume that the baryon-to-mass ratio in a galaxy can be well-represented by the cosmological ratio, i.e., $M_b/M_{\rm tot} \sim \Omega_b/\Omega_m$, the result from Jiang & Kochanek (2007) implies a large amount of gas

mass in early-type galaxies, which can be estimated by

$$M_{\rm gas,Q} = (M_{\rm baryon,Q} - M_{\star,\rm Q}) \sim M_{\star,\rm Q}\ (\frac{\Omega_b/\Omega_m}{M_\star/M_{\rm tot}} - 1). \tag{5.19}$$

The values of $M_\star/M_{\rm tot} \sim 0.026$ and 0.056 correspond to $M_{\rm gas,Q} = 5.77\ M_{\star,\rm Q}$ and $M_{\rm gas,Q} = 2.14\ M_{\star,\rm Q}$, respectively. Here we adopt the latter number to be more conservative in our estimation.

According to the observational results in Pannella et al. (2009), the stellar mass function $\frac{dn}{dM_\star,Q}$ evolves only slightly with redshift. Also, we find that the $\frac{dn}{dM_\star,Q}$ shown in Pannella et al. (2009) can be roughly fitted by the following function,

$$\frac{dn}{d(\log M_{\star,\rm Q})} = C_m\ \exp(-\frac{(\log M_{\star,\rm Q} - 10.7)^2}{2\sigma_m^2}) \tag{5.20}$$

where $C_m = 10^{-2.8}$ Mpc^{-3}, $\sigma_m = 0.56$, and $M_{\star,\rm Q}$ is in units of $M_\odot$. The Type Ia rate in quiescent galaxies provided in Sullivan et al. (2006) and the stellar mass function suggested by Pannella et al. (2009) (Eq. 5.20) give a cosmic Ia SN rate of $\mathcal{R}_{\rm Ia,Q}(z = 0) = 1.31 \times 10^{-5}$yr^{-1} Mpc^{-3}, and $\langle M_{\rm gas,Q}\rangle_{z=0} = 1.30 \times 10^{11}\ M_\odot$. Both of these numbers are constant with redshift, as a result of assuming a non-evolving stellar-mass function. However, we know that the cosmic Ia SN rate $R_{\rm Ia,Q}$ in quiescent galaxy must decrease at high redshift. Therefore we impose an artificial cutoff for the rate at redshift $z = 2$, which is the redshift when $\mathcal{R}_{\rm Ia,Q}$ equals the cosmic Type Ia rate in star-forming galaxies $\mathcal{R}_{\rm Ia,S}$ adopted in this paper (see Fig. 5.1).

The red curves in Fig. 5.3 plot the EGB estimation from Type Ia SNe in quiescent galaxies. Note that these results assume the same cosmic-ray acceleration efficiencies and cosmic-ray confinement in both quiescent galaxies and star-forming galaxies. The EGB emissions from SNe in star-forming galaxies are plotted as blue curves for comparison. The total EGB emissions from SNe in both star-forming and quiescent galaxies are plotted as black curves. The left panel plots results under the assumption of pure luminosity evolution

for the star-forming galaxies. The right panel shows the EGB predictions assuming pure density evolution for the quiescent galaxies.

Notice that the estimated EGB emission from Type Ia SNe in quiescent galaxies is significantly higher than the EGB emission from Type Ia events in star-forming galaxies. The increase in EGB emission is mainly from the larger amount of gas mass in quiescent galaxies. Based on the observational results in Pannella et al. (2009), the stellar mass of a quiescent galaxy is around $10^{11}\ M_{\odot}$, which corresponds to $\sim 2 \times 10^{11}\ M_{\odot}$ of the gas mass according to the conversion suggested in Jiang & Kochanek (2007). Comparing to the general gas mass of about $\sim 10^{9}\ M_{\odot}$ in star-forming galaxies (Fields et al., 2010), the gas mass in quiescent galaxies is about two orders-of-magnitude higher than that in star-forming galaxies. The total Type Ia SN rate in all quiescent galaxies integrated over the entire redshift range is lower than that in star-forming galaxies by around a factor of 5. Therefore the overall EGB emission from Type Ia events in quiescent galaxies is expected to be ~ 20 times higher than the EGB contribution from Type Ia SNe in star-forming galaxies. Additionally, our results indicate that the EGB emission from quiescent galaxies can exceed the EGB emission from CC SNe in star-forming galaxies under current assumptions. With this large EGB contribution from quiescent galaxies, the EGB emission from both quiescent and star-forming galaxies alone can fit the *Fermi* data to $E \sim 3$ GeV, regardless of whether we assume pure luminosity evolution or pure density evolution.

The large EGB production from Type Ia SNe in quiescent galaxies yields a high total EGB emission that is very close to the detections of *Fermi*. This implies two possibilities: (1) If we believe that all the assumptions we adopted are accurate, then quiescent galaxies turn out to be important sources for the EGB. Additionally, the EGB emission would be dominated by star-forming galaxies and quiescent galaxies, which leaves little room for blazars and starburst galaxies. (2) However, if we do believe that blazars and starburst galaxies also contribute a non-negligible amount to the EGB, some of the assumptions for the cosmic-ray production in quiescent galaxies must be wrong. The most uncertain assumptions in this

calculation are probably the cosmic-ray acceleration efficiency ϵ and the escape path length $\Lambda_{\rm esc}$. Although we treated the efficiency and the escape path length to be the same for both Type Ia and CC SNe in all environments, it is likely that these numbers are different in quiescent galaxies. In fact, Dorfi & Voelk (1996) have suggested that the efficiency in quiescent galaxies is at least 10 times lower than that in star-forming galaxies (Dorfi & Voelk, 1996), which could lower our prediction of the EGB from quiescent galaxies by a factor of 10 or even larger. Similarly, a smaller escape path length, i.e., a weaker cosmic-ray confinement, can also decrease our EGB estimation in quiescent galaxies.

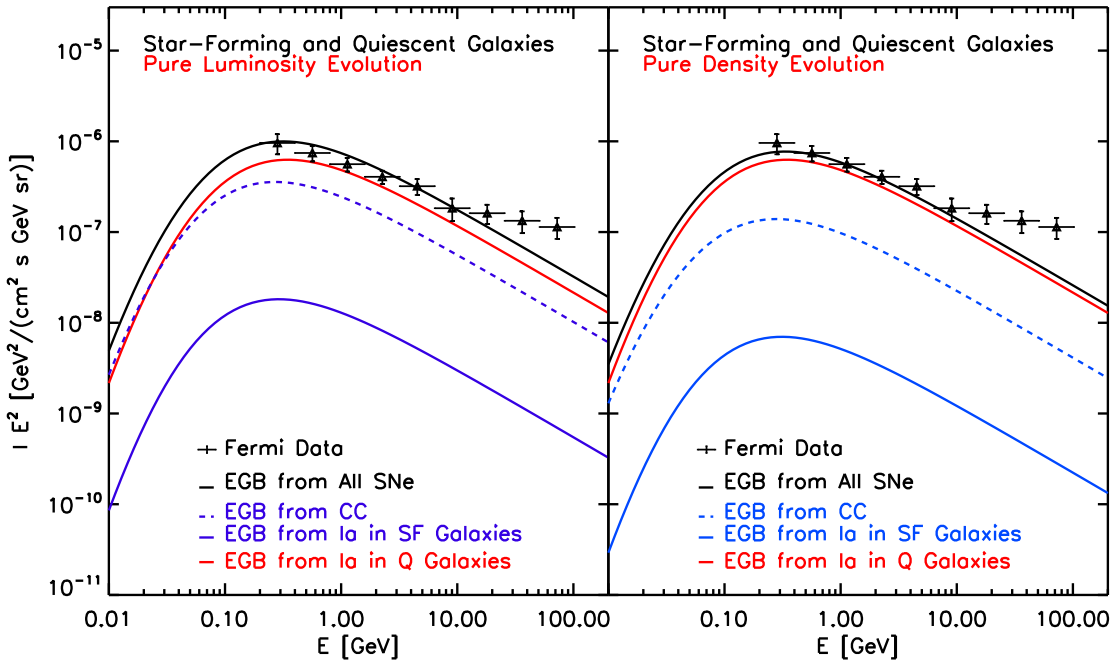

Figure 5.3: The EGB from SNe in both star-forming and quiescent galaxies. Results in the left panel assume pure luminosity evolution. Results in the right panel assume pure density evolution. The dashed blue line shows the contribution from CC SNe; the solid blue line shows the contribution from Ia SNe in star-forming galaxies; the solid red line shows the contribution from Ia SNe in quiescent galaxies; and the black line plots the total contribution from all SNe in both star-forming and quiescent galaxies. The *Fermi* data are obtained from Abdo et al. (2009a).

5.7 The Uncertainties in the Extragalactic Gamma-ray Background Analysis

For star-forming galaxies, currently the main uncertainties in the EGB prediction come from four factors, as described in Fields et al. (2010): (1) uncertainty in the pionic gamma-ray production rate $\Gamma^{\rm MW}_{\pi^0\to\gamma\gamma}(E_{\rm em})$, which is $\sim$ 30% (Abdo et al., 2009b), (2) uncertainty in the normalization of the Galactic supernova rate $R^{\rm MW}_{\rm SN}$, which is $\sim$ 40% (Robitaille & Whitney, 2010), (3) uncertainty in the luminosity scaling in $\langle M_{\rm gas,S}\rangle$, which is $\sim$ 25% (Fields et al., 2010), and (4) uncertainty in the normalization of the cosmic SN rate $\mathcal{R}_{\rm SN,S}$, which is $\sim$ 16% resulting from the uncertainties in the cosmic CC SN rate $\mathcal{R}_{\rm CC} \sim (1.0 \pm 0.2) \times 10^{-4}$ yr^{-1} Mpc^{-3} (Horiuchi et al., 2009) and the cosmic Ia rate $\mathcal{R}_{\rm Ia} \sim (0.25 \pm 0.05) \times 10^{-4}$ yr^{-1} Mpc^{-3} (Horiuchi & Beacom, 2010). The total uncertainty in the EGB prediction will then be $\sim 10^{\pm 0.25}$.

The upcoming large synoptic surveys, such as the LSST, will provide novel information in both the cosmic supernova rate and how they depend on the galaxy types out to high redshift. LSST will detect $\sim 10^5$ CC SNe per year out to redshift $z \sim 1$ (Lien & Fields, 2009) and $\sim 5.0 \times 10^4$ Type Ia events per year out to redshift $z \sim 0.8$ (Bailey et al., 2009). Within one year of observation, LSST is expected to achieve a statistical precision of less than a few percent in the cosmic SN rate. Hence, LSST will almost completely remove the uncertainty input from the cosmic SN rate in the EGB analysis and result in an uncertainty of $\sim 10^{\pm 0.24}$ in the EGB prediction that purely comes from the first three factors described in the previous paragraph.

For quiescent galaxies, many characteristics related to their gamma-ray emissions are poorly understood. Therefore our estimation for the EGB in quiescent galaxies is just to demonstrate possible EGB contribution from quiescent galaxies. Further studies about the gamma-ray emission from quiescent galaxies will be needed for a quantitative analysis of the uncertainty. In additional to detecting on the order of a million SNe throughout the

LSST lifetime, the survey is also expected to observe 10 billion galaxies out to redshift $z \sim 2$ (Ivezic et al., 2008). Thus LSST will be able to provide important information about the galaxy characteristics and supernova rate dependency of galaxy types out to high redshift, which will greatly improve the prediction of the EGB from quiescent galaxies.

5.8 Conclusions

We estimated the EGB contribution from Type Ia SNe in both star-forming and quiescent galaxies. For star-forming galaxies, most of the gamma-ray emission comes from cosmic rays accelerated by CC SNe. This is mainly because there are about 4.5 times more CC SNe than Type Ia events in star-forming galaxies.

However, the Type Ia contribution to the EGB becomes important for quiescent galaxies, where there are almost no CC SNe. Our predictions suggest that the EGB from Type Ia events in quiescent galaxies can be around 1 to 2 orders-of-magnitude higher than those produced by Type Ia SNe in star-forming galaxies, which will make galaxies the dominant source of the EGB. However, our prediction for the EGB in quiescent galaxies is quite uncertain due to several assumptions that contain substantial uncertainties: (1) a quiescent galaxy contains a large amount of hot gas, which is around 100 times more than a star-forming galaxy based on current observations (Pannella et al., 2009), (2) Type Ia rate in a quiescent galaxies is assumed to have no evolution with redshift, and is much lower than that in a star-forming galaxy, and (3) the cosmic-ray acceleration efficiencies and the cosmic-ray confinement are the same for all environments. The third assumption is probably the least understood. If the cosmic-ray acceleration efficiencies and the cosmic-ray confinement depend highly on the galaxy type, the normalization of the EGB from quiescent galaxies could change significantly. However, there exist only a few studies about the cosmic-ray efficiencies in quiescent galaxies, and even less information about how cosmic-ray confinement depends on galaxy types. Dorfi & Voelk (1996) suggest that the cosmic-ray acceleration

efficiency is probably lower in quiescent galaxies than in star-forming galaxies by at least a factor of 10. The EGB detection from *Fermi* along with EGB predictions from other sources, such as blazars and starburst galaxies, will provide important constraints on the cosmic-ray production efficiency of SNe and the cosmic-ray confinement.

In contrast to quiescent galaxies, Type Ia SNe in the star-forming galaxies are not likely to be the dominant source of the EGB based on current observations of the Type Ia rate in star-forming galaxies. CC SNe will still be the major contributors to the EGB due to their larger population. It is thus important to understand the characteristics of CC SNe in order to correctly predict their contribution to the EGB. We conclude that the large supernova sample provided by LSST will offer critical information about the cosmic supernova rate for both CC and Ia events, and their dependence on galaxy types out to high redshift.

The *Fermi* detection of the EGB contains crucial information about the extragalactic gamma-ray source spectrum. Particularly, it can provide an important probe to the cosmic-ray acceleration efficiency and the cosmic-ray confinement in quiescent galaxies. With our knowledge about supernovae increasing rapidly as future synoptic surveys come online, the EGB contribution from supernovae in galaxies can possibly be disentangled from other source candidates.

Acknowledgments We thank Don Ellison, Robert Brunner, Tijana Prodanovic, and Vasiliki Pavlidou for helpful conversations.

5.9 Supplement: The Delay-Time Distribution of Type Ia Supernovae and Detailed Calculation of $\langle M_{\rm gas,S} \rangle$ in Eq. 5.9

The delay time of each Type Ia SN can differ from ~ 0.1 Gyr to ~ 10 Gyr (Mannucci et al., 2005; Scannapieco & Bildsten, 2005; Mannucci et al., 2006; Sullivan et al., 2006; Maoz et al.,

2011). Observationally, the delay times of Type Ia SNe are usually studied via comparison between measurements of the cosmic Type Ia SN rate and the cosmic star-formation rate, and are usually described by some functions of delay-time distribution, which describes the probability of a Type Ia event with a specific delay time. Current proposed delay-time distributions have included a single power law (e.g., Horiuchi & Beacom, 2010; Graur et al., 2011), a Gaussian (e.g., Strolger et al., 2004; Dahlen et al., 2008b), and a bimodal distribution (e.g., Sullivan et al., 2006). The difficulty in determining the delay-time distribution mainly comes from the uncertainty in the cosmic Ia SN rate measurements. Fortunately, the value $\langle M_{\rm gas,S}\rangle$ is independent of the choice of delay-time distribution, as we show in the following derivation.

Based on the relation between the gas mass $M_{\rm gas,S}$ and the star-formation rate ψ (Eq. 5.12), and also the connection between ψ and $L_{\rm H_{\alpha,z}}$, i.e, $\psi(L_{\rm H_\alpha}, z)/(1\ M_\odot\ {\rm yr}^{-1}) = {\rm L_{H_{\alpha,z}}}/(1.26 \times 10^{34}\ {\rm W})$), the $M_{\rm gas,S}$ for a galaxy at redshift z can be directly linked to the observable H_α luminosity $L_{\rm H_{\alpha,z}}$ by $M_{\rm gas,S} = 2.8 \times 10^9\ M_\odot\ (1+z)^{-\beta}\ (\frac{L_{\rm H_{\alpha,z}}}{1.26\times10^{34}\ {\rm W}})^{\omega}$. Additionally, the Type Ia rate can also be related to $L_{\rm H_{\alpha,z}}$ by

$$R_{\rm Ia,S} \propto \int_0^t L_{H_\alpha}(t-\tau)\ \Delta(\tau)\ {\rm d}\tau, \tag{5.21}$$

where $L_{H_\alpha}(t-\tau) \equiv L_{\rm H_{\alpha,z+\Delta z}}(t,\tau)$, which is the H_α luminosity measured at some earlier time $t-\tau$ or larger redshift $z+\Delta z$. Therefore $\langle M_{\rm gas,S}\rangle$ can be expressed in terms of $L_{\rm H_{\alpha,z}}$,

$$\langle M_{\rm gas,S}\rangle \propto \frac{\int dL_{\rm H_{\alpha,z}}\ (1+z)^{-\beta}\ (L_{\rm H_{\alpha,z}})^{\omega}\ (\int_0^t\ L_{\rm H_{\alpha,z+\Delta z}}(t,\tau)\ {\rm DTD}(\tau)\ {\rm d}\tau)\frac{{\rm dn_{galaxy,S}}}{{\rm dL_{H_{\alpha,z}}}}}{\int dL_{\rm H_{\alpha,z}}\ (\int_0^t\ L_{\rm H_{\alpha,z+\Delta z}}(t,\tau)\ {\rm DTD}(\tau)\ {\rm d}\tau)\ \frac{{\rm dn_{galaxy,S}}}{{\rm dL_{H_{\alpha,z}}}}} \tag{5.22}$$

This equation expresses only the redshift-dependent terms and we will further calculate how $\langle M_{\rm gas,S}\rangle$ evolves with redshift in the case of pure luminosity evolution and pure density evolution respectively in § 5.9.1 and § 5.9.2. Fields et al. (2010) shows that the local value of $\langle M_{\rm gas,S}\rangle_{z=0} = 6.8 \times 10^9\ M_\odot$.

5.9.1 Pure Luminosity Evolution

In the case of pure luminosity evolution, the star-formation rate in each galaxy traces the general evolution of the cosmic star-formation rate, i.e. $\frac{\psi(z+\Delta z)}{\psi(z)} = \frac{\dot{\rho}_\star(z+\Delta z)}{\dot{\rho}_\star(z)}$. Therefore from the directly proportional relation between the star-formation rate ψ in a galaxy and the galaxy H_α luminosity $L_{\mathrm{H}_{\alpha,\mathrm{z}}}$, one can trace the evolution of the H_α luminosity via the history of cosmic star-formation rate, which is well-known out to redshift $z \sim 1$ (e.g., Hopkins, 2004; Hopkins & Beacom, 2006, and references therein). That is, $\frac{L_{\mathrm{H}_{\alpha,\mathrm{z}+\Delta\mathrm{z}}}}{L_{\mathrm{H}_{\alpha,\mathrm{z}}}} = \frac{\psi(z+\Delta z)}{\psi(z)} = \frac{\dot{\rho}_\star(z+\Delta z)}{\dot{\rho}_\star(z)}$. Therefore the galaxy luminosity at different redshifts can be found by

$$L_{\mathrm{H}_{\alpha,\mathrm{z}+\Delta\mathrm{z}}} = L_{\mathrm{H}_{\alpha,\mathrm{z}}}\ \frac{\dot{\rho}_\star(z+\Delta z)}{\dot{\rho}_\star(z)} \equiv L_{\mathrm{H}_{\alpha,\mathrm{z}}}\ \frac{\dot{\rho}_\star(t-\tau)}{\dot{\rho}_\star(t)}. \tag{5.23}$$

With this relation, $\langle M_{\mathrm{gas,S}} \rangle$ in Eq. 5.22 can be simplified to

$$\langle M_{\mathrm{gas,S}} \rangle \propto \frac{\int dL_{\mathrm{H}_{\alpha,\mathrm{z}}} (1+z)^{-\beta}\ (L_{\mathrm{H}_{\alpha,\mathrm{z}}})^{\omega}\ (\int_0^t\ L_{\mathrm{H}_{\alpha,\mathrm{z}}}\ \frac{\dot{\rho}_\star(t-\tau)}{\dot{\rho}_\star(t)}\ \Delta(\tau)\ d\tau) \frac{dn_{\mathrm{galaxy,S}}}{dL_{\mathrm{H}_{\alpha,\mathrm{z}}}}}{\int dL_{\mathrm{H}_{\alpha,\mathrm{z}}}\ (\int_0^t\ L_{\mathrm{H}_{\alpha,\mathrm{z}}}\ \frac{\dot{\rho}_\star(t-\tau)}{\dot{\rho}_\star(t)}\ \Delta(\tau)\ d\tau)\ \frac{dn_{\mathrm{galaxy,S}}}{dL_{\mathrm{H}_{\alpha,\mathrm{z}}}}} \tag{5.24}$$

$$= \frac{(1+z)^{-\beta}\ (\int_0^t\ \frac{\dot{\rho}_\star(t-\tau)}{\dot{\rho}_\star(t)}\ \Delta(\tau)\ d\tau)\ \int dL_{\mathrm{H}_{\alpha,\mathrm{z}}}\ (L_{\mathrm{H}_{\alpha,\mathrm{z}}})^{\omega+1}\ \frac{dn_{\mathrm{galaxy,S}}}{dL_{\mathrm{H}_{\alpha,\mathrm{z}}}}}{(\int_0^t\ \frac{\dot{\rho}_\star(t-\tau)}{\dot{\rho}_\star(t)}\ \Delta(\tau)\ d\tau)\ \int dL_{\mathrm{H}_{\alpha,\mathrm{z}}}\ L_{\mathrm{H}_{\alpha,\mathrm{z}}}\ \frac{dn_{\mathrm{galaxy,S}}}{dL_{\mathrm{H}_{\alpha,\mathrm{z}}}}} \tag{5.25}$$

$$= \frac{(1+z)^{-\beta}\ \int dL_{\mathrm{H}_{\alpha,\mathrm{z}}}\ (L_{\mathrm{H}_{\alpha,\mathrm{z}}})^{\omega+1}\ \frac{dn_{\mathrm{galaxy,S}}}{dL_{\mathrm{H}_{\alpha,\mathrm{z}}}}}{\int dL_{\mathrm{H}_{\alpha,\mathrm{z}}}\ L_{\mathrm{H}_{\alpha,\mathrm{z}}}\ \frac{dn_{\mathrm{galaxy,S}}}{dL_{\mathrm{H}_{\alpha,\mathrm{z}}}}}. \tag{5.26}$$

Therefore $\langle M_{\mathrm{gas,S}} \rangle$ is independent of the choice of delay-time distribution.

The assumption of pure luminosity evolution implies that $n_{\star,z}$ in the Schechter function remains constant and $L_{\star,z}$ in the Schechter function evolves as $\dot{\rho}_\star$ (Eq. 5.23). Hence the

redshift dependence of $\langle M_{\rm gas,S}\rangle$ can be further calculated using the Schechter function,

$$\langle M_{\rm gas,S}\rangle \propto (1+z)^{-\beta}\ L^{\omega}_{\star,z}\ \frac{\int^{L_{\rm max}} d(\frac{L_{\rm H_{\alpha,z}}}{L_{\star,z}})\ (\frac{L_{\rm H_{\alpha,z}}}{L_{\star,z}})^{\omega+1}\ \frac{n_{\star,z}}{L_{\star,z}}\ (\frac{L_{\rm H_{\alpha,z}}}{L_{\star,z}})^{-\alpha}\ e^{-L_{\rm H_{\alpha,z}}/L_{\star,z}}}{\int^{L_{\rm max}} d(\frac{L_{\rm H_{\alpha,z}}}{L_{\star,z}})\ \frac{L_{\rm H_{\alpha,z}}}{L_{\star,z}}\ \frac{n_{\star,z}}{L_{\star,z}}\ (\frac{L_{\rm H_{\alpha,z}}}{L_{\star,z}})^{-\alpha}\ e^{-L_{\rm H_{\alpha,z}}/L_{\star,z}}} \tag{5.27}$$

$$= (1+z)^{-\beta}\ L^{\omega}_{\star,z=0}\ (\frac{\dot\rho_\star(z)}{\dot\rho_\star(z=0)})^{\omega}\ \frac{\int^{L_{\rm max}} d(\frac{L_{\rm H_{\alpha,z}}}{L_{\star,z}})\ (\frac{L_{\rm H_{\alpha,z}}}{L_{\star,z}})^{\omega+1}\ \frac{n_{\star,z}}{L_{\star,z}}\ (\frac{L_{\rm H_{\alpha,z}}}{L_{\star,z}})^{-\alpha}\ e^{-L_{\rm H_{\alpha,z}}/L_{\star,z}}}{\int^{L_{\rm max}} d(\frac{L_{\rm H_{\alpha,z}}}{L_{\star,z}})\ \frac{L_{\rm H_{\alpha,z}}}{L_{\star,z}}\ \frac{n_{\star,z}}{L_{\star,z}}\ (\frac{L_{\rm H_{\alpha,z}}}{L_{\star,z}})^{-\alpha}\ e^{-L_{\rm H_{\alpha,z}}/L_{\star,z}}} \tag{5.28}$$

$$\propto (1+z)^{-\beta}\ (\frac{\dot\rho_\star(z)}{\dot\rho_\star(z=0)})^{\omega} \tag{5.29}$$

where $L_{\rm max}$ is the maximum luminosity for star-forming galaxies, which corresponds to the maximum star formation defined in Fields et al. (2010). Galaxies with luminosities greater than $L_{\rm max}$ are considered starburst galaxies and are not included in this calculation. Additionally, we adopt the cosmic star-formation rate $\dot\rho_\star$ described in Horiuchi et al. (2009) based on current observations. Note that because the factors related to delay-time distribution canceled out, this result turns out to be the same as the one obtained in Fields et al. (2010).

5.9.2 Pure Density Evolution

In the case of pure density evolution $L_{\rm H_{\alpha,z+\Delta z}} = L_{\rm H_{\alpha,z}}$ as discussed in § 5.5.2. Thus in the Schechter function, $L_{\star,z}$ remains constant while $n_{\star,z}$ evolves as $\dot\rho_\star$. With similar calculations shown in the case of pure luminosity evolution (§ 5.9.1) and adopting the Schechter function for $\frac{dn_{\rm galaxy,S}}{dL_{\rm H_{\alpha,z}}}$, we can derive the redshift evolution of $\langle M_{\rm gas,S}\rangle$ in the case of pure density

evolution:

$$\langle M_{\rm gas,S}\rangle \propto \frac{\int dL_{\rm H_{\alpha,z}}(1+z)^{-\beta}\ (L_{\rm H_{\alpha,z}})^{\omega}\ (\int_0^t\ L_{\rm H_{\alpha,z}}\ \Delta(\tau)\ d\tau)\frac{dn_{\rm galaxy,S}}{dL_{\rm H_{\alpha,z}}}}{\int dL_{\rm H_{\alpha,z}}\ (\int_0^t\ L_{\rm H_{\alpha,z}}\ \ \Delta(\tau)\ d\tau)\ \frac{dn_{\rm galaxy,S}}{dL_{\rm H_{\alpha,z}}}} \tag{5.30}$$

$$= \frac{(1+z)^{-\beta}\ (\int_0^t\ \Delta(\tau)\ d\tau)\ \int dL_{\rm H_{\alpha,z}}\ (L_{\rm H_{\alpha,z}})^{\omega+1}\ \frac{dn_{\rm galaxy,S}}{dL_{\rm H_{\alpha,z}}}}{(\int_0^t\ \Delta(\tau)\ d\tau)\ \int dL_{\rm H_{\alpha,z}}\ L_{\rm H_{\alpha,z}}\ \frac{dn_{\rm galaxy,S}}{dL_{\rm H_{\alpha,z}}}} \tag{5.31}$$

$$= \frac{(1+z)^{-\beta}\ \int dL_{\rm H_{\alpha,z}}\ (L_{\rm H_{\alpha,z}})^{\omega+1}\ \frac{dn_{\rm galaxy,S}}{dL_{\rm H_{\alpha,z}}}}{\int dL_{\rm H_{\alpha,z}}\ L_{\rm H_{\alpha,z}}\ \frac{dn_{\rm galaxy,S}}{dL_{\rm H_{\alpha,z}}}} \tag{5.32}$$

$$\propto (1+z)^{-\beta}. \tag{5.33}$$

Again, because $\langle M_{\rm gas,S}\rangle$ is independent of the choice of delay-time distribution, the result is identical to the one calculated in Fields et al. (2010).

Chapter 6

Conclusions

The coming decade will be an exciting time for astrophysics and cosmology, with several large synoptic surveys, such as DES, Pan-STARRS 1, LSST, EVLA, and SKA, either running in earnest or ready to come online.

These surveys will provide new insights into the transient sky, and supernovae in particular. In this chapter, we will summarize the main results from our current work and discuss possible future prospects.

6.1 Summary of Current Work

We have primarily focused on the discoveries of core-collapse supernovae and their science potential when combined with multi-messenger observations. Our main conclusions are summarized below.

6.1.1 Core-Collapse Supernovae in the LSST Era

LSST will increase the number of core-collapse supernova detections from a few hundreds in current synoptic surveys to about a million by observing $\sim 10^5$ core-collapse events per year out to redshift $z \sim 1$ if we include the particularly luminous supernova population, and to redshift $z \sim 0.5$ if we do not. This complete and unbiased sample of core-collapse events will measure the cosmic core-collapse supernova rate via *direct counting* and will significantly decrease the statistical uncertainty in cosmic core-collapse supernova rate to less than $\sim 5\%$ within one year of observation. Consequently, the uncertainty of the cosmic star-formation

rate will also be greatly reduced. Moreover, observational characteristics of core-collapse supernovae, such as their luminosity function, their distribution in types and host galaxies, and the possible evolution as a function of redshift, will be much better known.

Furthermore, we investigated core-collapse supernova harvests with multiple survey modes with different survey depth and observing time, and provided survey recommendations for maximizing core-collapse supernova discoveries in LSST. We conclude that a survey cadence of $\sim$ 4 days will be sufficient to obtain a well-sampled lightcurve that includes the peak brightness. Additionally, a deep survey mode with limiting magnitude reaching $26^{\rm mag}$ will yield core-collapse supernova detections out to redshift $z \sim 2$.

6.1.2 Core-Collapse Supernovae and Neutrinos

Current uncertainties in the DSNB come from two physics inputs: the cosmic core-collapse supernova rate and supernova neutrino physics. With LSST removing the uncertainty in the cosmic core-collapse supernova rate, DSNB will be a powerful tool for probing the supernova neutrino physics and the optically "invisible" supernovae.

We showed that within one year of observations with LSST, the improved statistical uncertainty in the cosmic core-collapse supernova rate will be sufficient to distinguish the three different DSNB flux estimated by current candidate models of supernova neutrino physics. Therefore LSST provides a new opportunity to study supernova neutrino physics when combined with neutrino detectors.

Additionally, the comparison between the DSNB detected by neutrino detectors and that estimated from LSST supernova observations encodes critical information on the "invisible events", which are invisible to optical surveys either due to dust obscuration, or collapse directly into black holes and thus fail to release detectable optical signals. Current observational constraints allow the invisible supernova fraction to be as high as $\sim$ 50%. There might be as many invisible supernovae as the visible ones! This fraction will be much better constrained with upcoming large synoptic surveys.

6.1.3 Core-Collapse Supernovae and Radio Observations

To date, only ~ 50 supernovae in the local universe have been seen in radio, none of which are Type Ia. This number will soon be increased enormously by the next generation radio telescope, the Square Kilometer Array (SKA). Based on the current knowledge of radio supernovae, our predictions show that SKA will be capable of detecting ~ 620 core-collapse supernovae per year per square degree out to redshift $z \sim 5$ with its unprecedented sensitivity of $S_{\rm min} = 50$ nJy. The precursors of SKA, such as EVLA, ASKAP, and MeerKAT, will achieve survey sensitivities around 1 μJy and will be able to observe ~ 160 events per year per square degree out to redshift $z \sim 3$. Therefore, SKA will be capable of performing a supernova synoptic survey, which will provide a brand new mode in radio supernova observations that are entirely different from the current targeted searches.

We have also provided survey strategies for SKA in order to maximize the science potential of core-collapse supernova discoveries. We conclude that SKA matches all the requirements for synoptic core-collapse supernova searches, except for those at lower redshift. Due to the limited observational volume, a 1 deg^2 field-of-view does not contain sufficient number of detections per year for synoptic surveys within redshift $z \sim 0.5$. Hence a targeted search based on optical surveys with a much larger sky coverage will offer the best chance of finding radio core-collapse supernovae.

Since dust is almost completely transparent to radio waves, radio observations might be the main, if not the only, method to detect supernovae in dust-obscured regions at high redshift. Comparison between discoveries in radio and optical synoptic surveys will provide important information about dust evolution and total supernova rate out to high redshift.

Our predictions for radio surveys also include Type Ia events. We conclude that SKA will bring hope of the first detection of radio Type Ia supernovae. However, radio follow-ups of optical observations will be the best way to search for such events due to their intrinsically low luminosity in radio.

6.1.4 Supernova Inputs of the Extragalactic Gamma-Ray Background

Following the calculation of the core-collapse supernova contribution to the diffuse extragalactic gamma-ray background (EGB) in Fields et al. (2010), we predict the Type Ia supernova inputs in the EGB. We conclude that in star-forming galaxies, core-collapse supernovae will be the dominant sources of pionic gamma-ray production due to the interaction between supernova-accelerated cosmic rays and interstellar medium. However, Type Ia supernovae in quiescent galaxies might produce unexpectedly large pionic gamma-ray emission if we assume similar cosmic-ray acceleration efficiency and cosmic-ray confinement as those in the star-forming galaxies. Consequently, gamma-ray emission from star-forming and quiescent galaxies will dominate the EGB source spectrum and leave little room for other candidates, such as blazars and starburst galaxies. To avoid this situation, one would need to significantly lower the cosmic-ray production efficiencies and/or the escape path length (which means a weaker cosmic-ray confinement) in quiescent galaxies. In any case, EGB will provide important information about cosmic-ray acceleration and propagation mechanism in galaxies.

Current uncertainty in the EGB from star-forming galaxies is about a factor of $10^{\pm 0.25}$. LSST will completely remove the EGB uncertainty from the cosmic supernova rate and also provide further information about the galaxy luminosity function, the dependency of supernova rate in different galaxy types, and how these relations evolve with redshift.

6.2 Future Prospects

Accompanying the enormous amount of data from future synoptic surveys are the challenges for data management and obtaining related follow-up information that are crucial to reaping the full scientific harvest from these data sets. For example, redshift measurements will need to rely mostly on photometric information. It will also be important to identify supernovae

and distinguish different supernova type with only lightcurves and crude spectroscopic data from the available bandpasses, for it will be impossible to follow-up every single supernova in these large surveys. Most of the existing supernova synoptic surveys have their own software to identify Type Ia supernova candidates before follow-up observations are performed in order to efficiently use the follow-up time. However, fewer efforts are made to identify core-collapse events without follow-up, and almost no attempts have been made to discover radio supernovae with only synoptic searches. Therefore, studying the properties of core-collapse supernovae, especially at radio wavelengths, in the proto-type synoptic surveys is crucial for maximizing the science potential of upcoming observations and be fully prepared for the era of large-scale synoptic surveys. An obvious next step to our current work would be refining the core-collapse supernova program we have developed with updated data and making it into a better tool for analyzing the properties of core-collapse events in both optical and radio wavelength to search for possible techniques capable of identifying supernovae automatically without follow-up information.

Moreover, synoptic surveys and archival data provide easy access to multi-messenger observations, and thus research connecting different fields of astronomy, astrophysics, and cosmology, will be increasingly important. Throughout this thesis, we have discussed several science possibilities to study supernova physics, star formation history, particle astrophysics, dust evolution, and cosmic-ray acceleration by combining surveys in different regime including optical, radio, gamma rays, and neutrinos. More work in exploring science potential of multi-messenger studies can be done.

For example, at least some of the long gamma-ray bursts (GRBs) are connected to core-collapse supernovae (Galama et al., 1998; Soderberg et al., 2006b; Woosley & Bloom, 2006; Gehrels et al., 2009). Long GRBs initially explode in gamma rays, but will later show afterglows in X-rays, radio, and optical wavelengths. Additionally, theories have suggested that long GRBs are likely to originate from supernovae that form spinning black holes (Heger et al., 2003), and thus might be connected to the invisible events discussed in Chapter

3. Therefore synergies between neutrino detections and multi-wavelength observations will provide important information about the origin of GRBs.

Furthermore, combining supernova surveys with galaxy searches will probe the supernova population as a function of host galaxy and galaxy clustering. Particularly, it will be interesting to measure the fraction of hostless supernovae, which are supernovae without visible host galaxies. These hostless events will provide an important insight into the possibility of intergalactic supernovae. Also, these events will be excellent probes of galaxies that are dimmer than the survey sensitivity and will thus provide an independent and possibly the only method to search for extremely dim dwarf galaxies.

As supernova observations firmly step into the synoptic survey era in the next decade, we conclude here with the optimistic expectation that these surveys will finally unveil the mystery of supernovae. We will learn about their origins, explosion mechanism, and their impact on the surrounding environment. Additionally, we look forward to seeing the next Galactic supernova, either in optical, radio, or neutrinos!

References

Abdo, A. A., et al. 2009a, Physical Review Letters, 103, 251101

—. 2009b, ApJ, 703, 1249

Acero, F., et al. 2010, A&A, 516, A62+

Adelberger, K. L., & Steidel, C. C. 2000, ApJ, 544, 218

Aharmim, B., et al. 2006, ApJ, 653, 1545

Ando, S. 2004, ApJ, 607, 20

Ando, S., & Pavlidou, V. 2009, *Mon. Not. Roy. Astron. Soc.*, 400, 2122

Ando, S., & Sato, K. 2004, New Journal of Physics, 6, 170

Ando, S., Sato, K., & Totani, T. 2003, Astroparticle Physics, 18, 307

Ashworth, Jr., W. B. 1980, Journal for the History of Astronomy, 11, 1

Astier, P., et al. 2006, A&A, 447, 31

Baade, W. 1926, Astronomische Nachrichten, 228, 359

Bailey, S., Bernstein, J. P., Cinabro, D., Kessler, R., & Kuhlma, S. 2009, ArXiv e-prints

Baklanov, P. V., Blinnikov, S. I., & Pavlyuk, N. N. 2005, Astronomy Letters, 31, 429

Balberg, S., & Shapiro, S. L. 2001, ApJ, 556, 944

Baldry, I. K., & Glazebrook, K. 2003, ApJ, 593, 258

Baron, E., Nugent, P. E., Branch, D., & Hauschildt, P. H. 2004, ApJ, 616, L91

Bazin, G., et al. 2009, A&A, 499, 653

Beacom, J. F., & Strigari, L. E. 2006, Phys. Rev. C, 73, 035807

Beacom, J. F., & Vagins, M. R. 2004, Phys. Rev. Lett., 93, 171101

Berezhko, E. G., & Ellison, D. C. 1999, ApJ, 526, 385

Berger, E., Kulkarni, S. R., Frail, D. A., & Soderberg, A. M. 2003, ApJ, 599, 408

Bernstein, J. P., Cinabro, D., Kessler, R., & Kuhlma, S. 2009, ArXiv e-prints

Bionta, R. M., et al. 1987, Phys. Rev. Lett., 58, 1494

Bisnovatyi-Kogan, G. S., & Seidov, Z. F. 1982, Sov. Astron., 26, 132

—. 1984, Annals of the New York Academy of Sciences, 422, 319

Blondin, S., & Tonry, J. L. 2007, ApJ, 666, 1024

Botticella, M. T., et al. 2008a, A&A, 479, 49

—. 2008b, A&A, 479, 49

Buras, R., Rampp, M., Janka, H.-T., & Kifonidis, K. 2006, A&A, 447, 1049

Cappellaro, E., Evans, R., & Turatto, M. 1999, A&A, 351, 459

Cappellaro, E., Turatto, M., Tsvetkov, D. Y., Bartunov, O. S., Pollas, C., Evans, R., & Hamuy, M. 1997, A&A, 322, 431

Cappellaro, E., et al. 2005, A&A, 430, 83

Carilli, C. L., & Rawlings, S. 2004, New Astronomy Review, 48, 979

Central Bureau for Astronomical Telegrams. 2008, http://www.cfa.harvard.edu/iau/cbat.html

Chen, H.-W., Prochaska, J. X., & Gnedin, N. Y. 2007, ApJ, 667, L125

Chevalier, R. A. 1982a, ApJ, 259, L85

—. 1982b, ApJ, 259, 302

—. 1998, ApJ, 499, 810

Chin, Y.-N., & Huang, Y.-L. 1994, Nature, 371, 398

Choi, P. I., et al. 2006, ApJ, 637, 227

Chomiuk, L., Soderberg, A. M., Chevalier, R., Badenes, C., & Fransson, C. 2011, in Bulletin of the American Astronomical Society, Vol. 43, American Astronomical Society Meeting Abstracts 217, 304.05

Cole, S., et al. 2001, *Mon. Not. Roy. Astron. Soc.*, 326, 255

Cooke, J. 2008, ApJ, 677, 137

Crockett, R. M., et al. 2007, *Mon. Not. Roy. Astron. Soc.*, 381, 835

Dahlén, T., & Fransson, C. 1999, A&A, 350, 349

Dahlén, T., & Goobar, A. 2002, PASP, 114, 284

Dahlen, T., Strolger, L., & Riess, A. G. 2010, in Bulletin of the American Astronomical Society, Vol. 42, American Astronomical Society Meeting Abstracts 215, 430.23

Dahlen, T., Strolger, L., Riess, A. G., & The GOODS Team. 2008a, The Extended HST Supernova Survey: The Rates of Type Ia and CC SNe at high-z, http://www.arcetri.astro.it/ filippo/snrate08/Home.html

Dahlen, T., Strolger, L.-G., & Riess, A. G. 2008b, ApJ, 681, 462

Dahlen, T., et al. 2004, ApJ, 613, 189

Daigne, F., Olive, K. A., Sandick, P., & Vangioni, E. 2005, Phys. Rev. D, 72, 103007

D'Andrea, C. B., et al. 2010, ApJ, 708, 661

Dar, A. 1985, Phys. Rev. Lett., 55, 1422

Dar, A., & Shaviv, N. J. 1995, Physical Review Letters, 75, 3052

de Blok, E. W. J. G., Booth, R., Jonas, J., & Fanaroff, B. 2010, ISKAF2010 Science Meeting

Dessart, L., & Hillier, D. J. 2005, A&A, 439, 671

—. 2008, *Mon. Not. Roy. Astron. Soc.*, 383, 57

Dessart, L., et al. 2008, ApJ, 675, 644

Dilday, B., et al. 2010, ApJ, 713, 1026

Djorgovski, S. G., et al. 2008, Astronomische Nachrichten, 329, 263

Doggett, J. B., & Branch, D. 1985, AJ, 90, 2303

Domogatskii, G. V. 1984, Sov. Astron., 28, 30

Dorfi, E. A., & Voelk, H. J. 1996, A&A, 307, 715

Drake, A. J., et al. 2009, ApJ, 696, 870

—. 2010, ApJ, 718, L127

Duan, H., Fuller, G. M., Carlson, J., & Qian, Y.-Z. 2006, Phys. Rev. D, 74, 105014

Eck, C. R., Cowan, J. J., Roberts, D. A., Boffi, F. R., & Branch, D. 1995, ApJ, 451, L53+

Ellison, D. C., Patnaude, D. J., Slane, P., Blasi, P., & Gabici, S. 2007, ApJ, 661, 879

Fichtel, C. E., Hartman, R. C., Kniffen, D. A., Thompson, D. J., Ogelman, H. B., Ozel, M. E., & Tumer, T. 1977, ApJ, 217, L9

Fichtel, C. E., Simpson, G. A., & Thompson, D. J. 1978, ApJ, 222, 833

Fields, B. D., Olive, K. A., Cassé, M., & Vangioni-Flam, E. 2001, A&A, 370, 623

Fields, B. D., Pavlidou, V., & Prodanović, T. 2010, ApJ, 722, L199

Filippenko, A. V. 1997, ARA&A, 35, 309

Filippenko, A. V. 2001, in American Institute of Physics Conference Series, Vol. 565, Young Supernova Remnants, ed. S. S. Holt & U. Hwang, 40–58

Frieman, J. A., et al. 2008, AJ, 135, 338

Fryer, C. L. 1999, ApJ, 522, 413

—. 2009, ApJ, 699, 409

Fryer, C. L., et al. 2009, ApJ, 707, 193

Fukugita, M., Ichikawa, T., Gunn, J. E., Doi, M., Shimasaku, K., & Schneider, D. P. 1996, AJ, 111, 1748

Fukugita, M., & Kawasaki, M. 2003, *Mon. Not. Roy. Astron. Soc.*, 340, L7

Gal-Yam, A., & Maoz, D. 2004, *Mon. Not. Roy. Astron. Soc.*, 347, 942

Gal-Yam, A., Maoz, D., & Sharon, K. 2002, in Astronomical Society of the Pacific Conference Series, Vol. 283, A New Era in Cosmology, ed. N. Metcalfe & T. Shanks, 289–+

Gal-Yam, A., et al. 2006, ApJ, 639, 331

—. 2009, Nature, 462, 624

Galama, T. J., et al. 1998, Nature, 395, 670

Gehrels, N., Ramirez-Ruiz, E., & Fox, D. B. 2009, ARA&A, 47, 567

Gezari, S., et al. 2009a, ApJ, 690, 1313

—. 2009b, ApJ, 690, 1313

Gnedin, N. I., & Ostriker, J. P. 1992, ApJ, 400, 1

Gnedin, N. Y., Kravtsov, A. V., & Chen, H.-W. 2008, ApJ, 672, 765

Graur, O., et al. 2011, ArXiv e-prints

Guseinov, O. K. 1967, Sov. Astron., 10, 613

Hamuy, M., & Pinto, P. A. 2002, ApJ, 566, L63

Hartmann, D. H., & Woosley, S. E. 1997, Astroparticle Physics, 7, 137

Hatano, K., Branch, D., & Deaton, J. 1998, ApJ, 502, 177

Heger, A., Fryer, C. L., Woosley, S. E., Langer, N., & Hartmann, D. H. 2003, ApJ, 591, 288

Helder, E. A., Kosenko, D., & Vink, J. 2010, ApJ, 719, L140

Hippelein, H., et al. 2003, A&A, 402, 65

Hirata, K., et al. 1987, Phys. Rev. Lett., 58, 1490

Hopkins, A. M. 2004, ApJ, 615, 209

—. 2007, ApJ, 654, 1175

Hopkins, A. M., & Beacom, J. F. 2006, ApJ, 651, 142

Horiuchi, S., & Beacom, J. F. 2010, ApJ, 723, 329

Horiuchi, S., Beacom, J. F., & Dwek, E. 2009, Phys. Rev. D, 79, 083013

Horiuchi, S., Beacom, J. F., Kochanek, C. S., Prieto, J. L., Stanek, K. Z., & Thompson, T. A. 2011, ArXiv e-prints

Hughes, D. H., et al. 1998, Nature, 394, 241

Hunter, S. D., et al. 1997, ApJ, 481, 205

Iben, Jr., I., & Tutukov, A. V. 1984, ApJS, 54, 335

Inoue, Y., & Totani, T. 2009, ApJ, 702, 523

Iocco, F., Mangano, G., Miele, G., Raffelt, G. G., & Serpico, P. D. 2005, Astroparticle Physics, 23, 303

Ivezic, Z., et al. 2008, ArXiv e-prints

Iwamoto, K., et al. 1998, Nature, 395, 672

Janka, H.-T., Langanke, K., Marek, A., Martínez-Pinedo, G., & Müller, B. 2007, Phys. Rep., 442, 38

Jewitt, D. 2003, Pan-STARRS Science Goals: Science Overview, http://pan-starrs.ifa.hawaii.edu/project/science/precodr.html

Jiang, G., & Kochanek, C. S. 2007, ApJ, 671, 1568

Johnston, S., Feain, I. J., & Gupta, N. 2009, in Astronomical Society of the Pacific Conference Series, Vol. 407, The Low-Frequency Radio Universe, ed. D. J. Saikia, D. A. Green, Y. Gupta, & T. Venturi, 446–+

Kaplinghat, M., Steigman, G., & Walker, T. P. 2000, Phys. Rev. D, 62, 043001

Keller, S. C., et al. 2007, Publ.Astron.Soc.Austral., 24, 1

Kiewe, M., et al. 2010, ArXiv e-prints

Kim, A., Goobar, A., & Perlmutter, S. 1996, PASP, 108, 190

Kim, A. G., & Miquel, R. 2007, Astroparticle Physics, 28, 448

Kim, S. S., & Lee, M. G. 2007, PASP, 119, 1449

Kirshner, R. P., & Kwan, J. 1974, ApJ, 193, 27

Kistler, M. D., Yuksel, H., Ando, S., Beacom, J. F., & Suzuki, Y. 2008a, ArXiv e-prints

Kistler, M. D., Yüksel, H., Beacom, J. F., & Stanek, K. Z. 2008b, ApJ, 673, L119

Kochanek, C. S., Beacom, J. F., Kistler, M. D., Prieto, J. L., Stanek, K. Z., Thompson, T. A., & Yüksel, H. 2008, ApJ, 684, 1336

Komatsu, E., et al. 2009, ApJS, 180, 330

Koyama, K., Petre, R., Gotthelf, E. V., Hwang, U., Matsuura, M., Ozaki, M., & Holt, S. S. 1995, Nature, 378, 255

Krauss, L. M., Glashow, S. L., & Schramm, D. N. 1984, Nature, 310, 191

Kudritzki, R.-P., & Puls, J. 2000, ARA&A, 38, 613

Kulkarni, S. R., et al. 1998, Nature, 395, 663

Kunz, M., Bassett, B. A., & Hlozek, R. A. 2007, Phys. Rev. D, 75, 103508

Kuznetsova, N., et al. 2008, ApJ, 673, 981

Lacki, B. C., Thompson, T. A., Quataert, E., Loeb, A., & Waxman, E. 2010, ArXiv e-prints

Le Floc'h, E., et al. 2005, ApJ, 632, 169

Leaman, J., Li, W., Chornock, R., & Filippenko, A. V. 2011, *Mon. Not. Roy. Astron. Soc.*, 412, 1419

Leibundgut, B., & Suntzeff, N. B. 2003, in Lecture Notes in Physics, Berlin Springer Verlag, Vol. 598, Supernovae and Gamma-Ray Bursters, ed. K. Weiler, 77–90

Leitherer, C., Robert, C., & Drissen, L. 1992, ApJ, 401, 596

Li, W., Chornock, R., Leaman, J., Filippenko, A. V., Poznanski, D., Wang, X., Ganeshalingam, M., & Mannucci, F. 2011a, *Mon. Not. Roy. Astron. Soc.*, 412, 1473

Li, W., et al. 2011b, *Mon. Not. Roy. Astron. Soc.*, 412, 1441

Li, Z.-Y., & Chevalier, R. A. 1999, ApJ, 526, 716

Liebendörfer, M., Rampp, M., Janka, H.-T., & Mezzacappa, A. 2005, ApJ, 620, 840

Lien, A., & Fields, B. D. 2009, *JCAP*, 1, 47

Lien, A., Fields, B. D., & Beacom, J. F. 2010, Phys. Rev. D, 81, 083001

Lunardini, C. 2006, Astroparticle Physics, 26, 190

Lunardini, C. 2007, Phys. Rev. D, 75, 073022

—. 2009, Phys. Rev. Lett., 102, 231101

Lunardini, C., & Peres, O. L. G. 2008, *JCAP*, 8, 33

MacFadyen, A. I., & Woosley, S. E. 1999, ApJ, 524, 262

MacFadyen, A. I., Woosley, S. E., & Heger, A. 2001, ApJ, 550, 410

Madau, P., della Valle, M., & Panagia, N. 1998, *Mon. Not. Roy. Astron. Soc.*, 297, L17+

Madau, P., Ferguson, H. C., Dickinson, M. E., Giavalisco, M., Steidel, C. C., & Fruchter, A. 1996, *Mon. Not. Roy. Astron. Soc.*, 283, 1388

Makiya, R., Totani, T., & Kobayashi, M. A. R. 2011, ApJ, 728, 158

Malaney, R. A. 1997, Astroparticle Physics, 7, 125

Malek, M., et al. 2003, Phys. Rev. Lett., 90, 061101

Mannucci, F., Della Valle, M., & Panagia, N. 2006, *Mon. Not. Roy. Astron. Soc.*, 370, 773

—. 2007, *Mon. Not. Roy. Astron. Soc.*, 377, 1229

Mannucci, F., Della Valle, M., Panagia, N., Cappellaro, E., Cresci, G., Maiolino, R., Petrosian, A., & Turatto, M. 2005, A&A, 433, 807

Maoz, D., & Gal-Yam, A. 2004, *Mon. Not. Roy. Astron. Soc.*, 347, 951

Maoz, D., Mannucci, F., Li, W., Filippenko, A. V., Valle, M. D., & Panagia, N. 2011, *Mon. Not. Roy. Astron. Soc.*, 412, 1508

Maoz, D., Waxman, E., & Loeb, A. 2005, ApJ, 632, 847

Mathews, W. G., & Brighenti, F. 2003, ARA&A, 41, 191

Mezzacappa, A., Liebendörfer, M., Messer, O. E. B., Hix, W. R., Thielemann, F.-K., & Bruenn, S. W. 2001, Phys. Rev. Lett., 86, 1935

Miknaitis, G., et al. 2007, ApJ, 666, 674

Miller, A. A., et al. 2009, ApJ, 690, 1303

Modjaz, M., et al. 2009, ApJ, 702, 226

Mokiem, M. R., et al. 2007, A&A, 473, 603

Montes, M. J., Weiler, K. W., & Panagia, N. 1997, ApJ, 488, 792

Mukherjee, R., & Chiang, J. 1999, Astroparticle Physics, 11, 213

Munari, U., Barbon, R., Piemonte, A., Tomasella, L., & Rejkuba, M. 1998, A&A, 333, 159

Nakamura, O., Fukugita, M., Brinkmann, J., & Schneider, D. P. 2004, AJ, 127, 2511

Nakano, S., & Aoki, M. 1997, IAU circ., 6795, 2

Nakazato, K., Sumiyoshi, K., Suzuki, H., & Yamada, S. 2008, Phys. Rev. D, 78, 083014

—. 2009, Phys. Rev. D, 79, 069901

Nomoto, K., Thielemann, F.-K., & Yokoi, K. 1984, ApJ, 286, 644

Nugent, P., et al. 2006, ApJ, 645, 841

Oda, T., & Totani, T. 2005, ApJ, 630, 59

Olivares, F. 2008, ArXiv e-prints

Padovani, P., Ghisellini, G., Fabian, A. C., & Celotti, A. 1993, *Mon. Not. Roy. Astron. Soc.*, 260, L21

Page, D. N., & Hawking, S. W. 1976, ApJ, 206, 1

Palanque-Delabrouille, N., et al. 2010, A&A, 514, A63+

Panagia, N., Van Dyk, S. D., Weiler, K. W., Sramek, R. A., Stockdale, C. J., & Murata, K. P. 2006, ApJ, 646, 369

Pannella, M., et al. 2009, ApJ, 701, 787

Papenkova, M., Li, W. D., Wray, J., Chleborad, C. W., & Schwartz, M. 2001, IAU circ., 7722, 1

Pastorello, A., et al. 2006, *Mon. Not. Roy. Astron. Soc.*, 370, 1752

Patat, F., Barbon, R., Cappellaro, E., & Turatto, M. 1993, *The Atlas, Astron. Astrophys. Suppl.*, 98, 443

—. 1994, A&A, 282, 731

Pavlidou, V., & Fields, B. D. 2001, ApJ, 558, 63

—. 2002, ApJ, 575, L5

Pavlidou, V., & Venters, T. M. 2008, ApJ, 673, 114

Pérez-González, P. G., Zamorano, J., Gallego, J., Aragón-Salamanca, A., & Gil de Paz, A. 2003, ApJ, 591, 827

Perlmutter, S., et al. 1999, ApJ, 517, 565

Phillips, M. M. 1993a, ApJ, 413, L105

—. 1993b, ApJ, 413, L105

Pisarski, R. L., Helfand, D. J., & Kahn, S. M. 1984, ApJ, 277, 710

Pohl, M. 1993, A&A, 270, 91

—. 1994, A&A, 287, 453

Pooley, D., et al. 2002, ApJ, 572, 932

Poznanski, D., Maoz, D., & Gal-Yam, A. 2007, AJ, 134, 1285

Price, P. A., et al. 2002, ApJ, 572, L51

Prodanović, T., & Fields, B. D. 2006, ApJ, 645, L125

Quimby, R. M., et al. 2009, ArXiv e-prints

Rau, A., et al. 2009, PASP, 121, 1334

Rest, A., et al. 2011, ApJ, 729, 88

Reynolds, S. P., & Chevalier, R. A. 1981, ApJ, 245, 912

Richardson, D., Branch, D., Casebeer, D., Millard, J., Thomas, R. C., & Baron, E. 2002, AJ, 123, 745

Riess, A. G., Press, W. H., & Kirshner, R. P. 1996, ApJ, 473, 88

Riess, A. G., et al. 1998, AJ, 116, 1009

Robitaille, T. P., & Whitney, B. A. 2010, ApJ, 710, L11

Rudaz, S., & Stecker, F. W. 1991, ApJ, 368, 406

Sako, M., et al. 2008, AJ, 135, 348

Salamon, M. H., & Stecker, F. W. 1998, ApJ, 493, 547

Salpeter, E. E. 1955, ApJ, 121, 161

Scannapieco, E., & Bildsten, L. 2005, ApJ, 629, L85

Scannapieco, E., Madau, P., Woosley, S., Heger, A., & Ferrara, A. 2005, ApJ, 633, 1031

Scheck, L., Kifonidis, K., Janka, H.-T., & Müller, E. 2006, A&A, 457, 963

Schlickeiser, R. 1989, ApJ, 336, 243

Shaw, R. L. 1979, A&A, 76, 188

Silk, J., & Srednicki, M. 1984, Physical Review Letters, 53, 624

SKA Design Reference Mission. 2009, http://www.skatelescope.org/PDF/DRM-v1.0.pdf

Smail, I., Ivison, R. J., & Blain, A. W. 1997, ApJ, 490, L5+

Smartt, S. J., Eldridge, J. J., Crockett, R. M., & Maund, J. R. 2009, *Mon. Not. Roy. Astron. Soc.*, 395, 1409

Smith, N., Li, W., Filippenko, A. V., & Chornock, R. 2011, *Mon. Not. Roy. Astron. Soc.*, 412, 1522

Smith, N., et al. 2007, ApJ, 666, 1116

Soderberg, A. M. 2007, in American Institute of Physics Conference Series, Vol. 937, Supernova 1987A: 20 Years After: Supernovae and Gamma-Ray Bursters, ed. S. Immler, K. Weiler, & R. McCray, 492–499

Soderberg, A. M., Chevalier, R. A., Kulkarni, S. R., & Frail, D. A. 2006a, ApJ, 651, 1005

Soderberg, A. M., Frail, D. A., & Wieringa, M. H. 2004, ApJ, 607, L13

Soderberg, A. M., Nakar, E., Berger, E., & Kulkarni, S. R. 2006b, ApJ, 638, 930

Spergel, D. N., et al. 2007, ApJS, 170, 377

Sreekumar, P., et al. 1998, ApJ, 494, 523

Stecker, F. W. 1971, NASA Special Publication, 249

—. 2007, Journal of Physics Conference Series, 60, 215

Stecker, F. W., Morgan, D. L., & Bredekamp, J. 1971, Phys. Rev. Lett., 27, 1469

Stecker, F. W., Salamon, M. H., & Malkan, M. A. 1993, ApJ, 410, L71

Stecker, F. W., & Venters, T. M. 2010, ArXiv e-prints

Stephenson, F. R. 2007, Highlights of Astronomy, 14, 303

Stephenson, F. R., & Green, D. A. 2005, Journal for the History of Astronomy, 36, 217

Stockdale, C. J., Kelley, M., Sramek, R. A., Williams, C. L., Van Dyk, S. D., Weiler, K. W., & Panagia, N. 2006, New Radio Supernova Results

Stockdale, C. J., Kelley, M. T., Weiler, K. W., Panagia, N., Sramek, R. A., Marcaide, J. M., Williams, C. L. M., & van Dyk, S. D. 2007, in American Institute of Physics Conference Series, Vol. 937, Supernova 1987A: 20 Years After: Supernovae and Gamma-Ray Bursters, ed. S. Immler, K. Weiler, & R. McCray, 264–268

Stockdale, C. J., Weiler, K. W., Van Dyk, S. D., Montes, M. J., Panagia, N., Sramek, R. A., Perez-Torres, M. A., & Marcaide, J. M. 2003, ApJ, 592, 900

Strigari, L. E., Beacom, J. F., Walker, T. P., & Zhang, P. 2005, *JCAP*, 4, 17

Strigari, L. E., Kaplinghat, M., Steigman, G., & Walker, T. P. 2004, *JCAP*, 3, 7

Strolger, L.-G., et al. 2004, ApJ, 613, 200

Strong, A. W., Moskalenko, I. V., & Reimer, O. 2000, ApJ, 537, 763

Strumia, A., & Vissani, F. 2003, Physics Letters B, 564, 42

Sullivan, M., Ellis, R., Nugent, P., Smail, I., & Madau, P. 2000, *Mon. Not. Roy. Astron. Soc.*, 319, 549

Sullivan, M., et al. 2006, ApJ, 648, 868

Sumiyoshi, K., Yamada, S., & Suzuki, H. 2007, ApJ, 667, 382

—. 2008, ApJ, 688, 1176

Tanimori, T., et al. 1998, ApJ, 497, L25+

The Dark Energy Survey Collaboration. 2005, ArXiv Astrophysics e-prints

The Large Synoptic Survey Telescope Collaboration. 2007, Science Requirements Document, http://www.lsst.org/Science/docs/SRD.pdf

Thompson, T. A., Burrows, A., & Pinto, P. A. 2003, ApJ, 592, 434

Thompson, T. A., Quataert, E., & Waxman, E. 2007, ApJ, 654, 219

Tonry, J. 2003, Pan-STARRS Science Goals: Supernova Science, http://pan-starrs.ifa.hawaii.edu/project/science/precodr.html

Tonry, J. L., et al. 2003, ApJ, 594, 1

Totani, T., & Sato, K. 1995, Astroparticle Physics, 3, 367

Tyson, J. A. 2002, in Presented at the Society of Photo-Optical Instrumentation Engineers (SPIE) Conference, Vol. 4836, Society of Photo-Optical Instrumentation Engineers (SPIE) Conference Series, ed. J. A. Tyson & S. Wolff, 10–20

Venters, T. M., & Pavlidou, V. 2011, ArXiv e-prints

Vink, J. S., de Koter, A., & Lamers, H. J. G. L. M. 2001, A&A, 369, 574

Vinkó, J., & Takáts, K. 2007, in American Institute of Physics Conference Series, Vol. 937, Supernova 1987A: 20 Years After: Supernovae and Gamma-Ray Bursters, ed. S. Immler, K. Weiler, & R. McCray, 394–398

Vogel, P., & Beacom, J. F. 1999, Phys. Rev. D, 60, 053003

Wang, Y. 2007, ApJ, 654, L123

Wang, Y., Kostov, V., Freese, K., Frieman, J. A., & Gondolo, P. 2004, *JCAP*, 12, 3

Watanabe, K., Hartmann, D. H., Leising, M. D., & The, L.-S. 1999, ApJ, 516, 285

Webbink, R. F. 1984, ApJ, 277, 355

Weiler, K. W., Panagia, N., Montes, M. J., & Sramek, R. A. 2002, ARA&A, 40, 387

Weiler, K. W., Panagia, N., & Sramek, R. A. 1990, ApJ, 364, 611

Weiler, K. W., Panagia, N., Sramek, R. A., van Dyk, S. D., Williams, C. L., Stockdale, C. J., & Kelley, M. T. 2009, in American Institute of Physics Conference Series, Vol. 1111, American Institute of Physics Conference Series, ed. G. Giobbi, A. Tornambe, G. Raimondo, M. Limongi, L. A. Antonelli, N. Menci, & E. Brocato, 440–447

Weiler, K. W., Sramek, R. A., Panagia, N., van der Hulst, J. M., & Salvati, M. 1986, ApJ, 301, 790

Weiler, K. W., van Dyk, S. D., Sramek, R. A., & Panagia, N. 2004, New Astronomy Review, 48, 1377

Weiler, K. W., Williams, C. L., Panagia, N., Stockdale, C. J., Kelley, M. T., Sramek, R. A., Van Dyk, S. D., & Marcaide, J. M. 2007, ApJ, 671, 1959

Wellons, S., & Soderberg, A. M. 2011, in Bulletin of the American Astronomical Society, Vol. 43, American Astronomical Society Meeting Abstracts #217, 337.15–+

Wesselink, A. J. 1946, *Bull. Astron. Inst. Netherlands*, 10, 91

Wood-Vasey, W. M., et al. 2007, ApJ, 666, 694

Woosley, S. E. 1993, ApJ, 405, 273

Woosley, S. E., & Bloom, J. S. 2006, ARA&A, 44, 507

Woosley, S. E., Eastman, R. G., & Schmidt, B. P. 1999, ApJ, 516, 788

Woosley, S. E., Wilson, J. R., & Mayle, R. 1986, ApJ, 302, 19

Wurm, M., von Feilitzsch, F., Göger-Neff, M., Hochmuth, K. A., Undagoitia, T. M., Oberauer, L., & Potzel, W. 2007, Phys. Rev. D, 75, 023007

York, D. G., et al. 2000, AJ, 120, 1579

Young, D. R., Smartt, S. J., Mattila, S., Tanvir, N. R., Bersier, D., Chambers, K. C., Kaiser, N., & Tonry, J. L. 2008a, A&A, 489, 359

—. 2008b, A&A, 489, 359

Yüksel, H., Ando, S., & Beacom, J. F. 2006, Phys. Rev. C, 74, 015803

Yüksel, H., & Beacom, J. F. 2007, Phys. Rev. D, 76, 083007

Yüksel, H., Kistler, M. D., Beacom, J. F., & Hopkins, A. M. 2008, ApJ, 683, L5

Zhao, F.-Y., Strom, R. G., & Jiang, S.-Y. 2006, Chinese J. Astron. Astrophys., 6, 635

Zheng, C., et al. 2008, AJ, 135, 1766